UNIVERSIDADE FEDERAL DE SANTA MARIA
CENTRO DE CIÊNCIAS NATURAIS E EXATAS
PROGRAMA DE PÓS-GRADUAÇÃO EM METEOROLOGIA

Osmar Evandro Toledo Bonfim

ELEVATION-DEPENDENT WARMING E SUAS POSSÍVEIS CAUSAS NOS ANDES

Santa Maria, RS
2022

Osmar Evandro Toledo Bonfim

ELEVATION-DEPENDENT WARMING E SUAS POSSÍVEIS CAUSAS NOS ANDES

Tese de Doutorado apresentada ao Programa de Pós-Graduação em Meteorologia, Área de Concentração em Estudos e Aplicações em Tempo e Clima, da Universidade Federal de Santa Maria (UFSM, RS), como requisito parcial para obtenção do grau de **Doutor em Meteorologia**. Defesa realizada por videoconferência.

ORIENTADOR: Prof. Luca Mortarini

Santa Maria, RS
2022

Bonfim, Osmar Toledo
ELEVATION-DEPENDENT WARMING E SUAS POSSÍVEIS CAUSAS NOS ANDES / Osmar Toledo Bonfim.- 2022.
73 p.; 30 cm

Orientador: Luca Mortarini
Tese (doutorado) - Universidade Federal de Santa Maria, Centro de Ciências Naturais e Exatas, Programa de Pós-Graduação em Meteorologia, RS, 2022

1. Elevation-dependent warming 2. Tendências regionais de temperatura. 3. Modelos climáticos 4. CORDEX 5. Projeções I. Mortarini, Luca II. Título.

Sistema de geração automática de ficha catalográfica da UFSM. Dados fornecidos pelo autor(a). Sob supervisão da Direção da Divisão de Processos Técnicos da Biblioteca Central. Bibliotecária responsável Paula Schoenfeldt Patta CRB 10/1728.

End. Eletr.: osmartoledob@gmail.com

Osmar Evandro Toledo Bonfim

ELEVATION-DEPENDENT WARMING E SUAS POSSÍVEIS CAUSAS NOS ANDES

Tese de Doutorado apresentada ao Programa de Pós-Graduação em Meteorologia, Área de Concentração em Estudos e Aplicações em Tempo e Clima, da Universidade Federal de Santa Maria (UFSM, RS), como requisito parcial para obtenção do grau de **Doutor em Meteorologia**

Aprovado em 17 de fevereiro de 2022

Luca Mortarini, Dr. (UFSM)
(Presidente/Orientador)

Elisa Palazzi, Dra. (ISAC-CNR)

Otávio Costa Acevedo, Dr. (UFSM)

Djane Fonseca da Silva, Dra. (UFAL)

Felipe Denardim Costa, Dr. (UNIPAMPA)

Santa Maria, RS
2022

DEDICATÓRIA

”Aos meus pais (José Osmar e Leodirce) e a meu irmão (Leandro) que mesmo aos prantos me deram carinho, apoio e ensinamentos para que eu pudesse derrubar os próprios muros e chegar até essa etapa da minha vida.”

AGRADECIMENTOS

Agradeço ao Programa de Pós-Graduação em Meteorologia (PPGMET) pela oportunidade de continuar os meus estudos, em especial aos professores Otávio Acevedo e Gervázio Degrazia.

Agradeço a todos meus amigos do curso de doutorado que estiveram comigo nos momentos de estudos e pesquisas, em especial ao GRUpo de Turbulência Atmosférica de Santa Maria (GRUTA): Daiane, Ivan Maurício, Rafael.

Aos meus amigos e professores do mestrado no ICAT-UFAL, especialmente à Professora Djane Fonseca.

Agradeço aos professores Luca Mortarini e Elisa Palazzi pelas orientações prestadas, pela confiança em mim depositada, pela disposição, pela paciência e pela ajuda em todas as etapas deste trabalho, os quais me proporcionaram um aprendizado louvável.

À CAPES pelo suporte financeiro dado a esta pesquisa.

E a minha família

"....porque eu vou conseguir, e eu vou até o fim. "

RESUMO

ELEVATION-DEPENDENT WARMING E SUAS POSSÍVEIS CAUSAS NOS ANDES

AUTOR: Osmar Evandro Toledo Bonfim
ORIENTADOR: Luca Mortarini

As regiões montanhosas foram reconhecidas como as mais sensíveis às mudanças climáticas e ambientais e, em particular, ao aquecimento global. Vários estudos relataram o elevation-dependent warmng (EDW), ou seja, quando as taxas de aquecimento diferem em diferentes faixas de altitude, particularmente com foco no aumento das taxas de aquecimento com a elevação. A Cordilheira dos Andes provou ser um *hot-spot* relevante às mudanças climáticas, com tendências positivas de temperatura e um recuo generalizado das geleiras nas últimas décadas. Para avaliar e entender melhor o EDW nesta região e identificar sua possível dependência da latitude, a Cordilheira dos Andes foi dividida em cinco domínios, três pertencentes à zona tropical e dois pertencentes aos subtrópicos. Além disso, para cada área, as faces leste e oeste da cordilheira foram analisadas separadamente. Um conjunto de simulações de modelos climáticos regionais (RCM) participantes do Experimento Coordenado de Redução Climática Regional (CORDEX), consistindo em um RCM aninhado em oito modelos climáticos globais (GCM) diferentes pertencentes do Projeto de Intercomparação de Modelos Acoplados (CMIP5) foi considerado neste estudo. O EDW foi avaliado calculando a diferença de temperatura entre o final do século (2071 - 2100) e o período histórico (1976 - 2005) e relacionando-a com a elevação. As projeções futuras foram baseadas nos cenários de alta emissão de CO_2 (RCP 8.5) e de estabilização das concentrações de CO_2 (RCP 4.5). Possíveis diferenças nos mecanismos condutores de EDW foram identificadas usando análises de correlação entre as mudanças de temperatura e todas as variáveis identificadas como possíveis mecanismos condutores de EDW. Para as temperaturas máximas, um sinal EDW positivo (ou seja, aumento das taxas de aquecimento com elevação) foi identificado em ambos os lados dos Andes Tropicais e Subtropicais e em todas as estações. Para as temperaturas mínimas, ao contrário, enquanto um EDW positivo foi identificado nos subtrópicos (particularmente evidente no lado oeste da cadeia), os trópicos foram caracterizados por um EDW negativo ao longo do ano. Portanto, a região tropical marca uma transição entre os comportamentos discordantes de EDW para a temperatura mínima. Nos trópicos diferentes mecanismos condutores de EDW foram identificados para a temperatura mínima, cujas mudanças estão principalmente associadas a mudanças na radiação de onda longa (ROL), e para a temperatura máxima, as mudanças são principalmente impulsionadas por mudanças na radiação de onda curta (ROC). Isso pode explicar o sinal EDW oposto encontrado nos Andes Tropicais durante o dia e a noite. Mudanças no albedo da neve foi o mecanismo condutor onipresente para

a intensificação do EDW nos subtrópicos, tanto para a temperatura mínima quanto para a máxima. Mudanças na ROL e umidade também foram condutores de EDW nos subtrópicos, mas com diferente relevância ao longo das estações do ano. Além disso, os lados oeste e leste da Cordilheira podem ser influenciados por diferentes mecanismos condutores de EDW..

Palavras-chave: Elevation-dependent warming. Tendências regionais de temperatura. Clima regional. Modelos climáticos. CORDEX. Projeções

ABSTRACT

ELEVATION-DEPENDENT WARMING AND ITS POSSIBLE CAUSES IN THE ANDES

AUTHOR: Osmar Evandro Toledo Bonfim
ADVISOR: Luca Mortarini

Mountain regions have been recognized to be more sensitive to climate and environmental changes, and to global warming in particular. Several studies report on elevation-dependent warming (EDW), i.e., when warming rates are different in different altitude ranges, particularly focusing on the enhancement of warming rates with elevation. The Andean chain proved to be a relevant climate change hot-spot with positive temperature trends and a widespread glacier retreat over the recent decades. To assess and to better understand elevation dependent warming in this mountain region and to identify its possible dependence on latitude, the Andean Cordillera was split into five domains, three pertaining to the tropical zone and two pertaining to the Subtropics. Further, for each area the eastern and western faces of the mountain range were separately analyzed. An ensemble of regional climate model (RCM) simulations participating in the Coordinated Regional Climate Downscaling Experiment (CORDEX), consisting of one RCM nested into eight different global climate models from the CMIP5 ensemble was considered in this study. EDW was assessed by calculating the temperature difference between the end of the century (20712100) and the historical period (19762005) and relating it to the elevation. Future projections were based in the high-emission scenario (RCP 8.5) and repeated for the stabilization of the CO_2 scenario (RCP 4.5). Possible differences in the EDW mechanisms were identified using correlation analyses between temperature changes and all the variables identified as possible EDW drivers. For the maximum temperatures, a positive EDW signal (i.e., enhancement of warming rates with elevation) was identified in each side of both the tropical and subtropical Andes and in all seasons. For the minimum temperatures, on the contrary, while a positive EDW was identified in the Subtropics (particularly evident in the western side of the chain), the Tropics are characterized by a negative EDW throughout the year. Therefore, the tropical boundary marks a transition between discordant EDW behaviors in the minimum temperature. In the Tropics and particularly in the inner Tropics, different EDW drivers were identified for the minimum temperature, whose changes are mostly associated with changes in downward longwave radiation, and for the maximum temperature, whose changes are mainly driven by changes in downward shortwave radiation. This might explain the opposite EDW signal found in the Tropical Andes during daytime and nighttime. Changes in albedo are an ubiquitous driver for positive EDW in the Subtropics, for both the minimum and the maximum temperature. Changes in longwave radiation and humidity are also EDW drivers in the Subtropics but with different relevance throughout the seasons and

during daytime and nighttime. Also, the western and eastern sides of the Cordillera might be influenced by different EDW drivers.

Keywords: Andes. Elevation-dependent warming. Regional temperature trends. Regional climate. Climate models. Projections

LISTA DE FIGURAS

LISTA DE TABELAS

LISTA DE ABREVIATURAS E SIGLAS

$a.s.l$	acima do nível do mar
AB	Alta da Bolívia
$C3S$	Copernicus Climate Change Service
$CMIP5$	Projeto de Intercomparação de Modelos Acoplados
$CORDEX$	Experimento Coordenado de Redução Climática Regional
DJF	Dezembro, Janeiro e Fevereiro
$ECMWF$	Centro Europeu de Previsões Meteorológicas de Médio Prazo
EDW	Elevation-dependent warming
$ENOS$	El Niño Oscilação Sul
EQM	Erro quadrático médio
$ERA5$	ECMWF Reanalysis version 5
$GCMs$	Modelos climáticos globais
GEE	Gases de efeito estufa
$GMS5$	Satélite meteorológico geoestacionário
GPS	Sistemas de posicionamento global
$IPCC$	Painel Intergovernamental sobre Mudanças do Clima
JJA	Junho, Julho e Agosto
LST	Temperatura superfície do terrestre
$MODIS$	Moderate Resolution Imaging Spectroradiometer
RCD	Redução Climática Regional
$RCMs$	Modelos climáticos regionais
$RCPs$	Vias de concentração representativas
ROC	Radiação de onda curta
ROL	Radiação de onda longa
SAM	domínio América do Sul
SON	Setembro, Outubro e Novembro
$Tasmax$	Temperatura máxima do ar em superfície

$Tasmin$	Temperatura mínima do ar em superfície
$WCRP$	Programa mundial de pesquisas climáticas
$WRF-CHEM$	Modelo de Pesquisa e Previsão Numérica do Tempo acoplado à Química

SUMÁRIO

1 INTRODUÇÃO

Referidas por muitos autores como torres de águas naturais do século XXI (MESSERLI, 2001; VIVIROLI; WEINGARTNER, 2004; IMMERZEEL et al., 2020), as regiões montanhosas compreendem cerca de 27% da superfície continental da Terra (PRICE, 2015) abastecendo cerca de 40% da população mundial com água doce através de sistemas fluviais fundamentais para irrigação, produção de alimentos e geração de energia hidrelétrica. Durante a segunda metade do século XX, as observações sugeriram que as regiões montanhosas são relativamente mais sensíveis e vulneráveis ao aquecimento global. O Painel Intergovernamental sobre Mudanças Climáticas (IPCC, 2021) considera as geleiras de montanhas como um indicador chave das mudanças climáticas recentes, e apontam que elas ainda continuaram derretendo por décadas ou séculos. De fato, os recuos das geleiras são um dos efeitos mais evidentes do aquecimento global em seu estágio inicial.

Durante a estação chuvosa ocorre o armazenamento da precipitação de neve nas geleiras, que garante a disponibilidade de água para a comunidade a jusante na estação seca. Porém, à medida que as Bacias glaciais desaparecem, a disponibilidade e a qualidade da água são comprometidas (BRADLEY et al., 2006). Nas áreas tropicais, como em parte dos Andes, as variações sazonais da temperatura do ar são pequenas, a quantidade e o tempo de escoamento das geleiras ao longo do ano são controlados principalmente pela alternância das estações chuvosas e secas. Beniston (2003) afirmou que de 30% a 50% da massa glacial de montanha existente em todo o mundo pode desaparecer até 2100. Entre o período passado recente (1986 - 2005) e o futuro próximo (2031 - 2050), a profundidade da neve deverá diminuir em 25% em muitas regiões elevadas, como os Alpes Europeus, Oeste da América do Norte, Cordilheira do Himalaia e Andes Subtropicais, independentemente do cenário de emissão de gases de efeito estufa (GEE) (IPCC, 2021).

Uma das questões importantes relacionadas às mudanças climáticas nas montanhas é se elas estão aquecendo mais do que as planícies adjacentes ou em comparação com o aquecimento médio global. Muitos estudos (PEPIN et al., 2015; PALAZZI et al., 2017; MINDER et al., 2018; NIU et al., 2021) relataram tendências na mudança da temperatura do ar em relação à elevação, um fenômeno conhecido como Elevation-Dependent Warming (EDW). O EDW não implica necessariamente que o aquecimento se intensifique com a altitude, mas significa que a taxa de aquecimento (por exemplo, em $^{\circ}$ C por década) não é uniforme nas cadeias de montanhas. Apesar de ter recebido grande atenção nos últimos anos, o EDW ainda não é completamente compreendido. A identificação dos mecanismos que conduz o EDW e como eles se combinam é complexo e varia conforme as diferentes cadeias de montanhas, estações do ano e indicadores de temperatura (por exemplo, temperatura média, mínima ou máxima), portanto, nenhum padrão de EDW ainda

foi definido.

Vários processos físicos contribuem para o EDW, e a quantificação de suas contribuições relativas permanecem em grande parte imprecisas (MINDER et al., 2018; PALAZZI et al., 2019). Por exemplo, em ambientes montanhosos, a sensibilidade da temperatura do ar ao forçamento radiativo aumenta em baixas temperaturas (OHMURA, 2012). A relação entre umidade específica e radiação de onda longa (ROL) não é linear, em uma atmosfera seca e fria típica de altitudes elevadas, qualquer aumento na umidade atmosférica causado pelo aumento da temperatura, levaria a um aquecimento desproporcionalmente grande (RANGWALA, 2013). O feedback do albedo da neve desempenha um papel importante, pois a redução na cobertura de neve implica em aumento da absorção da radiação solar na superfície que, no que lhe concerne, leva ao aumento da temperatura do ar e intensifica o derretimento da neve (PEPIN; LUNDQUIST, 2008).

Para melhorar o entendimento do EDW, as medições de temperatura do ar nas estações meteorológicas são essenciais. Dado que a maioria das estações meteorológicas estão instaladas em regiões relativamente de baixa altitude, as estações localizadas em regiões de montanhas são escassas, e essas áreas atualmente são sub-representadas. De acordo com o banco de dados da Rede Global de Climatologia Histórica (RGCHv3), das 7.297 estações cadastradas, apenas 191 (3%) estão acima de 2.000 metros de altitude e 54 (0,7%) acima de 3.000 metros, e os dados de longo prazo são simplesmente inexistentes para estações acima de 5.000 metros em qualquer região montanhosa (LAWRIMORE et al., 2011).

Os Andes Tropicais configuram como uma região de elevada incerteza, devido a localizações de estações terrestres esparsas e não homogêneas e ainda apresentar uma maior variação nas simulações de modelos em comparação com as áreas vizinhas (ou seja, o Oceano Pacífico e a Bacia hidrográfica amazônica) (URRUTIA; VUILLE, 2009; BUYTAERT et al., 2010).

Além disto, a Cordilheira dos Andes difere das outras cadeias de montanhas como os Alpes europeus, as Montanhas Rochosas do Colorado e a Cordilheira do Himalaia de várias maneiras. Em particular, a Cordilheira dos Andes é bastante estreita, mas muito íngreme ao longo da costa oeste do continente, ascendendo da costa do Oceano Pacífico a uma altitude média de 3.500 m em menos de 300-400 km, dependendo da latitude. A presença da Cordilheira dos Andes, desempenha um papel fundamental na determinação do clima da América do Sul. Devido à sua latitude e altitude, os Andes interrompem a circulação atmosférica, resultando em uma variedade de fenômenos de mesoescala e circulação regional, contrastando as condições climáticas ao longo das encostas leste e oeste, e planícies adjacentes (GARREAUD, 2009).

Sob esta ótica, o conhecimento do EDW e dos seus possíveis mecanismos de condução, destacando as diferenças em função da latitude, da sazonalidade, das variáveis consideradas (tanto a temperatura mínima quanto a temperatura máxima) e das faces

(leste e oeste) da Cordilheira dos Andes, visa compreender como as mudanças climáticas futuras podem impactar o zoneamento dos ecossistemas, a economia e a sociedade a jusante dos Andes.

2 REVISÃO BIBLIOGRÁFICA

2.1 ELEVATION-DEPENDENT WARMING

Uma das principais questões enfrentadas pela comunidade científica que trabalha com mudanças climáticas nas montanhas é se as taxas de aquecimento, bem como as tendências de outras variáveis como precipitação e profundidade da neve, exibem uma dependência da altitude e, em particular, se são intensificadas em altitudes mais elevadas quando comparadas com as áreas mais baixas ou com a média global. Isso teria claramente várias implicações para a criosfera de altitude, ecossistemas de montanha, biodiversidade e, finalmente, para a sociedade. Vários estudos globais e regionais relataram o aquecimento dependente da elevação, também conhecido no inglês como Elevation-dependent warming (EDW) (PEPIN et al., 2015; PALAZZI et al., 2019, MILLER et al., 2021, entre outros).

Em princípio, avaliar a taxa e o padrão de aquecimento com elevação nas últimas décadas deveria ser simples. No entanto, muitos fatores e condições dificultam a verificação da taxa de aquecimento em regiões montanhosas. Em primeiro lugar, as estações meteorológicas de longa duração (com mais de 20 anos de registros) são extremamente escassas em altitudes elevadas, muito poucas estão em picos ou platôs isolados, e a maioria das observações em regiões montanhosas são feitas em vales com microclimas distintos e propensos à drenagem do ar frio. Além disso, a extrema temperatura local, topografia, inclinação e exposição dificultam a coleta de dados e a preservação da estação in-situ (PEPIN et al., 2011; 2015).

Distintas metodologias são aplicadas para avaliar o EDW, dentre elas, as mais utilizadas são observações *in situ*, dados de satélite, reanálise dados e modelos climáticos (RANGWALA; MILLER, 2012; PEPIN et al., 2015; PALAZZI et al., 2017; 2019; MINDER et al., 2018; NIU et al., 2021; CHIMBORAZO et al., 2022). A maioria dos estudos sobre EDW baseia-se na análise de observações *in situ* e apontam para uma amplificação nas taxas de aquecimento em razão da elevação. Em contrapartida, os autores admitem que essa amplificação do aquecimento pode não ser considerada universal. Alguns estudos como Tudoroiu et al. (2016) mostraram que na porção oriental dos Alpes europeus há um aquecimento negativo dependente da elevação em torno de 2100 metros de altitude, Vuille e Bradley (2000) encontraram tendências de aquecimento reduzidas com o aumento da elevação nos Andes Tropicais, e You et al. (2010) não encontraram sinais de EDW utilizando dados de reanálises no Platô Tibetano oriental e central para o intervalo de 1961 a 2005.

Outros estudos sugeriram que as regiões montanhosas podem estar aquecendo a

taxas mais altas do que o resto da superfície terrestre global. Liu et al. (2006) examinaram tendências nas temperaturas mínimas e máximas no período de 1961 a 2003 no Platô Tibetano. Os autores descobriram que as temperaturas mínimas estão aumentando mais rapidamente do que as temperaturas máximas em todos os meses, com um aquecimento mais pronunciado no inverno e na primavera. Wang et al. (2016) utilizaram um conjunto de observações globais no período de 1961 a 2010 e notaram que as regiões de altitudes mais elevadas globalmente estão se aquecendo a taxas mais rápidas do que as planícies próximas.

Os estudos observacionais de EDW enfrentam desafios associados à falta de registros climáticos em terrenos montanhosos, conforme discutido acima. No entanto, modelos climáticos numéricos têm sido úteis para superar algumas limitações de conjuntos de dados observacionais. Eles podem representar cenários climáticos futuros e possibilitar o diagnóstico de mecanismos físicos (MINDER et al., 2018). Vários estudos (RANGWALA et al., 2016; PALAZZI et al., 2017; 2019, YOU et al., 2019) investigaram EDW utilizando dados de modelos climáticos globais (GCMs) e quase todos encontraram um sinal claro de EDW, com um aquecimento amplificado com a elevação ou mostrando algum aquecimento máximo nas elevações intermediárias.

A resolução do modelo também desempenha um papel importante na avaliação do EDW. Executando o EC-Earth GCM em cinco resoluções diferentes (T159 (aprox. 125 km), T255 (aprox. 80 km), T511 (aprox. 40 km), T799 (aprox. 25 km), T1279 (aprox. 16 km)), PALAZZI et al. (2019) investigaram o impacto da resolução espacial no sinal do EDW sobre as Montanhas Rochosas do Colorado, Região dos Alpes europeus e o Platô Tibetano. Nenhuma dependência de resolução evidente na capacidade do modelo de simular EDW foi encontrada, no entanto, as diferentes resoluções simularam diferentes intensidades de EDW e atribuíram uma importância diferente aos vários mecanismos de condução do EDW.

2.2 MECANISMOS RESPONSÁVEIS PELO ELEVATION-DEPENDENT WARMING

O conhecimento dos mecanismos e processos físicos que podem estar ligados ao EDW é essencial para explicar as variações no fluxo líquido de energia sobre as regiões montanhosas. Vários estudos mostraram que o maior aquecimento observado em altitudes mais elevadas pode ser atribuído ao feedback do albedo da neve (ZAZULIE et al., 2018; MINDER et al., 2018; PALAZZI et al., 2019; GUO et al., 2021; SHEN et al., 2021), cobertura de nuvens (LIU et al., 2009), modulação do vapor de água do aquecimento de ondas longas (RANGWALA et al. 2009; PALAZZI et al., 2019, NIU et al., 2021), vapor de água superficial (RANGWALA, 2013) e aerossóis (LAU et al., 2010). Outros fatores como mudanças na cobertura do solo foram considerados no estudo de Tudoroiu et al. (2016), no entanto, na

literatura não há consenso sobre o papel desse mecanismo no desencadeamento do EDW. A Tabela 1 resume os possíveis mecanismos responsáveis pelo EDW e seus efeitos.

2.2.1 Feedback do albedo de neve/gelo

O feedback do albedo da neve é certamente um dos feedbacks mais fortes do sistema climático. Relevante em regiões de altitudes elevadas dominadas por neve, também tem um papel crucial na amplificação polar (ou arctic amplification, no inglês). A definição de Albedo está relacionada à quantidade de energia solar refletida pela superfície da Terra. Superfícies brilhantes, como geleiras, têm um albedo alto e, portanto, refletem uma maior quantidade de energia solar do que absorvem (Figura 1) (PEPIN et al., 2015).

A mudança no albedo atua para reforçar a anomalia positiva de temperatura inicial na área de gelo levando a mais aquecimento. O aquecimento tende a diminuir a cobertura de gelo, portanto, diminuir o albedo, aumentando a quantidade de energia solar absorvida e levando a mais aquecimento. Como esse feedback modula a absorção da superfície da radiação solar incidente, afeta principalmente as mudanças na temperatura máxima. Aumento na temperatura mínima também é possível se a diminuição da cobertura de neve for acompanhada de aumento na umidade do solo e umidade específica, que podem facilitar uma maior retenção diurna de energia solar na superfície durante o dia e amplificar o aquecimento de ondas longas da superfície terrestre à noite (RANGWALA; MILLER, 2012).

Figura 1 – Feedback Albedo da Neve/Gelo.

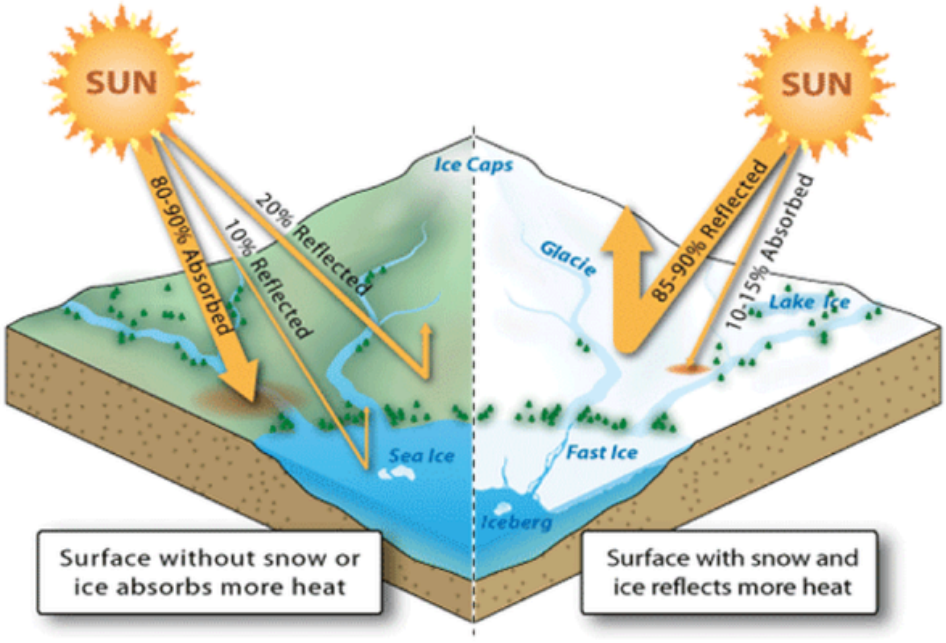

Fonte: Pistone et al. (2014).

Tabela 1 – Possíveis mecanismos do EDW juntamente com seu efeito, relevância sazonal e resposta à temperatura.

Condutor climático	Efeito	Relevância sazonal	Resposta à Temperatura
Redução no albedo da neve	Aumento absorção superficial da insolação	Principalmente primavera; inverno em altitudes mais baixas; verão em altitude mais elevada.	Aumento Tasmax
Aumento na cobertura de nuvens (diurno)	Redução insolação da superfície	Todas as estações, mas efeitos maiores no verão.	Redução Tasmax
Aumento na cobertura de nuvens (noturno)	Aumento ROL	Todas as estações, porém, maiores efeitos no inverno.	Aumento Tasmin
Aumento na umidade específica	Aumento ROL	Principalmente inverno; efeitos menores são possíveis no outono e na primavera.	Aumento Tasmin
Aumento de aerossóis absorventes (Carbono negro, poeira)	Redução no albedo das nuvens; Redução do albedo da neve sobre a superfície; Aumento aquecimento da troposférica média	Dependente da emissão sazonal e insolação	Aumento Tasmin; Aumento Tasmax (cobertura de nuvens reduzida)

Fonte: Adaptado de Pepin e Lundquist (2008); Rangwala et al. (2009).

Sobre a Região dos Alpes europeus, Giorgi et al. (1997) encontraram uma mudança mais pronunciada na temperatura e precipitação em altitudes mais elevadas induzidas pelo aquecimento de CO_2. Este aquecimento foi associado a uma diminuição da cobertura de neve e, portanto, impulsionado pelo feedback do albedo da neve, especialmente no inverno e na primavera.

No Platô Tibetano, Guo et al. (2019) descobriram que o declínio da cobertura de neve está fortemente correlacionado com as tendências de temperatura no inverno e na primavera. Nas análises de satélite, os autores mostraram um pico de aquecimento em torno de 3.500m - 4.000m no inverno e 4.000m - 4.500m na primavera, confirmando o feedback positivo do albedo da neve nessas faixas de elevação. Palazzi et al. (2019) identificaram o feedback do albedo da neve como o principal mecanismo condutor do EDW nos meses de setembro, outubro e novembro (SON) para as Montanhas Rochosas do Colorado e Cordilheira do Himalaia utilizando GCMs com alta (aprox. 25km) e muito alta resolução (aprox. 16km).

O tempo sazonal da cobertura de neve varia com a elevação, e as taxas máximas de aquecimento geralmente ocorrem perto do 0°C isotérmica anual (ou linha de neve). Espera-se que a atual linha de neve, que varia com a altitude em diferentes cadeias de montanhas, recue para altitudes mais altas à medida que o sistema climático aqueça. Esta intensificação do aquecimento também atrasa o início da cobertura de neve por vários dias ou semanas em altitudes mais baixas e médias (TERZAGO et al., 2017) e espera-se que essa tendência continue e se intensifique no futuro, envolvendo altitudes mais altas.

Nos Andes Tropicais, durante a fase quente do El Niño Oscilação Sul (ENOS), a precipitação diminuiu em cerca de 10% a 30% e os períodos secos ocorreram com mais frequência durante o verão austral (VUILLE et al., 2000). Essa situação reduz a cobertura de nuvens, aumenta a incidência de radiação de onda curta (ROC), reduz o acúmulo de neve e diminui o albedo nas geleiras. As condições de ENOS na fase fria, por outro lado, são caracterizadas por temperaturas mais baixas, ventos mais constantes e maior volume de precipitação de neve que, aumentam o albedo e a sublimação na região (FRANCOU et al., 2004).

Outros fatores como urbanização (ilhas de calor) (CAMPOVERDE, 2018) e a migração ascendente da linha de árvores (substituição da cobertura de neve por vegetação, LUTZ et al., 2013), estão associados com o aumento de temperatura do ar e redução do albedo da neve nos Andes. Segundo Pepin et al. (2015), restringir a análise somente para estações meteorológicas acima de 500 metros provavelmente subestimaria esses efeitos. No entanto, na Cordilheira dos Andes, algumas grandes cidades estão localizadas acima desta faixa de elevação.

2.2.2 Cobertura de Nuvens

Segundo o quarto relatório do IPCC (2007) o efeito do feedback das nuvens nos modelos climáticos exerce dois efeitos concorrentes na forçante radiativa da Terra. Ao refletir a ROC de volta para o espaço (o efeito albedo das nuvens) e ao capturar a ROL emitida pela superfície e pela baixa troposfera (o efeito estufa das nuvens). Já no quinto relatório do IPCC (2013), propriedades adicionais foram acrescentadas no feedback das nuvens como: mudanças na altitude, quantidade, profundidade óptica das nuvens de alto e de baixo nível (figura 2).

Figura 2 – Diferentes propriedades radiativas das nuvens de baixo e alto nível e seu feedback.

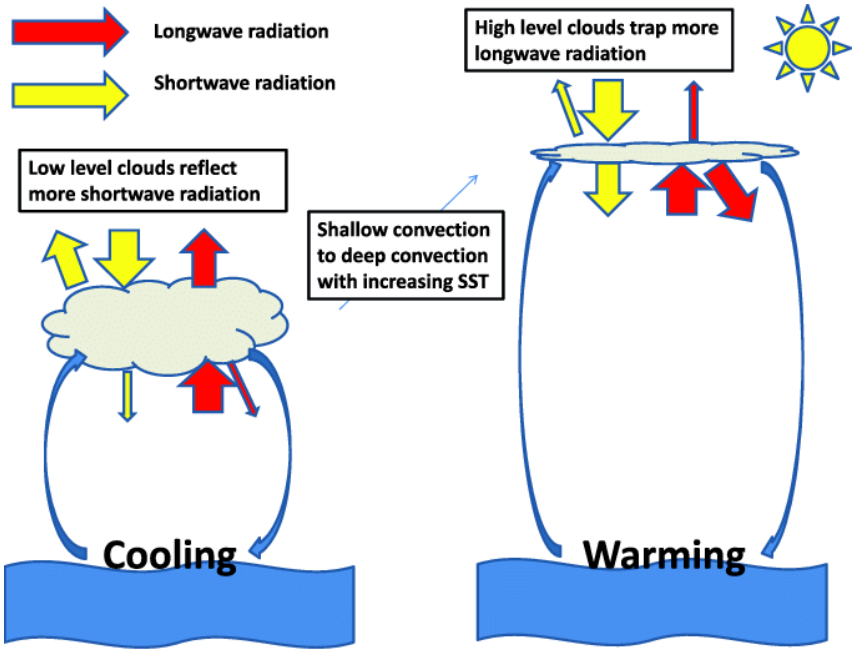

Fonte: Liu et al. (2013).

Segundo Vuille et al. (2003) observações de mudanças de longo prazo em nuvens e propriedades de nuvens são esparsas, particularmente em regiões de elevada altitude. Poucos estudos discutiram como as mudanças nas nuvens podem afetar o EDW. As variações na cobertura de nuvens e nas propriedades das nuvens influenciam fortemente a ROL e ROC, portanto, o balanço de energia da superfície (PEPIN et al., 2015).

Através de observações e projeções de modelos na região do Platô Tibetano, Liu et al. (2009) demonstraram que o aumento da concentração atmosférica de GEE intensifica a cobertura média anual de nuvens em altitudes inferiores a 2.000 m, devido ao aumento na umidade atmosférica e alterações no ciclo hidrológico. Acima de 3000 m, as nuvens totais diminuem e mostram pouca dependência de elevação. Isso favorece o aumento da radiação solar líquida de superfície e a diminuição da profundidade da neve. Os efeitos combinados de profundidade de neve e cobertura de nuvens, resultam em um maior au-

mento de temperatura em altitudes mais altas, em relação a altitudes mais baixas, levando a EDW.

Duan e Wu (2006) relataram um aumento na cobertura de nuvens de baixos níveis no período noturno sobre as partes central e oriental do Platô Tibetano entre 1961 e 2003, apesar da diminuição da cobertura total de nuvens durante o mesmo período. Os autores sugeriram que esse aumento na cobertura de nuvens de baixos níveis é capaz de explicar, em parte, o aumento mínimo na temperatura sobre o planalto na segunda metade do século XX.

Sicart et al. (2016) investigaram que nos Andes Tropicais, fortes mudanças sazonais na cobertura de nuvens e precipitação controlam amplamente o balanço de massa das geleiras, sendo que as propriedades radioativas das nuvens na região desempenham papeis distintos. A atenuação de ROC a emissão de ROL oriundas das nuvens foram maiores no verão (Dezembro, Janeiro e Fevereiro -DJF) (cerca de 20-30%) do que no inverno (Junho, Julho e Agosto -JJA), provavelmente porque a maioria das nuvens de verão são do tipo cúmulos, de baixos níveis e associados à convecção local, enquanto as nuvens de inverno são frequentemente altostratos associadas as perturbações extratropicais.

2.2.3 Vapor de água e fluxos radiativos

As tendências positivas de temperatura produzidas pelo aumento dos níveis de GEE antropogênicos (por exemplo, dióxido de carbono) levam a mais vapor de água na atmosfera que, por sua vez, absorve e emite ROL, aumentando assim o aquecimento da superfície (IPCC, 2021). Os aumentos na umidade específica da superfície foram sugeridos como parcialmente responsáveis por um rápido aumento no aquecimento da superfície na Europa Central (PHILIPONA et al., 2005) e no Platô Tibetano (RANGWALA et al., 2009) no final do século XX. Embora esses estudos sugerem que os aumentos na umidade específica causem aumentos significativos na ROL, Minder et al. (2018) não encontraram evidências sobre a contribuição do feedback do vapor de água para a intensificação do EDW.

Sobre o Platô Tibetano Central, durante a estação das monções, Kuwagata et al. (2001) observaram padrões diurnos no vapor de água usando dados de satélite meteorológico geoestacionário (GMS-5). O total de água precipitável diminuiu durante o dia nos vales, enquanto aumentou nas montanhas. Usando sistemas de posicionamento global (GPS), Wu et al. (2003) sugeriram que a umidade específica da superfície atinge o pico à noite em ambos os períodos secos e úmidos sobre o Platô Tibetano. No entanto, as implicações dos padrões diurnos de vapor d'água, formação de nuvens e precipitação no balanço de energia em relação à elevação ainda precisam de maiores investigações.

Em regiões de altitude elevada, particularmente nos subtrópicos, a baixa atmosfera

tende a ser subsaturada na absorção de vapor de água, especificamente durante a estação fria. Portanto, aumentos no vapor de água durante o inverno, quando a umidade específica é mais baixa, causariam um aumento maior na ROL (RANGWALA et al., 2010). Esses aumentos na ROL aumentariam principalmente a temperatura mínima. Ruckstuhl et al. (2007) sugeriram que a sensibilidade da ROL ao vapor de água da superfície aumenta com a altitude na região dos Alpes suíços. A mesma mudança na quantidade do vapor de água da superfície causará uma mudança maior no ROL em áreas de altitude elevada quando comparados às planícies adjacentes.

As mudanças na umidade são especialmente relevantes no contexto das variações das geleiras devido ao impacto significativo do vapor d'água. Nos Andes, não existem registros *in-situ* contínuos e de longo prazo para documentar tais mudanças. No entanto, novos conjuntos de dados de vapor de água troposférico tornaram-se disponíveis graças a técnicas aprimoradas de sensoriamento remoto. Vuille et al. (2003) encontraram um aumento significativo da umidade relativa entre 1950 e 1995 de até 2.5% por década. Dado esse aumento significativo, segue-se que a pressão de vapor (ou umidade específica) também aumentou significativamente.

2.2.4 Aerossóis

Concentrados principalmente em altitudes relativamente baixas, existem uma variedade de aerossóis atmosféricos (carbono negro, poeiras, fumaça) que contribuem para o aquecimento atmosférico. A diminuição no fluxo de ROC nas encostas mais baixas das montanhas são um dos efeitos esperados (conhecido como efeito de escurecimento da superfície), mas têm efeitos limitados ou nenhum efeito nas regiões mais elevadas acima da camada atmosférica de aerossóis. Durante a estação pré-monção, Ramanathan e Carmichael (2008) encontraram uma camada atmosférica de poeira de desertos e altos níveis de carbono negro em altitudes de até 5000 metros na Cordilheira do Himalaia e no Platô Tibetano. No entanto, existem poucos estudos sobre o alcance de poluentes antropogênicos em altitudes elevadas nas regiões de montanhas.

O carbono negro afeta o balanço de radiação de duas maneiras: absorve radiação na troposfera (principalmente, troposfera média a baixa) e diminui o albedo da superfície quando depositado sobre a neve (Figura 3) (GAUTAM et al., 2013). Devido à complexidade de seu feedback, é muito difícil avaliar seu efeito na intensificação do EDW. Dependendo da altitude em que foi depositado, o carbono negro pode aumentar ou reduzir o EDW. Xu et al. (2009) sugeriram que o carbono negro depositado pode aumentar a absorção de radiação visível de 10 a 100% nas geleiras do Tibete.

Ramanathan et al. (2007) propuseram que o aumento do aquecimento atmosférico regional sobre o Platô Tibetano poderia ser atribuído à formação de nuvens marrons at-

mosféricas, que consistem em uma mistura de aerossóis absorventes de luz resultantes da queima de biomassa e consumo de combustível fóssil provenientes do sul da Ásia.

Figura 3 – Ciclo do Carbono Negro na hidrogeosfera

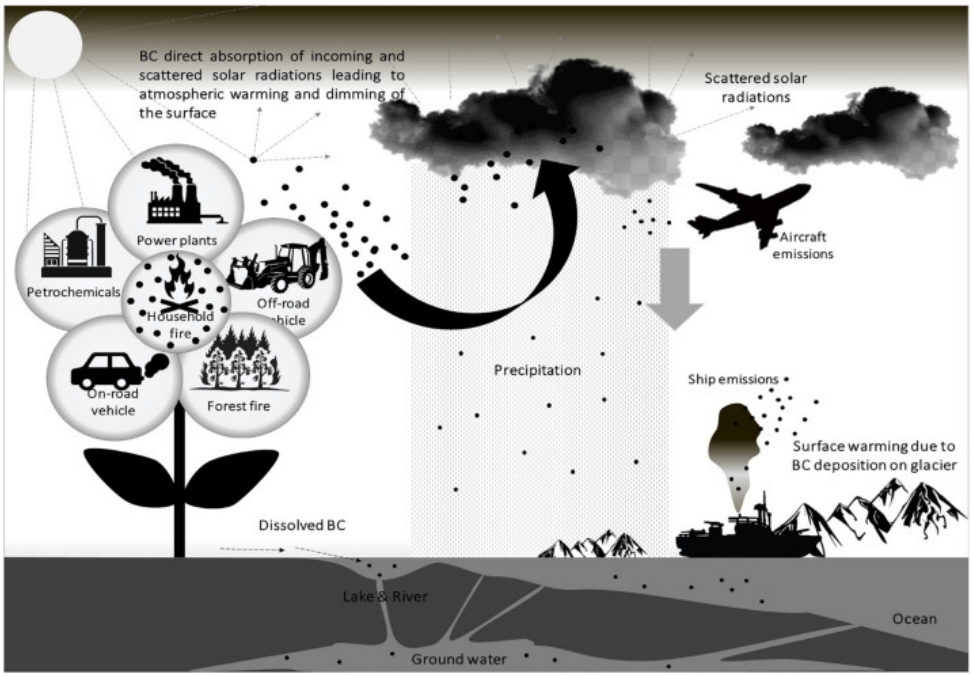

Fonte: Mukherjee e Kumar (2021).

Aerossóis como poeira dependem de outros fatores, como mudança no uso da terra. Por exemplo, Painter et al. (2007) analisaram vários eventos de neve nas Montanhas Rochosas do Colorado e descobriram que as perturbações antropogênicas na cobertura do solo, transfere poeira para a atmosfera através de ventos sazonais da primavera oriundas das regiões áridas para as montanhas. Este fenômeno causa uma redução significativa do albedo da neve na região, em razão do derretimento da neve durante a primavera e o aumento da absorção da radiação solar na superfície. Da mesma forma que o carbono negro, o impacto da poeira no EDW dependerá da elevação na qual ela foi depositada.

Utilizando dados de satélite no período de 2000 a 2016, Bolaños-Ortiz et al. (2019) verificaram uma redução no albedo da neve causados pela deposição de carbono negro proveniente das áreas industriais e urbanas do Chile, principalmente durante os meses da primavera. Além disso, utilizando o modelo de Pesquisa e Previsão Numérica do Tempo acoplado à Química (WRF-Chem), os autores mostraram que ocorre uma predominância dos ventos de oeste no transporte de carbono negro para as Bacias glaciais localizadas em regiões mais elevadas do Chile.

2.3 CORDILHEIRA DOS ANDES

A Cordilheira dos Andes é a mais extensa cordilheira continental do globo terrestre, localizada na costa ocidental da América do Sul, estendendo-se por 7.000 km de aproximadamente 7°N a 45°S. Ao longo de suas porções tropicais e subtropicais, as alturas máximas (picos) dos Andes são superiores a 4.000 metros acima do nível do mar (a.s.l.) (Figura 4). Em contraste com sua altitude, os Andes são uma cordilheira relativamente estreita com uma largura típica de menos de 200 km. Sua altura, extensão latitudinal e orografia proeminente exibem diversos padrões de tempo e clima, incluindo características tropicais, subtropicais e extratropicais (GARREAUD et al., 2009).

Os Andes Tropicais abrigam mais de 99% de todas as geleiras tropicais (KASER, 1999). O estudo de Francou e Vincent (2007) estimou a área total da superfície das geleiras nos Andes Tropicais em cerca de 1.920 km^2. As geleiras nos Andes desempenham um importante serviço, tanto econômico, agrícola e ambiental para as populações das planícies a jusante, liberando água proveniente das geleiras para a parte árida do Oeste (Peru e Bolívia) durante a estação seca (maio - setembro), quando ocorre pouca ou nenhuma chuva. Grande parte da oferta de água doce consumida na agricultura, consumo doméstico, processo industrial e hidroeletricidade origina-se das Bacias glaciais dos Andes (VUILLE et al., 2008a).

Consistente com a maioria das geleiras de montanhas em todo o mundo, as geleiras nos Andes Tropicais vêm recuando a uma taxa crescente desde o final da década de 1970. Considerando o cenário A2 do IPCC, para o século XXI é previsto um aumento na temperatura de mais de 4 °C para as altitudes superiores à 4000 metros (BRADLEY et al., 2006; URRUTIA; VUILLE, 2009). Conforme a análise realizada por Vuille et al. (2008b) utilizando cerca de 280 estações in situ localizadas entre 1°N e 23°S (Andes tropicais), foi detectado um aumento da temperatura do ar próximo à superfície de 0,68 °C no período de 1939 a 2008, com uma taxa de 0,10°C por década. De modo geral, as geleiras tropicais encolhem em resposta ao aumento da temperatura do ar, o que de fato foi observado na região dos Andes (VUILLE et al., 2003; MARK; SELTZER, 2005).

Estudos de modelagem sugeriram que as geleiras na Cordilheira Branca do Peru (onde 70% de todas as geleiras tropicais estão localizadas) continuarão recuando significativamente nas próximas décadas e podem desaparecer completamente em algumas Bacias hidrográficas até 2080, com consequências drásticas para o escoamento (Juen et al., 2007). O fluxo pode aumentar durante a estação chuvosa, mas diminuirá durante a estação seca, consequentemente aumentando a amplitude sazonal do escoamento.

As tendências de precipitação de neve na Cordilheira dos Andes são difíceis de avaliar devido às medições esparsas de queda de neve com observação intermitente, poucos registros de longo prazo e categorias de medidores variáveis (GARREAUD et al., 2009; RASMUSSEN et al., 2012). As informações de cobertura de neve são obtidas por satélites

Figura 4 – Mapa hipsométrico da América do Sul

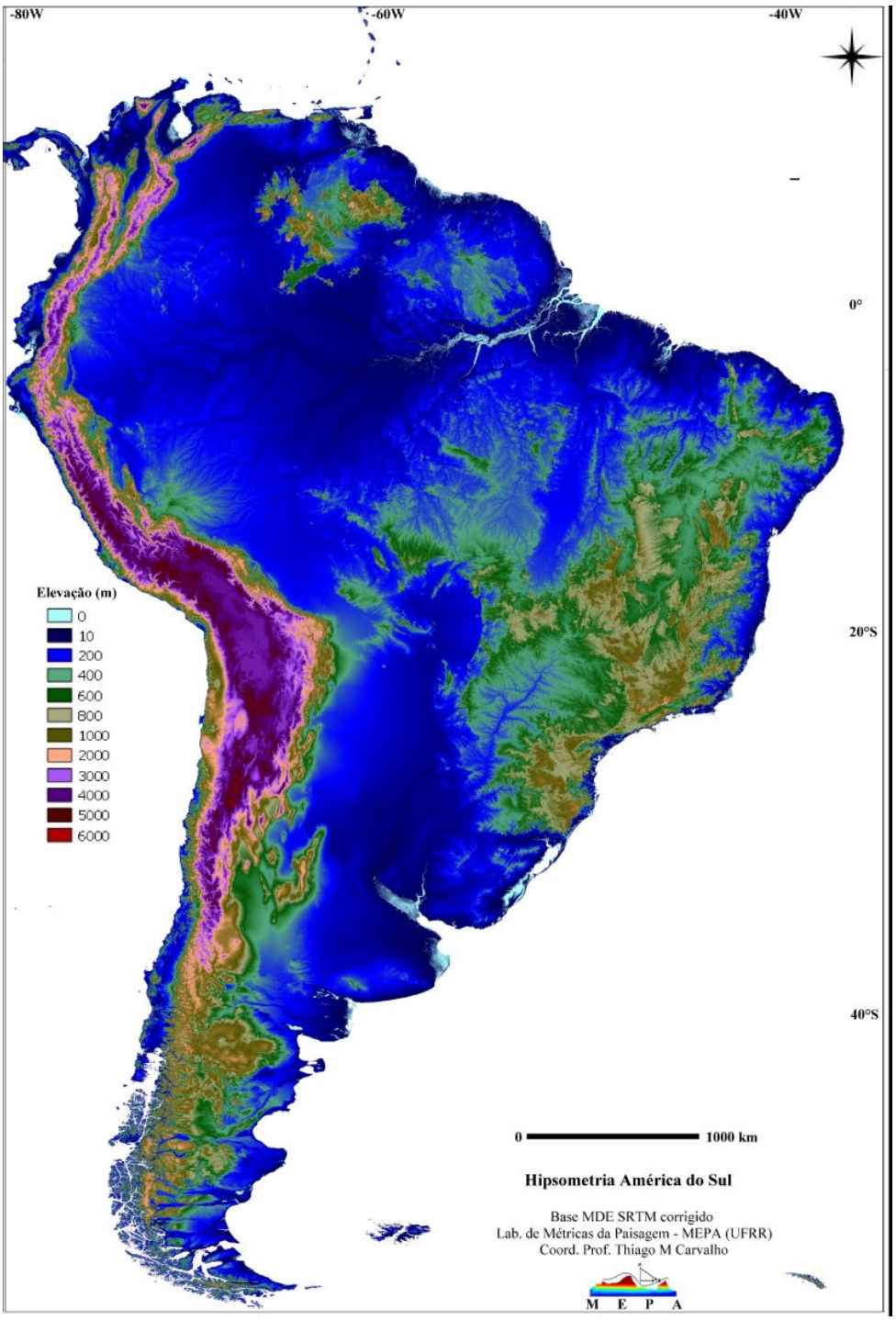

Fonte: MRE (2022).

(STEHR et al., 2009; NOLIN, 2010). No entanto, simulações de modelos, como os GCM e modelos climáticos regionais (RCM), provaram ser uma ferramenta útil para estimar as propriedades da neve (por exemplo, extensão da neve, duração, início, fim, profundidade, densidade e equivalente da água da neve) e suas tendências, principalmente devido à deficiência observacional na Cordilheira dos Andes (FLATO; MAROTZKE, 2013).

Do ponto de vista climatológico, os Andes Tropicais são caracterizados por uma radiação solar incidente constante ao longo do ano. Por outro lado, nas regiões extratropicais (por exemplo, Andes Subtropicais) a radiação solar é influenciada pela variação da cobertura de nuvens de acordo com as estações do ano (cobertura máxima de nuvens durante o verão austral). Da mesma forma que a radiação solar, a umidade nos Andes Tropicais permanece quase inalterada ao longo do ano (a Bacia Amazônica fornece grande parte do transporte de umidade), enquanto os Andes Subtropicais são caracterizados por uma pronunciada sazonalidade de umidade específica e precipitação.

Em termos de circulação de larga escala em altos níveis, os Andes Tropicais situados entre o norte do equador e 15°S são propensos aos ventos de leste, enquanto as porções subtropicais e extratropicais da cadeia estão sujeitas a ventos de oeste. Nos meses de Dezembro, Janeiro e Fevereiro (DJF), os ventos de leste se estendem além de 15°S e a intensa convecção amazônica favorece o estabelecimento da Alta da Bolívia (AB), uma das características mais proeminentes da circulação de verão nos Andes (LENTERS; COOK, 1997). Nos meses de Junho, Julho e Agosto (JJA) os ventos de leste não ultrapassam 10°S de latitude e o jato subtropical de oeste tem seu máximo em torno de 30°S. A circulação de baixo nível é bastante complexa e extremamente importante, pois controla o transporte de umidade e, portanto, os padrões de precipitação. Garreaud et al. (2009) mostraram como a elevação orográfica do ar de baixo nível sobre as encostas oeste das Cordilheiras dos Andes produz precipitação duas a três vezes mais intensa do que ao nível do mar e sobre o lado oriental dos Andes Subtropicais, especialmente na Patagônia Argentina.

A precipitação sobre os Andes Centrais apresent um comportamento anual marcante, com a maior parte das chuvas concentradas durante o verão (dezembro-fevereiro), quando a circulação atmosférica favorece o soerguimento do ar úmido das planícies baixas para o leste da cordilheira (GARREAUD, 1999). A umidade transportada da Bacia Amazônica é a principal fonte de umidade para chuva nos Andes Orientais (GARREAUD, 1999; GARREAUD et al., 2003; GARREAUD et al., 2009). No entanto, a variabilidade da umidade por si só não poderia explicar a precipitação superficial sobre os Andes (GARREAUD et al., 2003).

2.4 EXPERIMENTO DE REDUÇÃO CLIMÁTICA REGIONAL COORDENADA (CORDEX)

Os modelos climáticos globais (GCMs) provaram ser as ferramentas mais valiosas para entender os processos que determinam a resposta do sistema climático às forças antropogênicas, como aumentos nas concentrações de GEE, mudanças na cobertura do solo e uso da terra e na distribuição dos aerossóis na atmosfera. Embora na última década ocorreram melhorias significativas nesses modelos, a resolução horizontal da maioria dos

GCMs atuais ainda é da ordem de centenas de quilômetros. No entanto, os impactos das mudanças climáticas e as estratégias de adaptação e mitigação necessárias para lidar com elas, ocorrem mais frequência em escalas regionais e nacionais. Por isso a Redução Climática Regional (RCD) tem um papel importante em desempenhar e fornecer projeções com mais detalhes e representação mais precisa, por exemplo, da superfície terrestre e de processos atmosféricos como os eventos extremos, sendo de vital importância para as regiões mais vulneráveis (GIORGI et al., 2009; ZHAO et al., 2021).

O Experimento Coordenado de Redução Climática Regional (CORDEX) é um programa patrocinado pelo World Climate Research Program (WCRP) para desenvolver uma estrutura aprimorada e gerar projeções climáticas em escala regional, de modo a melhorar os estudos de avaliação de impacto e outros usos de informações climáticas, planejadas em apoio ao Quinto Relatório de Avaliação do IPCC (OYERINDE, 2018). No entanto, uma das fraquezas do conjunto de simulações CORDEX é a heterogeneidade na disponibilidade dos GCMs nos diferentes domínios. Por exemplo, várias dezenas de modelos estão disponíveis para domínios como Europa, África, América do Norte, enquanto apenas alguns foram incluídos para, por exemplo, Austrália e Ásia Central (GIORGI et al., 2021). Um domínio é a região para a qual o RCD está ocorrendo, por exemplo, o domínio da América do Sul (SAM) cobre todo o continente Sul Americano (Figura 5).

Figura 5 – Domínios do CORDEX

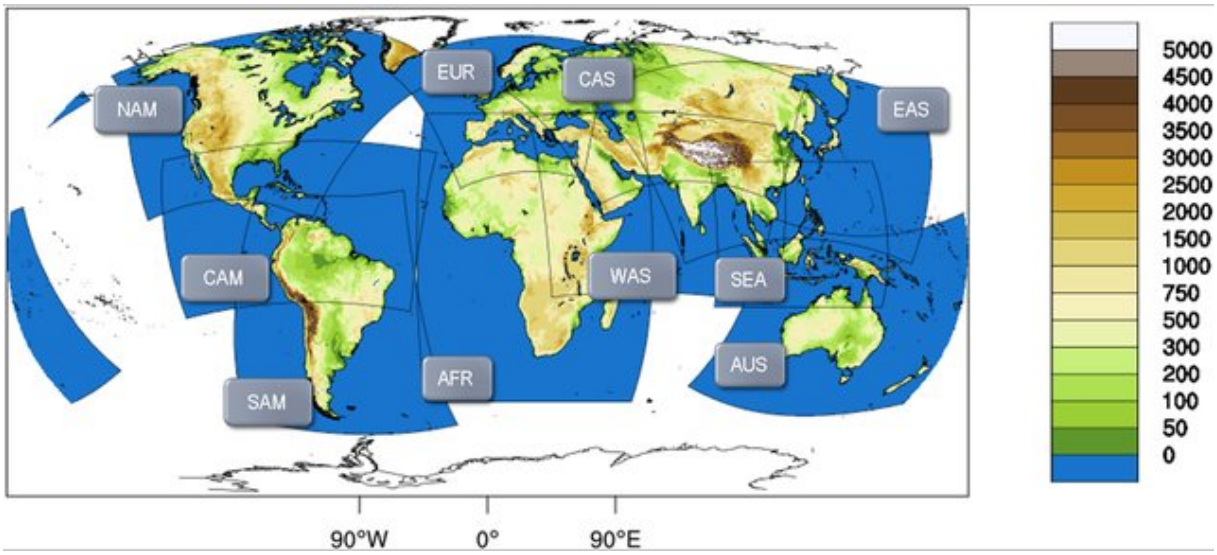

Fonte: Remedio et al. (2019).

A estrutura de projeção climática dentro do CORDEX inclui um grande número de experimentos de previsão decenal, incluindo o ciclo do carbono e experimentos destinados a investigar mecanismos individuais de feedbacks. Além disto, dispõe de simulações baseadas em cenários futuros chamadas vias de concentração representativas (RCPs), ou seja, vias de concentração de GEE ao longo do século XXI, correspondendo os diferentes níveis de estabilização das forçantes radiativas (W/m^2) até o ano 2100 (GIORGI et al.,

2009; OYERINDE, 2018; NIU et al., 2021).

O conjunto de simulações CORDEX foi utilizado sobre a América do Sul com intuito de avaliar a capacidade do CORDEX-SAM em reproduzir as condições climáticas médias do continente. No geral, a média multi-modelos reproduz as principais características climatológicas de verão e inverno. No entanto, as simulações individuais exibiram uma grande dispersão inter-modelos, superestimando a intensidade da precipitação ao longo da Cordilheira dos Andes (FALCO et al., 2020), nas encostas orientais dos Andes (PABÓN-CAICEDO et al., 2020) e subestimando a temperatura do ar em diferentes altitudes das montanhas (PABÓN-CAICEDO et al., 2020). Porém, até o momento, essas simulações são as melhores disponíveis para a América do Sul em termos de resolução espacial e disponibilidade de diferentes conjuntos de GCMs.

2.5 DADOS DE REANÁLISES ERA5

Os dados ERA5 (ECMWF Reanalysis version 5) são a quinta geração de reanálise atmosférica produzida pelo Centro Europeu de Previsões Meteorológicas de Médio Prazo (ECMWF) e mantidos pelo Copernicus Climate Change Service (C3S) (THÉPAUT et al., 2018). Atualmente os dados fornecem estimativas horárias de um grande número de variáveis climáticas a uma resolução espacial de 0,25° (aprox. 30km). Desta forma, abrange um registro detalhado da atmosfera global, superfícies terrestres e ondas oceânicas disponíveis a partir de 1950 (C3S, 2021).

As reanálises atmosféricas suportam uma ampla gama de aplicações abrangendo de avaliações intergovernamentais das mudanças climáticas globais até casos de uso específicos e únicos que exigem representações precisas do clima local. Assim, as reanálises visam fornecer homogeneidade e precisão na representação de variáveis climáticas globais e regionais em escalas de tempo multi-decadais, bem como acurácia na representação de eventos de escala sinótica em resolução temporal sub-diária (BELL et al., 2021).

Nas comparações entre os dados de reanálises e RCMs, o ERA5 produz temperaturas relativamente mais frias no inverno. À medida que a resolução espacial aumenta, o ERA5 intensifica a quantidade de cobertura da neve (WANG et al., 2020) e profundidade da neve (ORSOLINI et al., 2019) em altitudes elevadas na região do Platô Tibetano, provavelmente intensificando o efeito do albedo da neve.

Dados de reanálises ERA-Interim (versão anterior do ERA5) foram usados como referência para validar o desempenho dos GCMs no passado recente (1980 - 2005) para a região dos Andes Subtropicais. O conjunto de dados ERA-Interim representou mal a precipitação do verão, mas forneceu uma representação satisfatória para a precipitação e temperatura do ar no inverno (ZAZULIE et al., 2018).

2.6 SENSOR MODIS

O sensor MODIS (Moderate Resolution Imaging Spectroradiometer) é um instrumento de crucial importância, acoplado aos satélites Terra (conhecido como EOS AM-1) e Aqua (conhecido como EOS PM-1). O Terra MODIS e o Aqua MODIS visualizam toda a superfície da Terra a cada 1 ou 2 dias, adquirindo dados com alta resolução de radiação solar, atmosfera, oceanos e superfície em 36 bandas espectrais. Desta forma, esta ferramenta auxilia na compreensão da dinâmica global, no entendimento de processos climáticos e de mudanças ambientais bem como seus impactos (AGHELPOUR et al., 2020).

O produto MODIS de cobertura de neve diária (MODIS/Terra Snow Cover Daily) fornece dados de cobertura de neve média mensal em uma resolução de 0,05° (aprox. 5 km), sendo muito utilizado para avaliar cobertura de neve regional e mapeamento de albedo. A desvantagem desse método é que o sensor MODIS foi criado no ano de 2000 e, antes disso, não haviam imagens disponíveis para monitoramento da cobertura de neve (FAUSTO et al., 2015).

Os dados do sensor MODIS, em teoria, podem solucionar o problema de falta de dados meteorológicos em altitude elevadas, pois fornece imagens detalhadas, menos turva e parcialmente livre da cobertura de nuvens se comparado a outros sensores ópticos. Isto amplia a gama de aplicações para regiões como a Cordilheira dos Andes. Por exemplo, Delbart et al. (2015) constataram que no período de 2001 a 2014, a tendência decrescente da cobertura de neve durante o inverno explica claramente a tendência decrescente observada na vazão anual de água de quatro rios (Mendoza, Tunuyán, Diamante, Atuel) na região argentina de Cuyo. Já Saavedra et al. (2018) notaram uma perda significativa de cobertura de neve permanente em uma grande área (34.370km^2) entre 29°S e 36°S (Andes Subtropicais) correlacionada com a diminuição da precipitação e o aumento da temperatura.

Utilizando dados de temperatura superfície do terrestre (LST) derivados do sensor MODIS, Qin et al. (2009) examinou os padrões de elevação em todo o Platô Tibetano e encontrou um aquecimento mais forte em torno de 4800 - 6000 m. Já Aguillar-Lome et al. (2019) notaram que as tendências de Tasmax e Tasmin na região dos Andes Tropicais (7°S e 20°S), apresentam padrão de comportamento distintos em função da elevação. No inverno, a Tasmax apresentou uma tendência positiva mais intensa com o aumento da elevação, exibindo um claro sinal de EDW. No entanto, este padrão de aquecimento encontrado na Tasmax, não está presente para a tendência de Tasmin nas altitudes elevadas.

3 ARTIGO - COMPARISON OF ELEVATIONDEPENDENT WARMING AND ITS DRIVERS IN THE TROPICAL AND SUBTROPICAL

Climate Dynamics
https://doi.org/10.1007/s00382-021-06081-4

Comparison of elevation-dependent warming and its drivers in the tropical and subtropical Andes

Osmar Toledo[1] · **Elisa Palazzi**[2,3] · **Iván Mauricio Cely Toro**[1] · **Luca Mortarini**[1,3]

Received: 29 January 2021 / Accepted: 26 November 2021

Abstract
Mountain regions have been recognized to be more sensitive to climate and environmental changes, and in particular to global warming. Several studies report on elevation-dependent warming (EDW), i.e., when warming rates are different in different altitude ranges, particularly focusing on the enhancement of warming rates with elevation. The Andean chain proved to be a relevant climate change hot-spot with positive temperature trends and a widespread glacier retreat over the recent decades. To assess and to better understand elevation dependent warming in this mountain region and to identify its possible dependence on latitude, the Andean Cordillera was split into five domains, three pertaining to the tropical zone and two pertaining to the Subtropics. Further, for each area the eastern and western faces of the mountain range were separately analyzed. An ensemble of regional climate model (RCM) simulations participating in the Coordinated Regional Climate Downscaling Experiment (CORDEX), consisting of one RCM nested into eight different global climate models from the CMIP5 ensemble was considered in this study. EDW was assessed by calculating the temperature difference between the end of the century (2071–2100) and the period 1976–2005 and relating it to the elevation. Future projections refer to the RCP 8.5 high-emission scenario. Possible differences in EDW mechanisms were identified using correlation analyses between temperature changes and all the variables identified as possible EDW drivers. For the maximum temperatures, a positive EDW signal (i.e. enhancement of warming rates with elevation) was identified in each side of both the tropical and subtropical Andes and in all seasons. For the minimum temperatures, on the contrary, while a positive EDW was identified in the Subtropics (particularly evident in the western side of the chain), the Tropics are characterized by a negative EDW throughout the year. Therefore, the tropical boundary marks a transition between discordant EDW behaviours in the minimum temperature. In the Tropics and particularly in the inner Tropics, different EDW drivers were identified for the minimum temperature, whose changes are mostly associated with changes in downward longwave radiation, and for the maximum temperature, whose changes are mainly driven by changes in downward shortwave radiation. This might explain the opposite EDW signal found in the tropical Andes during daytime and nighttime. Changes in albedo are an ubiquitous driver for positive EDW in the Subtropics, for both the minimum and the maximum temperature. Changes in longwave radiation and humidity are also EDW drivers in the Subtropics but with different relevance throughout the seasons and during daytime and nighttime. Also, the western and eastern sides of the Cordillera might be influenced by different EDW drivers.

Keywords Andes · Elevation-dependent warming · Regional temperature trends · Regional climate · Climate models · CORDEX · Projections

✉ Elisa Palazzi
e.palazzi@isac.cnr.it

✉ Luca Mortarini

[1] Universidade Federal de Santa Maria, Santa Maria, RS, Brazil

[2] Dipartimento di Fisica, Università degli Studi di Torino, Via Pietro Giuria 1, 10125 Torino, Italy

[3] Institute of Atmospheric Sciences and Climate – National Research Council, Torino, Italy

1 Introduction

Covering about 25% of the world's land surface and hosting about 12% of the world population, mountains provide a multitude of goods and services to both high-altitude environments and to downstream regions. Water is one of the most precious and critical resources delivered by mountains (e.g. Kohler and Maselli 2009; Price 2015), and about 40% of the world population depends on that water

Published online: 21 December 2021

for drinking purposes, agriculture, hydroelectricity. In the arid and semiarid regions of the Tropics and Subtropics, in particular, mountain regions play a very crucial role since they contain more than 80% of the freshwater made available to the countries around, especially when precipitation is scarce or absent (Viviroli et al. 2007, 2011). For example in the Andean countries, particularly Bolivia and Peru, water supply during the dry season depends on glaciated basins located at high elevations (Vuille et al. 2008).

Mountain regions have been recognized to exhibit enhanced sensitivity to climate and environmental changes, and in particular to global warming, overall showing larger temperature trends (0.3 °C/decade) compared to the globally-averaged trend (0.2 °C/decade, IPCC 2019, and references therein). The widespread glacier retreat observed in most mountain areas of the globe over the last decades is one of the most striking evidences of the temperature increase, though other changes, such as those in precipitation, are also at play (Bradley et al. 2006; Tennant et al. 2014).

The tropical Andes, hosting more than 99% of all the glaciers located in the Tropics (Kaser 1999), are a climate hotspot with increasing temperature trends both at the surface (Nogués-Bravo et al. 2007) and in the atmosphere (Bradley et al. 2006). The literature reports several studies which document the widespread retreat of Andean glaciers over the recent decades (Ceballos et al. 2006; Mark and McKenzie 2007; Seimon et al. 2007; Thompson et al. 2006; Vuille et al. 2008) in conjunction with the observed regional climate change (e.g. Vuille and Bradley 2000; Vuille et al. 2003). Past studies based on observations identified the increase in near-surface air temperature in the tropical Andes as the main driver of the glacier retreat occurred in the second half of the twentieth century. Also, warming was found to be markedly larger in the western side than in the eastern side of the chain (Vuille et al. 2003). According to the analysis performed by Vuille et al. (2008) over about 280 in-situ stations located between 1 °N and 23 °S, a near-surface air temperature increase of 0.68 °C was detected from 1939 to 2008, with a rate of 0.1 °C/decade. Changes in precipitation were found to be less notable and more regionally varying along the chain than the temperature changes (Vuille et al. 2008). Regional climate model (RCM) studies, focusing on projected temperature changes over South America, overall agree in showing a generalized warming trend all over the continent and identifying the Andean region as a climate hot-spot also by the end of the twenty-first century, with projected temperature increases larger than 4 °C (Solman 2013) compared to pre-industrial levels.

One of the main issues facing the research community working on mountain climate change is whether warming rates exhibit a dependence on the elevation and in particular if they are enhanced at higher elevations compared to lower-elevation counterparts. This would have several implications for the high-altitude cryosphere, mountain ecosystems, biodiversity and ultimately for the human societies which depend on the services delivered by mountains. Several global and regional studies report on elevation-dependent warming (EDW), i.e., whether warming rates are different in different altitude ranges (e.g., Palazzi et al. 2019; Pepin et al. 2015). The majority of them, analysing either observations or model simulations, point toward an amplification of warming rates with elevation (i.e. a positive EDW), but many uncertainties remain, including the strength of EDW, its dependence on the specific mountain region, and its drivers. On the one hand, these uncertainties are related to the difficulty of measuring EDW, because of the sparseness or even the lack of in-situ stations up to the highest elevations providing long-term temperature timeseries. On the other hand, uncertainties are inherent in numerical simulations with climate models with limited spatial resolution when applied in mountain environments and whose parameterizations of sub-grid processes are imperfect (Minder et al. 2018; Pepin et al. 2015). Most studies aiming at better understanding and disentangling the mechanisms leading to EDW have been based on climate models rather than on observations (Palazzi et al. 2017, 2019; Rangwala and Miller 2012) since the output of numerical models is spatially and temporally continuous and contains all the key variables that provide, at least in principle, a complete picture of the possible EDW drivers and of their mutual relationships. In studies analysing mid-latitude mountains, EDW has been frequently attributed to elevation-dependent changes in albedo (associated with, but not exclusively to, changes in snow cover), in downward longwave radiation and in specific humidity (e.g. Minder et al. 2018; Palazzi et al. 2017, 2019; Rangwala et al. 2016). However, the majority of those studies also concurs in recognizing that other mechanisms are at play which are currently not (or not sufficiently well) implemented in the models (e.g. Pepin et al. 2015).

Compared to the studies focused on the northern hemisphere mid-latitude mountains, EDW in the Andes and especially in the tropical Andes has not been extensively studied. Recently, analysing satellite Land Surface Temperature (LST) trends in the period 2000–2017 in winter and their dependence on elevation in the Andean region between 7 and 20 °S, Aguilar-Lome et al. (2019) found different behaviours in daytime and nighttime LST trends as a function of elevation. While the daytime winter LST showed a strong positive trend with elevation, the same warming pattern was not found in the nighttime LST. Among the first studies analysing future climate changes in the tropical Andes (10 °N–27 °S) is the paper by Urrutia and Vuille (2009) who used a regional climate model (RCM) based on two different emission scenarios (A2 and B2, belonging to the family of scenarios that preceded the Representative Concentration Pathways, RCPs, employed in the fifth IPCC assessment

report) to show a significant warming in the area, enhanced at higher elevations and further amplified in the middle and upper troposphere. For the subtropical Andes (from 30 to 37 °S), the model study by Zazulie et al. (2018) analysed future climate projections using five GCMs under the RCP 4.5 and RCP 8.5 greenhouse gas concentration scenarios (Riahi et al. 2011; Thomson et al. 2011), identifying an expected warming of 5 °C in winter at the highest elevations by 2075–2100 compared to the period 1980–2005. The authors also found a reduction in albedo by 20–60% at high elevations, which was identified as one key EDW driver.

The present paper focuses on future projections of warming rates in the southern hemisphere tropical and subtropical Andes, and in particular on the existence and driving mechanisms of EDW, highlighting possible differences as a function of the latitude, the season, the considered variable (either the minimum or the maximum temperature) and the side of the Andean Cordillera, i.e. considering its western and eastern slopes separately. Results for the end of the twenty-first century (2071–2100) are presented and compared to a historical model climatology (evaluated over the period 1976–2005) using simulations performed with one regional climate model (the RCA4 RCM, Samuelsson et al. 2011) nested into eight global model simulations whose projections are based on the RCP 8.5 greenhouse gas concentration scenario (Moss et al. 2010).

The paper is structured as follows: Sect. 2 introduces the area of study, the employed data and the methods used for their analysis; Sect. 3 presents the results on EDW, its existence and spatial variability, and considerations about its driving mechanisms; Sect. 4 discusses and concludes the paper.

2 Study area, data and methods

2.1 Climatic characteristics of the study areas

The Andean mountain chain is a relatively narrow mountain range extending all along the western coast of South America, encompassing tropical and extra-tropical latitudes which exposes it to diverse climatic conditions. North of 30 °S, relatively cold and arid conditions prevail along the western slopes of the Andes, while the Andean eastern slopes are comparatively moister, warmer, and prone to higher precipitation (Garreaud 2009; Rangwala and Miller 2012; Solman 2013). This pattern reverses south of 30 °S where precipitation mainly occurs on the western side (owing to the influence of westerly winds) while the eastern slopes are characterized by semiarid conditions (Garreaud 2009). The seasonal shift of the inter tropical convergence zone (ITCZ) controls climate conditions over the tropical part of the Cordillera.

In terms of large-scale upper-level circulation, the tropical Andes between north of the equator and 15 °S are prone to mild easterly winds while the subtropical and extra-tropical portions of the chain are subject to westerly winds. In DJF (austral summer), the easterly winds extend beyond 15 °S and the Amazon deep convection favors the establishment of the upper level Bolivian High (Lenters and Cook 1997), one of the most prominent features of the summertime circulation in the Andes. The summertime subtropical westerly jet displaces southwards and becomes less intense. In JJA (austral winter) the easterly winds do not cross 10 °S latitude and the subtropical westerly jet has its maximum around 30 °S. Low-level circulation is rather complex and extremely important since it controls the transport of humidity and, thus, the precipitation patterns. Between about 10 °S and 35 °S low-level winds mostly flow from the south along the western Pacific coast and from the north along the eastern Andes slopes.

The present study considers the tropical and subtropical parts of the Andes Cordillera, between 0 and 37 °S latitude and 64 °W and 80 °W longitude. The domain study was divided into five sub-regions depicted as coloured boxes in Fig. 1 where they are sketched above two orography maps. One (panel a) is derived from the land elevation data provided by the NASA Shuttle Radar Topographic Mission (SRTM, Farr et al. 2007), while the other (panel b) is the orography used in the CORDEX regional climate model simulations employed in this study (see Sect. 2.2).

2.2 Model data

We considered an ensemble of model simulations obtained with the Rossby Centre Atmospheric regional model (RCA4, Samuelsson et al. 2011) nested into eight different global climate models - CanESM2, CSIRO-Mk3-6-0, EC-EARTH, CM5A-MR, MIROC5, HadGEM2-ES, MPI-ESM-LR, and GFDL-ESM2M from the Climate Model Intercomparison Project phase 5 (CMIP5) ensemble, whose spatial resolution and a key reference are summarised in Table 1. The RCA4 simulations are part of the Coordinated Regional Climate Downscaling Experiment (Giorgi et al. 2009)—South American domain (CORDEX-SAM) and have a spatial resolution of 0.44 degrees latitude–longitude (approx. 50 km). To date and to our knowledge, these simulations are the best available for South America in terms of spatial resolution and availability of different ensemble members. The results discussed in the paper refer to the the Representative Concentration Pathway emission scenario RCP 8.5 corresponding to an anthropogenic radiative forcing of 8.5 Wm^{-2} by the end of the twenty-first century (Chou et al. 2014; Riahi et al. 2011). It is worth pointing out that all the analyses were repeated for the less extreme emission scenario RCP 4.5, pointing to a stabilization of the CO_2 concentrations by the end of the century, showing no differences in the spatial pattern of the

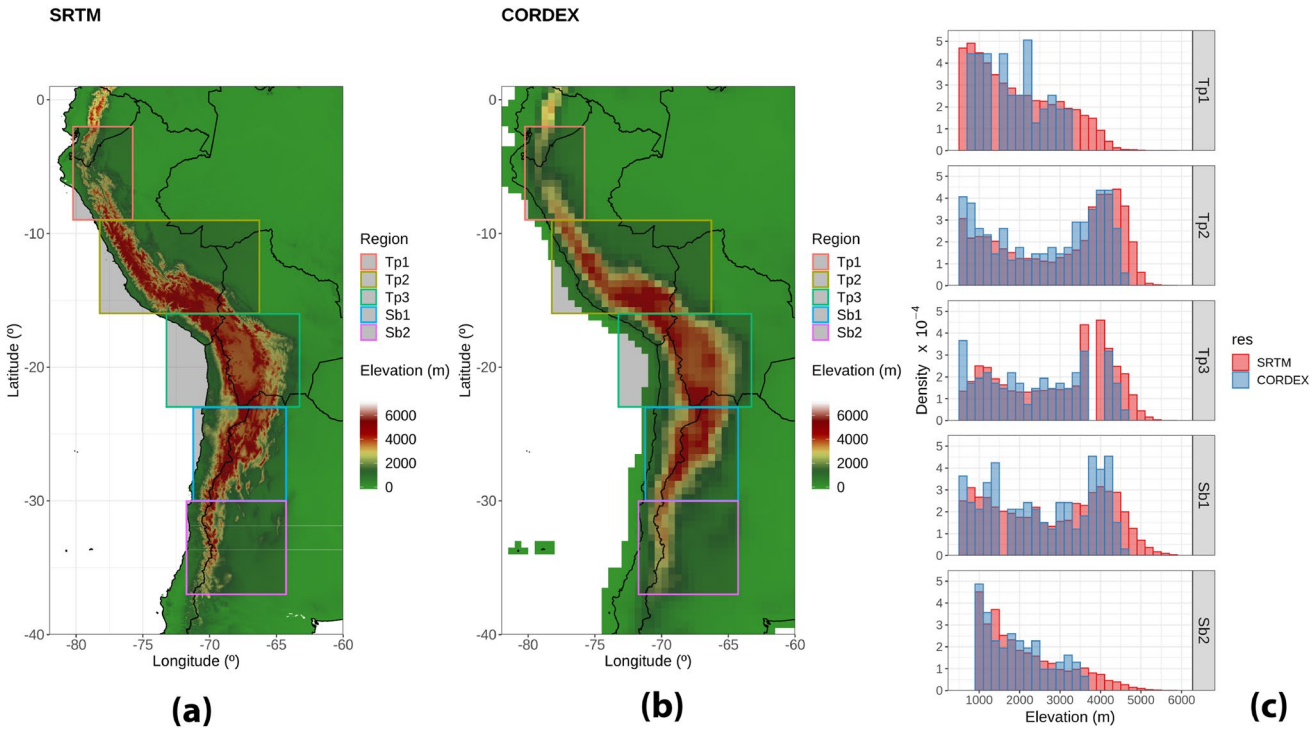

Fig. 1 **a** and **b** Topographic map of the Andean Cordillera from (**a**) land elevation data provided by the NASA Shuttle Radar Topographic Mission (SRTM) with a resolution of 3 arc second (approximately 90 m, Farr et al. 2007) and **b** from CORDEX models (0.44° longitude-latitude resolution). The tropical (Tp1, Tp2, Tp3) and subtropical (Sb1, Sb2) study areas are delimited by coloured boxes. **c** Fraction of grid cells in each 200m-thick elevational bin across the five study areas for the SRTM (red) and the CORDEX (cyan) data, only grid cells with elevation above 500 m were considered

Table 1 Characteristics of the eight GCMs driving the RCA4 RCM in this study

GCM name	Institution	Resolution lon x lat°Lev	Key reference
CanESM2	CCCMA	2.8125 × 2.8125L35	Arora et al. (2011)
CSIRO-Mk3-6-0	CSIRO-QCCCE	1.875 × 1.875L18 (T63)	Rotstayn et al. (2012)
EC-Earth	EC-EARTH	1.125 × 1.125L62 (T159)	Hazeleger et al. (2012)
CM5A-MR	IPSL	1.25 × 2.5L39	Dufresne et al. (2013)
MIROC5	MIROC	1.40625 × 1.40625L40 (T85)	Watanabe et al. (2010)
HadGEM2-ES	MOHC	1.25 × 1.875L38 (N96)	Bellouin et al. (2011)
MPI-ESM-LR	MPI-M	1.875 × 1.875L47 (T63)	Giorgetta et al. (2013)
GFDL-ESM2M	GFDL	2.5 × 2L24(M45)	Delworth et al. (2006)

seasonal temperature changes but just in the magnitude of the changes (which are strongest in the most extreme RCP 8.5 scenario). The projection period taken into account is 2071–2100 and it is compared to historical simulations in the period 1976–2005.

Figure 1c shows the density of grid points in each 200 m-thick elevation bin for the CORDEX RCM simulations (~ 50 km resolution) compared to the density distribution for high-resolution (~ 90 m) land elevation data, for the five study areas. With the exception of the highest elevations, the shape of the modeled elevation density distribution quite well reproduces the land elevation data distribution in Tp2, Tp3 and Sb1, and to a lesser extent in Sb2. The modeled elevation distribution in Tp1 is, instead, in less agreement with the observations, both in the representation of the lowest and highest elevations and in correctly simulating the shape of the distribution overall. As expected, the highest altitudes (above ~ 3300 m for Tp1; above ~ 4700 m for Tp2, Tp3 and Sb1; above ~ 3700 m for Sb2) are not reproduced in the RCM grid. It is worth stressing that the smoothing of higher altitudes due to the model grid resolution could potentially compromise the assessment of EDW and its drivers, especially those related to changes in snow cover and related feedbacks. To assess the capability of the CORDEX

models in reproducing a reasonable snow cover distribution, which is also coherent with the topography of the area, we evaluated the snow cover area in the models, limited to the multi-model mean, against the state-of-the-art Moderate Resolution Imaging Spectroradiometer (MODIS) satellite data. We used MODIS/Terra Snow Cover Monthly L3 Global 0.05Deg CMG Version 6 data, providing monthly averaged snow cover in 0.05 degree (approx. 5 km) resolution Climate Modeling Grid (CMG) cells. Monthly averages are computed from daily snow cover observations in the MODIS/Terra Snow Cover Daily L3 Global 0.05Deg CMG (MOD10C1) dataset. MODIS data were downloaded from https://nsidc.org/data/MOD10CM/versions/6. We performed the comparison on a seasonal basis by analysing the snow cover climatology over the period 2000–2020. Data from the CORDEX models have been averaged over that period through an extension of the historical runs ending in December 2005 using the RCP 4.5 scenario data. Results of this comparison are shown in Figs. S1–S3 of the Supplementary Information. Figures S1 and S2 show the climatological seasonal maps of the snow cover fraction in the period 2000–2020 for CORDEX and MODIS, respectively. The latter are in agreement with those shown in the study by Saavedra et al. (2018), who analysed the changes in Andes snow cover in the period 2000–2016 using the binary 8-days product from MODIS (MOD10A2). The only remarkable difference with Saavedra et al. (2018) are the high snow fraction values which we found around 20 °S latitude, which we did not found to be associated with the longer time period considered in our study. The seasonal snow fraction anomaly (CORDEX–MODIS) in Fig. S3 shows that the largest differences between the model mean and the satellite data are seen in the two subtropical areas (Sb1 and Sb2) along the Chile-Argentina border in JJA and SON, where CORDEX models overestimate snow cover from observations. Noteworthy, in the tropical areas (Tp1, Tp2 and Tp3) the measured and modelled data show a particularly good agreement. However, a well defined area is identified in Tp3 where the models underestimate the MODIS observations, in southwestern Bolivia near the border with Chile, around 20 °S. As mentioned above, this is related to the high snow fraction data observed in MODIS.

2.3 Methods

In order to assess and quantify EDW in the five study areas, the difference (or change) between the average in the period 2071–2100 (projection period) and the average in the period 1976–2005 (historical period) of the minimum (tasmin) and maximum (tasmax) surface air temperature was calculated and, then, fitted against elevation using, first, a linear regression model. This calculation was performed for each GCM–RCM pair of the model ensemble as well as for the multi-model mean. When not differently specified, the results of the present work mainly refer to the multi-model ensemble mean, the single GCM-RCM pairs being used to discuss the robustness of the results across the ensemble. A seasonal based analysis using the standard definition of seasons for the Southern Hemisphere has been performed: winter (June to August, JJA), autumn (March to May, MAM), summer (December to February, DJF), and spring (September to November, SON). Minimum and maximum temperatures were separately analyzed because they can exhibit different EDW signals owing to the mechanisms at play during nighttime and daytime. Due to the different climates of the western and eastern sides of the Cordillera, the two sides are analyzed separately. With eastern and western sides we refer to grid points respectively to the East and to the West of the highest grid point at each latitude. Similarly to other studies focused on different areas (e.g. Giorgi et al. 2014; Palazzi et al. 2019), in this study to reduce some of the influence of the coastal areas, only grid cells with elevation above 500 m a.s.l. were kept in the analysis.

The slope of the linear regression between warming rates and elevation along with its statistical significance provides a measure of the sign and strength of EDW. A positive slope identifies a positive EDW (i.e., the warming rates increase with elevation), while a negative slope identifies situations in which warming rates decrease as the elevation increases (negative EDW). The statistical significance of the linear regression slope is assessed following Bendat and Piersol (2000), as briefly summarized in the following. Given the random variable $w = \frac{1}{2} ln\left(\frac{1+\rho}{1-\rho}\right)$, where ρ is the theoretical covariance of the two variables (the temperature change and the elevation in our case), having a Gaussian distribution with mean $\mu = \frac{1}{2} ln\left(\frac{1+r}{1-r}\right)$ and variance $\sigma^2 = \frac{1}{N-3}$, where r is the empirical correlation of the two variables and N is the number of observations, at a confidence level of 0.05 the null hypothesis of no correlation between the two variables can be rejected if (Bendat and Piersol 2000):

$$\left| \frac{\sqrt{N-3}}{2} ln\left(\frac{1+r}{1-r}\right) \right| > 1.96 \quad (1)$$

The linear regression model allows a description of the general behaviour of the relationship between warming rates and the elevation. However, it is also known from previous studies that linearity can oversimplify the real EDW pattern, which might be better represented by more than a unique slope (e.g. Palazzi et al. 2019; Vuille et al. 2003; You et al. 2010). Therefore, using the same approach as in Palazzi et al. (2019) we investigated possible departures from linearity with a LOcal regrESSion (LOESS) method. Then,

the altitudes where the EDW signal changes its slope were identified with a piecewise linear regression. The piecewise regression model estimates the slope shift in the temperature change series fitting two altitude segments across a breakpoint, z_α (Toms and Lesperance 2003), as follows:

$$\Delta T_i = \begin{cases} \beta_0 + \beta_1 z_i + \epsilon_i & \text{if } z_i \leq z_\alpha \\ \beta_0 + \beta_1 z_i + \beta_2 (z_i - \alpha) + \epsilon_i & \text{if } z_i > z_\alpha \end{cases}$$

where the index i varies between 1 and the total number of points in the model grid, z_i represents the vector of elevations and ΔT_i the vector of the temperature change (either minimum or maximum temperature change), ϵ_i are the fit residuals (considered as independent and identically distributed random errors with zero mean and finite variance). z_α represents the breakpoint, i.e. the altitude at which the regression line changes the slope. β_0, β_1 and β_2 are the regression coefficients: β_0 is the intercept, β_1 is the slope value before the breakpoint and $\beta_1 + \beta_2$ is the slope after the breakpoint, so that β_2 can be interpreted as the difference in the two slopes, before and after the breakpoint. The model parameters β_0, β_1, and β_2 were estimated choosing the breakpoint, z_α, that minimizes the residual sum of squares (Chiu et al. 2006). This piecewise fitting procedure assumes one single breakpoint and forces continuity at it (Toms and Lesperance 2003).

In the literature, EDW has been linked to several mechanisms (Pepin et al. 2015): snow-albedo feedback, changes in vegetation and the tree line, changes in cloud cover and properties, processes associated with moisture and radiative fluxes, changes in atmospheric loading and properties of aerosol particles. To evaluate their possible contribution to EDW, following Rangwala and Miller (2012) and Rangwala et al. (2013, 2016) we considered as drivers the model variables whose changes mostly influence the energy balance at the surface, leading to temperature changes, i.e. albedo, surface downwelling longwave and shortwave radiation (*rlds*, *rsds*), and near-surface specific humidity (*huss*). For each season, the absolute change between the average in the projection period and the average in the historical period for each driver mentioned above ($\Delta albedo$, $\Delta rlds$, $\Delta rsds$, and $\Delta huss$) was calculated. Besides considering the absolute changes of *rlds*, *rsds*, and *huss*, we also took into account their relative changes ($\Delta rlds/rlds_0$, $\Delta rsds/rsds_0$, and $\Delta huss/huss_0$), i.e. the change of each variable relative to an average climatology, since previous studies have shown that they can be more effective, at least in the mid-latitude mountains, in determining elevation-dependent warming signals (Palazzi et al. 2017, 2019; Rangwala et al. 2013, 2016). In this study we focused on the tropical and subtropical Andes and both absolute and normalized changes were considered to assess the relative role of the EDW drivers and to highlight possible differences with the more explored mid-latitude mountain regions.

In order for the simulated $\Delta albedo$, $\Delta rlds$, $\Delta rsds$, $\Delta huss$, $\Delta rlds/rlds_0$, $\Delta rsds/rsds_0$, and $\Delta huss/huss_0$ to be considered as evidence of EDW mechanisms, some conditions need to be satisfied. First, the drivers have to exhibit a dependence on the elevation that is physically consistent with the EDW sign. In other words, all the drivers but $\Delta albedo$ must increase with height if EDW (in either the minimum temperature or the maximum temperature) is positive, and decrease with height if EDW is negative. Since $\Delta albedo$ has an opposite effect on the temperature change (i.e. decreases in albedo lead to temperature increases), for clarity in presenting the results, $-\Delta albedo$ was used in the analysis. Second, the drivers and the temperature changes must exhibit a positive spatial correlation even when they are altitude-detrended, i.e., when their dependence on the elevation is removed. The reader is referred to Palazzi et al. (2017, 2019) for further details on this methodology.

3 Results

Before discussing the specific results on EDW following the methodology described in Sect. 2.3, we present a comparison between the model climatology and an observation-based reference climatology over a common historical period. To this aim, we considered the recent ERA5 global reanalysis dataset (Hersbach et al. 2020) and used the reference period 1979–2005 to evaluate the historical model data against ERA5.

We first compared the annual cycle climatology of both the minimum and the maximum temperature and we show the results in Figs. 2 and 3, respectively. ERA5 data are shown in red while the model results are in black (multi-model mean of the GCM-RCM ensemble) and in grey (individual GCM-RCM pairs). The mean annual cycle is calculated over the period 1979–2005 in the five study areas considered in this study (columns in the figures) and for the East and West sides of the mountain range (rows). It is interesting to observe that the models (both individual realizations and their mean) exhibit a cold bias compared to ERA5 when the minimum temperature is taken into account (Fig. 2). Instead, the models either overestimate or underestimate ERA5 when the maximum temperature is analysed (Fig. 3), but the difference between model data and the reanalysis is considerably lower than for the minimum temperature. The study by Urrutia and Vuille (2009) also showed a cold bias exhibited by one RCM over the southern Andes (compared to CRU observations) related to the excess precipitation simulated by the model, which reduces incoming solar radiation and lowers air temperature, particularly over

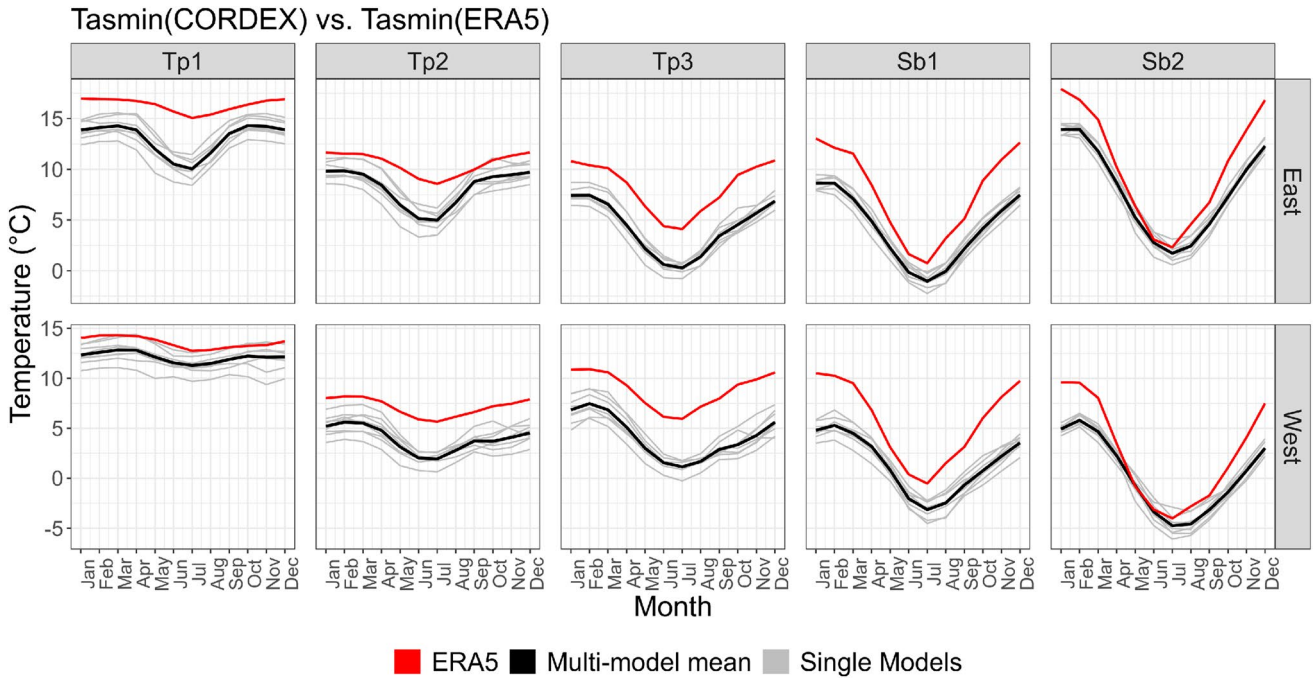

Fig. 2 Model ensemble representation (in black the multi-model mean, in grey the individual GCM-RCM pairs) of the minimum temperature mean annual cycle evaluated over the period 1979–2005, against the ERA5 climatology (red). The five analysed areas are shown in the columns, while the two sides of the Cordillera in the rows

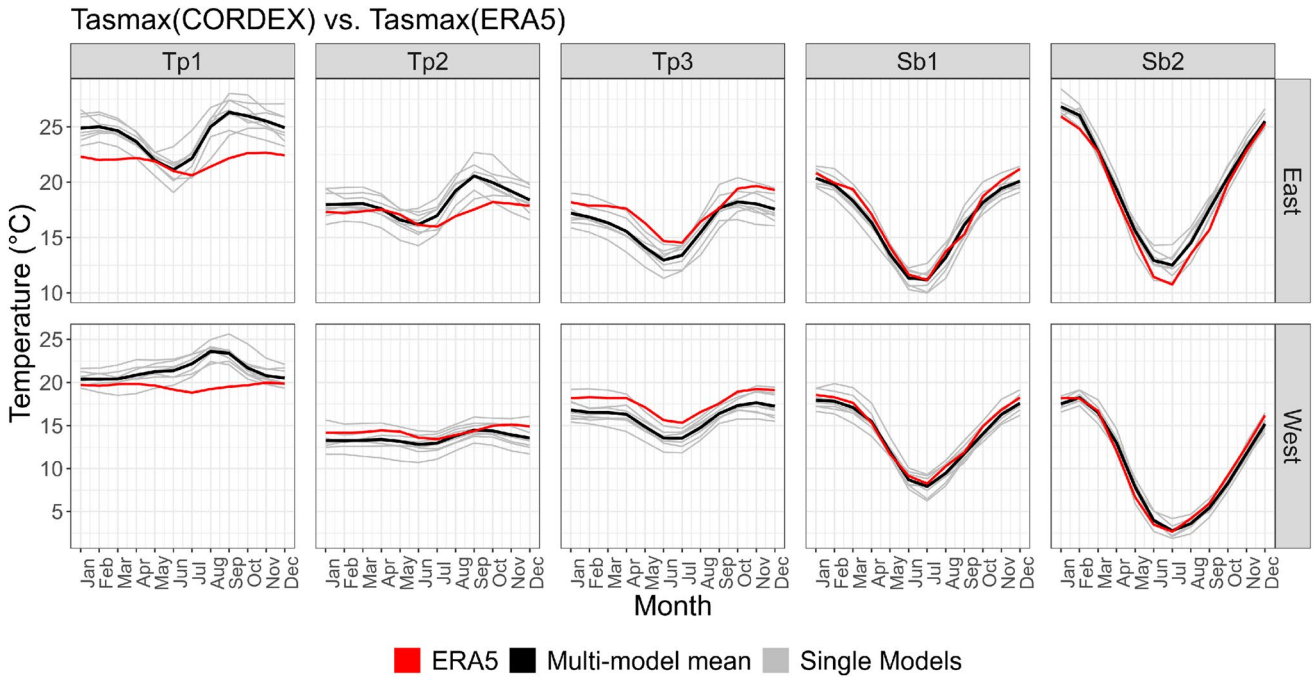

Fig. 3 The same as Fig. 2 but for the maximum temperature

the eastern Andean slope. Similar findings were discussed in other studies (e.g. Fernandez et al. 2006) using regional climate models. Table S1 of the Supplementary Information shows the numerical values of the biases (CORDEX–ERA5), at the seasonal and annual basis, for the minimum and the maximum temperature and the two

sides of the Cordillera. Tp3 and Sb1 show the largest minimum temperature bias, larger for the western than for the eastern side of the Cordillera; for the maximum temperature, Tp1 shows the largest CORDEX–ERA5 discrepancy (see Table S1). It is interesting to note that, for the minimum temperature, the magnitude of the bias is higher than the magnitude of the temperature perturbation in the RCP8.5 scenario (i.e., the change of the minimum temperature between the average in the period 2071–2100 and the average in the period 1976–2005), while it is lower for the maximum temperature. This comparison is shown in Table S2 of the Supplementary Information. Nevertheless and regardless of the temperature bias magnitude, the models reproduce roughly well the shape of temperature annual cycle, overall. For the minimum temperature in east facing Tp1 and Tp2, however, the amplitude of the annual cycle appears overestimated. This could indicate excess model sensitivity to climatic drivers which decrease during the austral winter, maybe humidity-driven downward longwave radiation. For the maximum temperature in east facing Tp1 and Tp2 the CORDEX simulations produce an annual temperature maximum in September and relatively warm conditions in August which are not seen in ERA5, which could again be indicative of an enhanced model sensitivity to a specific climate driver. The maximum temperature annual cycle for west facing Tp1 is not correctly simulated by the models compared to ERA5, as both the annual maxima and minima occur in the wrong points of the annual cycle. For completeness, a further evaluation of the model skills is presented in Figs. S4 and S5 (and in Table S3) of the Supplementary Information showing the time series (and the trends) of the minimum and maximum temperature in the models and in ERA5 for the five study areas and the two sides of the Cordillera. As for the model bias, similar considerations as for the climatological annual cycle apply in this case. In addition, Table S4 of the Supplementary Information compares the interannual variability of the minimum and maximum temperature time series in ERA5 and in the model ensemble. The interannual variability is calculated as the standard deviation of the detrended time series shown in Figures S4 and S5 of the Supplementary Information. For most of the seasons, sub-regions and sides of the Cordillera the interannual variability in ERA5 is within the range of variability displayed by the GCM-RCM pairs.

As stated in Sect. 2.3, the EDW assessment is based on the analysis of the temperature difference between two climates (and its relationship with the elevation). For this, the bias of the models against ERA5 has a negligible impact on the results, because we analysed the temperature differences between the end of the twenty-first century and the historical climatology, so any bias is removed.

3.1 Elevation-dependent warming assessment

Elevation-dependent warming is assessed by exploring the dependence of the minimum and of the maximum temperature change (*Δtasmin* and *Δtasmax* respectively) on elevation for each area in the tropical and in the subtropical Andes and for each season. We recall that the change is calculated as the difference between the 2071–2100 climatology (evaluated under the RCP 8.5 scenario) and the 1976–2005 climatology. For completeness, the spatial maps of *Δtasmin* and *Δtasmax* in the five study areas obtained from the multi-model mean of the GCM-RCM ensemble are shown in Figures S6 and S7 in the Supplementary Information. Both variables are expected to undergo a pronounced warming in the future with respect to the past; however, the maps highlight different EDW patterns between the minimum and the maximum temperature, further the warming is not homogeneous throughout the latitude range. For example, in the tropical areas *Δtasmin* is higher at lower elevations, at variance with the situation encountered in the subtropical areas (see Figure S6). This and other characteristics of a possible differential warming with elevation, i.e. of the EDW, in the five study areas are discussed in detail in the following analysis.

Figures 4 and 5 show the scatter plot between the elevation and, respectively, *Δtasmin* and *Δtasmax*. Two different colors are used to highlight the western (blue) and eastern (red) sides of the mountain range. For each of the five study areas and for each season three different regression lines are displayed to assess the dependence of the temperature changes on elevation (see Sect. 2.3 for details): a linear regression (dark blue and dark red for the eastern and western sides respectively), a LOESS fitting curve (light blue and orange for the eastern and western sides respectively) and a piecewise regression (lavender and red for the eastern and western sides respectively). The LOESS regression lines in Figs. 4 and 5 suggest that, in some cases, a nonlinear fitting able to capture the possible complex pattern of EDW may be more appropriate than a linear relationship. It can be noticed that in quite a few cases the LOESS (light blue and orange) and piecewise (lavender and red) regression lines overlap quite well throughout the whole elevation range, indicating that splitting the altitude domain into two segments and fitting with two separate lines could more properly describe the relationship between warming rates and elevation than a single linear regression line (dark blue and dark red). To better assess the robustness of a piecewise EDW behaviour across the entire model ensemble, Figures S8 and S9 of the Supplementary Information depict the piecewise regression lines for all individual GCM-RCM pairs (colored lines) and for their mean (black lines) for *Δtasmin* and *Δtasmax*, respectively. In those figures the two sides of the Cordillera are depicted with different line types (continuous for

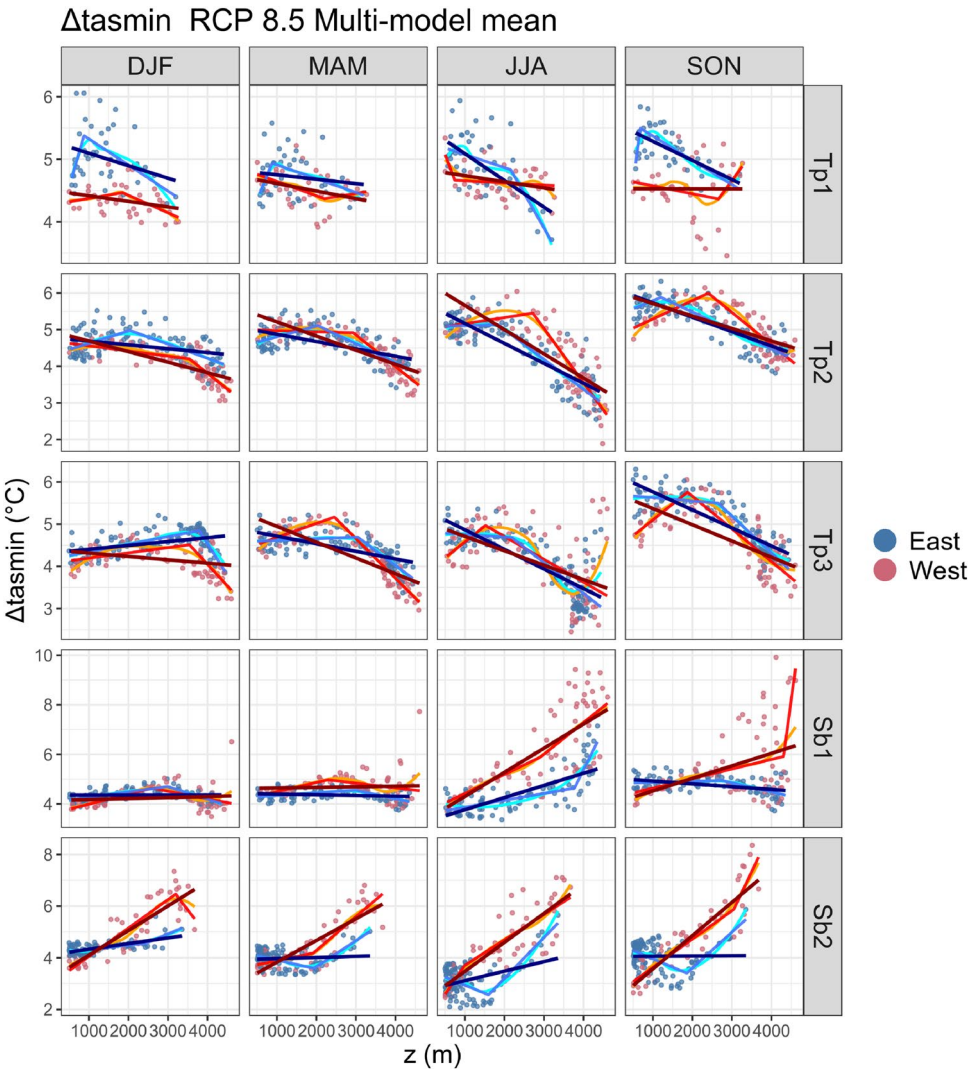

Fig. 4 Scatterplots of the seasonal minimum temperature changes versus altitude for the multi-model mean in the five study areas and in the RCP 8.5 scenario. The dark blue and dark red lines represent the linear regression model for the eastern and western sides of the Cordillera, respectively, the light blue (eastern side) and orange (western side) lines represent the LOESS fit and the piecewise regression is shown in lavender (eastern side) and red (western side). Point data referring to the eastern (western) side of the mountain range are colored in blue (red)

the western side and dashed for the eastern side) and they will be used in the discussion of the following EDW analysis. In particular, these plots highlight how each different GCM-RCM identifies the breakpoints and the slopes of the piecewise regression in the different seasons, areas and sides of the Andean Cordillera.

The minimum temperature in the Tropics (Tp1, Tp2, Tp3 in Fig. 4) shows no evidence of increased warming with elevation, i.e. of positive EDW, while the two subtropical areas show an opposite behaviour characterized by positive elevational gradients of warming rates, overall. These considerations apply to both eastern and western sides of the Andean Cordillera. Nonetheless, the two sides can exhibit different warming rates. This is particularly evident in Tp1 and in the two subtropical domains, in all seasons: in Tp1 the warming is larger in the eastern side (blue) while in the subtropics the western part exhibits amplified warming. This further justifies splitting the analysis in the two sides of the Cordillera. In Tp2 and Tp3 a smaller spread in the data is present and a different warming in the two sides of the Cordillera is not clearly detectable.

Figure 4 shows that, for both the eastern and western sides of the chain, the piecewise regression (lavender and red lines) almost overlaps with the LOESS curve (light blue and orange lines) in all cases but one (Tp3 in JJA). The different slopes of the two fitting lines (piecewise regression line) mark a breakpoint, i.e. an elevation where the EDW behaviour changes. In most of the seasons, areas, and sides of the Cordillera, the change in the EDW slope is remarkable. The position of the breakpoint depends on the season, on the latitude and on the side of the Cordillera. In Fig. S8 of the Supplementary Information we compare the position of the breakpoint in all GCM-RCM pairs. Though in some cases the models do not agree with each other, the model ensemble is mostly coherent in providing a robust estimate of the breakpoint height.

Unlike for the minimum temperature, the maximum temperature change (Fig. 5) is overall positively correlated

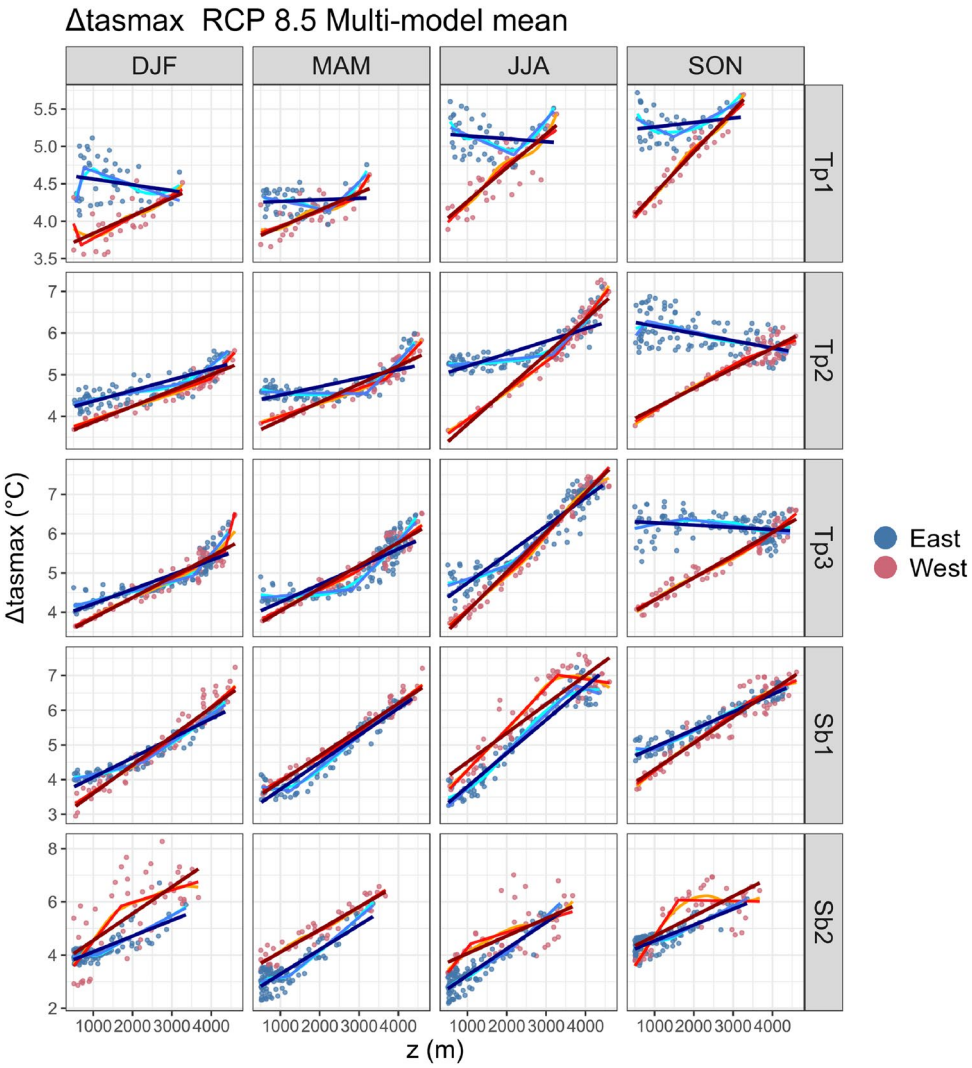

Fig. 5 The same as Fig. 4, but for the maximum temperature change

with the elevation. A distinction between the EDW behaviour found in the western and eastern sides of the mountain range is evident. This is particularly emphasised in the tropical areas where, at lower altitudes, larger temperature changes in the eastern side (blue points) than in the western side (red points) are observed. Overall, the eastern side is characterized by a twofold EDW behavior (light blue piecewise regression line). In Tp1 a negative EDW at lower altitudes is followed by a positive one at higher altitudes. In Tp2 and Tp3 a slightly positive EDW at lower altitudes and a more positive one above are found in DJF, MAM and JJA; in SON EDW is negative throughout the whole elevation range. In Tp1, Tp2 and Tp3 the western side behaves similarly throughout the seasons, showing a linear increase of *Δtasmax* with elevation. In DJF, MAM, and JJA, the height where the EDW signal changes its slope in the eastern side, also marks the height where the relationship between *Δtasmax* and the elevation is the same in the eastern and western sides of the mountain range. In SON, the eastern and western sides present similar *Δtasmax* values only at the highest elevations. In the Tropics, SON in the season with the most pronounced difference between the eastern and western warming.

In the two subtropical areas, the difference between the two sides of the mountain chain is less evident than for the three tropical areas but still existent. In Sb1 the relationship between *Δtasmax* and the elevation is overall well described by a linear regression, especially in the western side and with the exception of JJA. In Sb2, the warming pattern is reversed with respect to the Tropics, being characterised by an amplified warming in the western part. Here, a twofold behavior with a steeper slope at the lower altitudes is found in DJF, JJA and SON. Figure S9 of the Supplementary Information, depicting the piecewise regression lines for the individual GCM-RCM pairs of the model ensemble, shows that where the EDW slope before and after the breakpoint markedly changes in the multi-model mean (see Fig. 5), the agreement between the

individual GCM-RCM pairs is high in both the slopes and the breakpoint elevation.

Though the relationship between warming rates and elevation can deviate from linearity as discussed above, in the literature the strength of EDW is commonly quantified considering the slope of the linear regression over the whole elevation range. Besides, using a unique slope, rather than two slopes and a breakpoint altitude, enables a straightforward comparison among subdomains, seasons and sides of the Cordillera. Figure 6 summarizes the linear regression slopes for *Δtasmin* and *Δtasmax* in all the seasons, for all the five areas and for all GCM-RCM model pairs (colored symbols) as well as the multi-model mean (black symbol) in the RCP 8.5 scenario. In this figure the different sides of the mountain range are also depicted (West is indicated with the square red symbol while East with a blue triangle). The solid line connects, for each side of the Cordillera, the multi-model mean point of the five areas.

The upper panels referring to the minimum temperature confirm the distinct EDW behaviour between the tropical and subtropical regions. In the western mountain side (red points) the EDW is negative in the three tropical areas and positive in the subtropics. In DJF and MAM, in particular, Sb1 behaves like a transition region between the negative EDW in Tp1, Tp2, and Tp3 and the positive EDW in Sb2. In the eastern side, a less uniform behaviour is found throughout the seasons though, overall, EDW is negative in the tropics (with the exception of Tp3 in DJF) and positive (or neutral in Sb1) in the subtropics with the exception of SON. The two subtropical areas overall exhibit a larger inter-model spread compared to the tropical areas.

For the maximum temperature (lower panels), the slopes are overall positive in all seasons, for all areas and almost all individual model members. The slopes are larger in the western side than in the eastern side, except for Sb1 and Sb2 in MAM and JJA. The EDW slope gradually increases with latitude in all cases except in JJA for the western side, in which EDW increases (decreases) from lower to higher latitudes in the tropics (subtropics), and in SON for the eastern side, where EDW is constant and almost neutral in the three tropical areas while positive in the subtropics.

The different EDW sign found for the minimum and the maximum temperature in the Tropics is a quite robust feature across the whole model ensemble. Remarkably, to our knowledge, the contrasting behaviour between nighttime and daytime EDW—with minimum temperatures displaying negative slopes and maximum temperatures displaying positive slopes—differs from the behaviour most commonly observed in other mountain areas in the mid-latitudes such as the Tibetan Plateau-Himalayas (e.g., Palazzi et al. 2017) where the minimum and the maximum temperatures display a coherent EDW signal (same sign, positive) and the

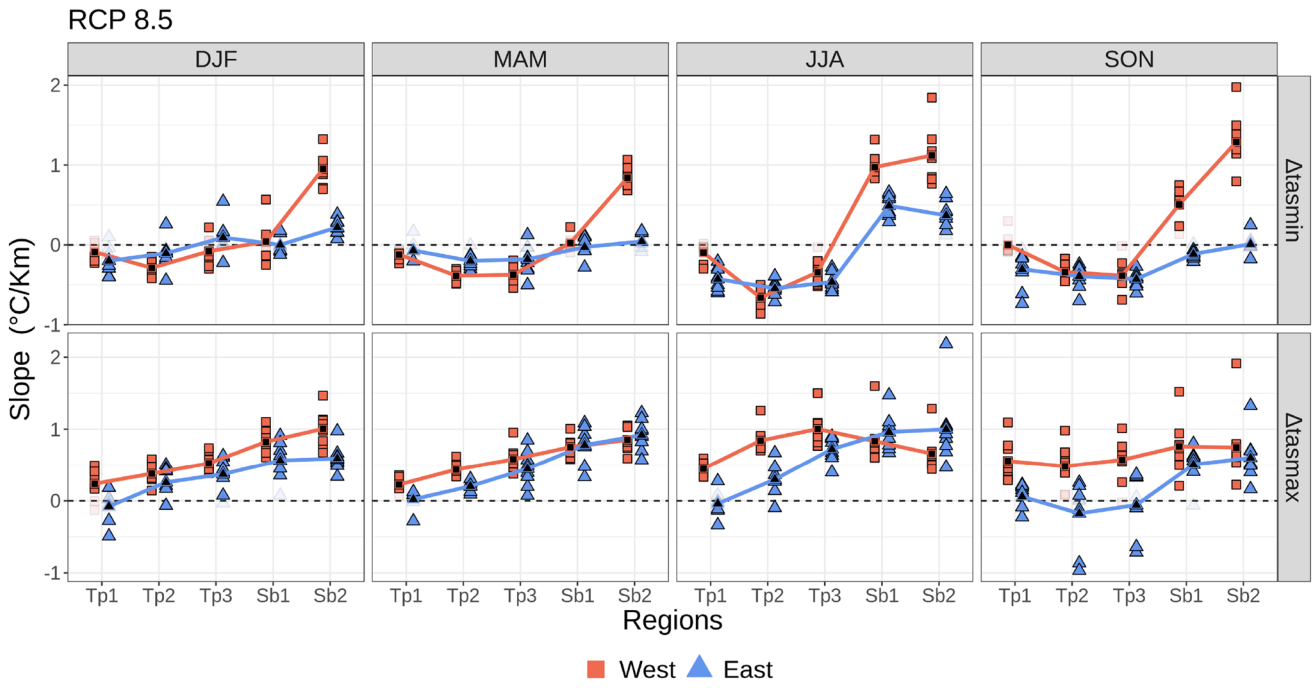

Fig. 6 Elevational gradients of the seasonal temperature change in the tropical (Tp1, Tp2, Tp3) and subtropical (Sb1, Sb2) Andes, for each side of the mountain chain (blue, east and red, west) and for the multi-model mean (black symbols) in the RCP8.5 scenario. The minimum and maximum temperature changes are shown in the top and bottom panels, respectively. The filled colored symbols represent statistically significant slopes while the transparent ones are not significant (Eq. 1). The colored lines connect the multi-model mean values in each area

minimum temperatures generally show larger warming and larger EDW than the maximum temperatures (Rangwala and Miller 2012). The different behavior found here, for nighttime and daytime EDW, corroborates the need to separately analyse the minimum and the maximum temperature in the Andes. It is interesting to note that, in a study focused on the tropical Andes based on the analysis of satellite LST data in the period 2000–2017, Aguilar-Lome et al. (2019) also found a different elevational gradient of LST trends in winter between daytime and nighttime conditions: daytime LST trends are amplified at higher elevations while nighttime LST trends exhibit a steady increase with altitude.

3.2 Analysis of the possible EDW drivers

To better understand the different EDW signals identified in the previous section, an assessment of the possible driving mechanisms is performed applying the methodology described in Sect. 2.3. The first step is to assess whether the elevational gradient of each relevant variable identified as possible EDW driver may in principle (i.e. based on physical considerations) explain the EDW sign. For this, Fig. 7 shows the slopes of the linear regression between each variable (-$\Delta albedo$, $\Delta rlds$, $\Delta rsds$, $\Delta huss$, $\Delta rlds/rlds_0$, $\Delta rsds/rsds_0$, and $\Delta huss/huss_0$) and the elevation in the RCP 8.5 scenario, for each season in the west (red) and east (blue) side of the Andean chain. The figure refers to the multi-model mean of the GCM-RCM ensemble only. For example, $\Delta tasmin$ in SON (upper right panel of Fig. 6) exhibits a positive EDW in Sb2 on the western side of the Cordillera (red squares). Since the slopes of -$\Delta albedo$, $\Delta rlds$, $\Delta rlds/rlds_0$ and $\Delta huss/huss_0$, shown in Fig. 7, are positive (same EDW sign), these variables are possible EDW drivers while those with negative slopes have to be excluded owing to physical considerations. As another example, $\Delta tasmax$ in SON exhibits a negative EDW in the Tp2 area in the eastern side of the Cordillera (blue triangles) that may be explained by $\Delta rlds$, since this is the only driver presenting a negative slope (Fig. 7). It is worth noting that, -$\Delta albedo$ in the Subtropics and the absolute and relative change in *huss* are the drivers showing the largest differences between the eastern and western side of the Cordillera.

As a second step, we calculated the correlation coefficient between the (minimum and maximum) temperature change and each of the variables that satisfied condition 1. Following Palazzi et al. (2017, 2019), all these variables were altitude-detrended and standardized (by dividing each change by its standard deviation over each of the considered domains) before calculating the spatial correlation with the temperature change. The aforementioned correlation coefficients are displayed in Figs. 8 and 9 for the minimum and the maximum temperature, respectively, and limited to the multi-model mean of the GCM-RCM ensemble. Analogous figures are shown in the Supplementary Information to present the results for all individual GCM-RCM pairs (Figs. S10–S13). White areas in the figures identify the cases in which either conditions 1 (a given possible EDW driver shows a dependence on the elevation which is physically consistent with the EDW sign) or 2 (the correlation between a given possible EDW driver and the temperature change is positive) are not satisfied. It is worth specifying that the correlations have been calculated after grouping and averaging the temperature change data and the drivers data into elevation bins, which makes the correlations stronger and more significant but not remarkably different from those that would have been obtained without data binning (not shown here). In the following, a discussion on EDW drivers in the tropical and subtropical Andes based on the correlations shown in Figs. 8 and 9 is presented. In order to assess the difference between the EDW mechanisms in the Tropics and in the Subtropics, major emphasis in the discussion is placed to the drivers which are persistent and robust in all three tropical areas and in all two subtropical areas.

As for the minimum temperature (Fig. 8), our analysis shows that in the tropics (Tp1, Tp2, and Tp3) EDW is overall not driven by the changes in albedo and in the incoming shortwave radiation, in both the west and east sides of the Cordillera (we recall that for the minimum temperature in the Tropics a negative EDW, i.e., decreasing warming rates with the elevation, was found). Only two exceptions are found, in Tp1 West MAM and Tp3 East SON where, however, the correlations are weak, lower than about 0.2. Instead, the (absolute and relative) change in the downward longwave radiation is a clear driver in all three tropical areas, whose role seems to become less relevant approaching the Subtropics (both $\Delta rlds$ and $\Delta rlds/rlds_0$ are strong drivers in Tp1, $\Delta rlds/rlds_0$ does not play a role in Tp3). For the minimum temperature, the most relevant difference in the EDW drivers between the Tropics and the Subtropics is that $\Delta albedo$ becomes a driver in the Subtropics, with stronger correlation in the west side of the Cordillera (in Sb1 in all seasons but JJA $\Delta albedo$ is a driver only in the West). The changes in *rlds* and in *huss*, particularly the relative changes, are also important drivers in the Subtropics. The individual GCM-RCM pairs (Figs. S10 and S11 of the Supplementary Information) overall provide the same picture as their mean. For the majority of models, $\Delta rlds$, $\Delta rlds/rlds_0$, and $\Delta huss$ are recognised as EDW drivers in the tropics (the signal becomes weaker moving southward); in the subtropics, also $\Delta albedo$ and $\Delta huss/huss_0$ play a role, particularly in Sb2. Tp1 is the region presenting not only the largest correlation between the drivers ($\Delta rlds$ and $\Delta rlds/rlds_0$) and $\Delta tasmin$ but also the largest agreement in the model ensemble, in both West and East sides of the Cordillera. Tp2 immediately follows, the correlation being slightly lower than for Tp1. In the subtropics, Sb2 is the region showing the highest correlation

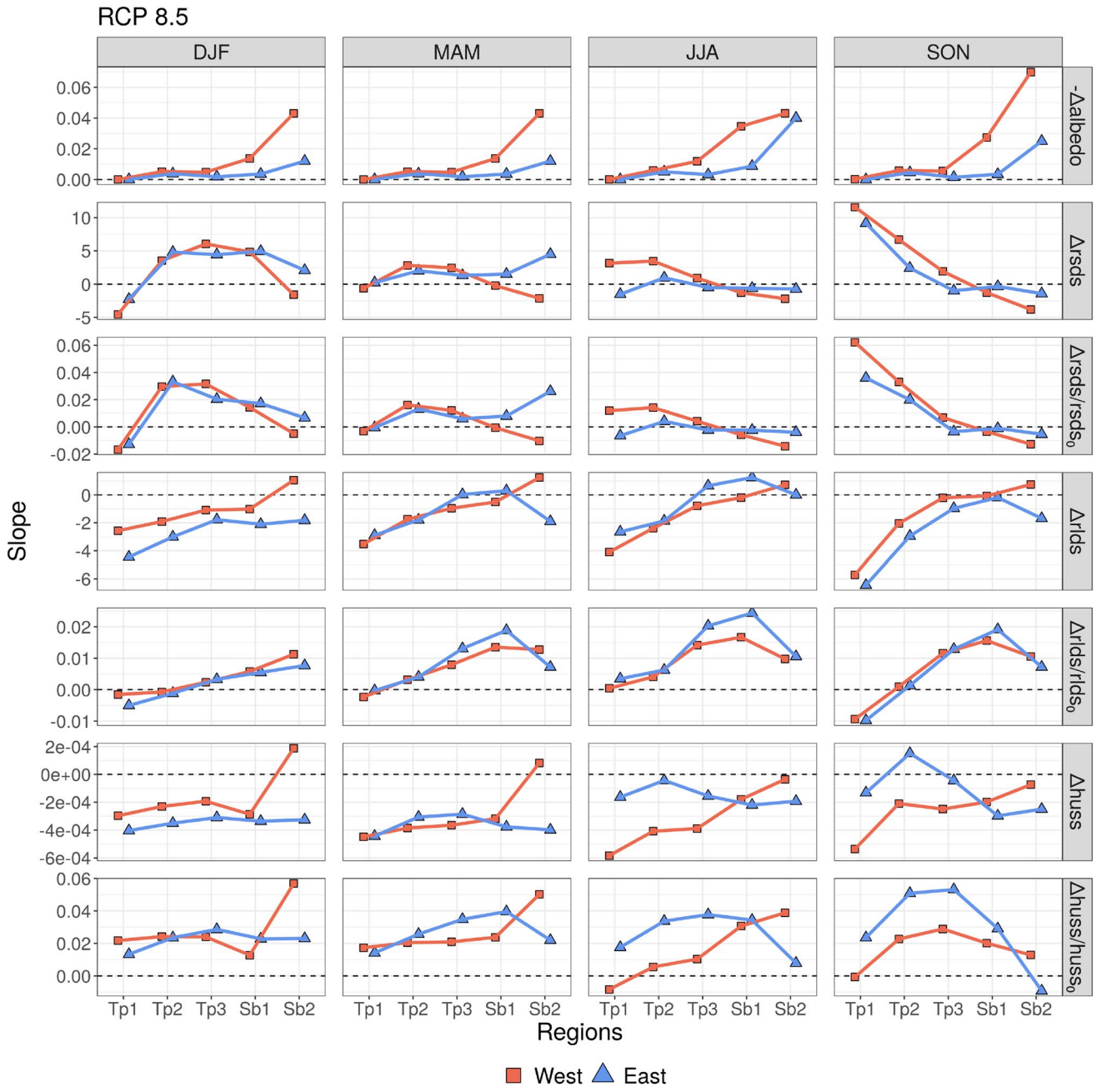

Fig. 7 Elevational gradient for the EDW drivers, for the RCP8.5 scenario, in the five areas areas (columns) and four seasons (rows) on each side of the Andean Cordillera

and agreement among the models, mainly in the western side.

As for *Δtasmax*, we recall that the EDW signal in the Tropics is opposite (and positive) with respect to the one found for *Δtasmin*. This also reflects in the identified EDW drivers. Changes in *Δtasmax* are mostly associated with changes in downward shortwave radiation (in Tp1 and Tp2) while for *Δtasmin* the main driver was the absolute and relative change in *rlds*. However, it is worth underlining that the correlations between the EDW drivers and the maximum temperature change is weaker than for *Δtasmin* (with a few exceptions) and the picture is less coherent across the seasons and the sides of the Cordillera. In Tp3, the EDW signal for *Δtasmax* is mainly associated with $\Delta rlds/rlds_0$ and, to a lesser extent, $\Delta huss/huss_0$. In Sb1, the identified drivers of EDW and their role for the minimum and the maximum temperature are very similar in the two sides of the Cordillera. While *Δalbedo* is the main driver in the west side, *Δrlds*

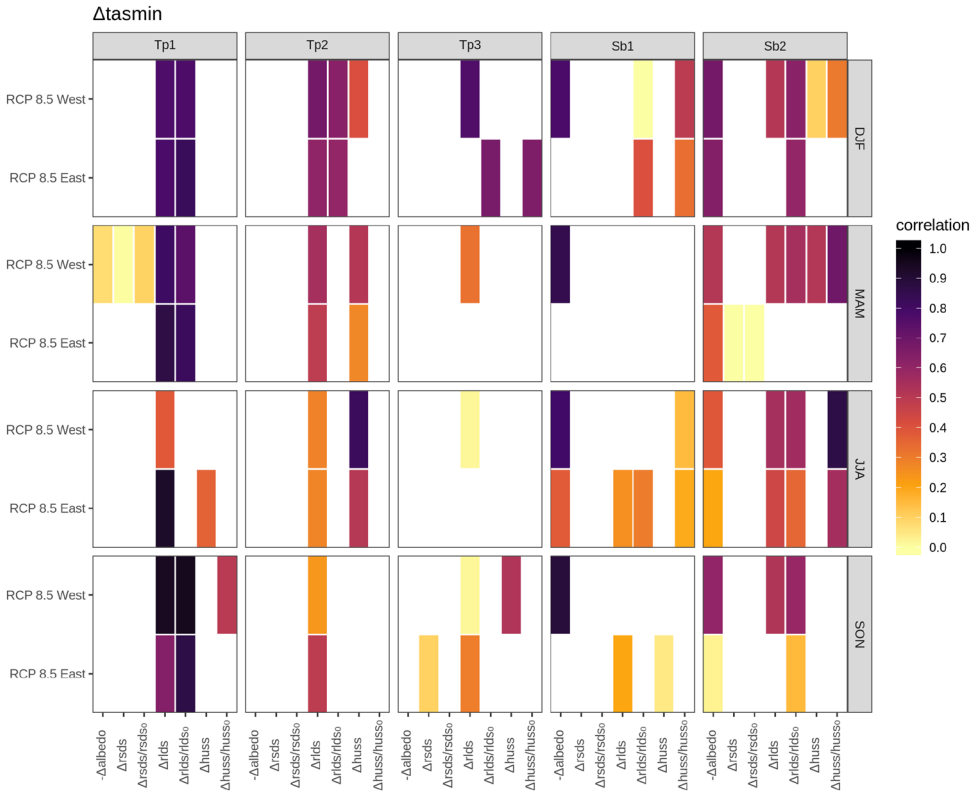

Fig. 8 Correlation coefficient between each of the seven possible EDW drivers and the minimum temperature change, for the RCP8.5 scenario, in the five areas areas (columns) and four seasons (rows) on each side of the Andean Cordillera. The drivers are displayed along the x-axis. White boxes identify the cases in which the correlation is negative and/or the elevational dependence of a given driver has not the same sign as EDW (see text for details)

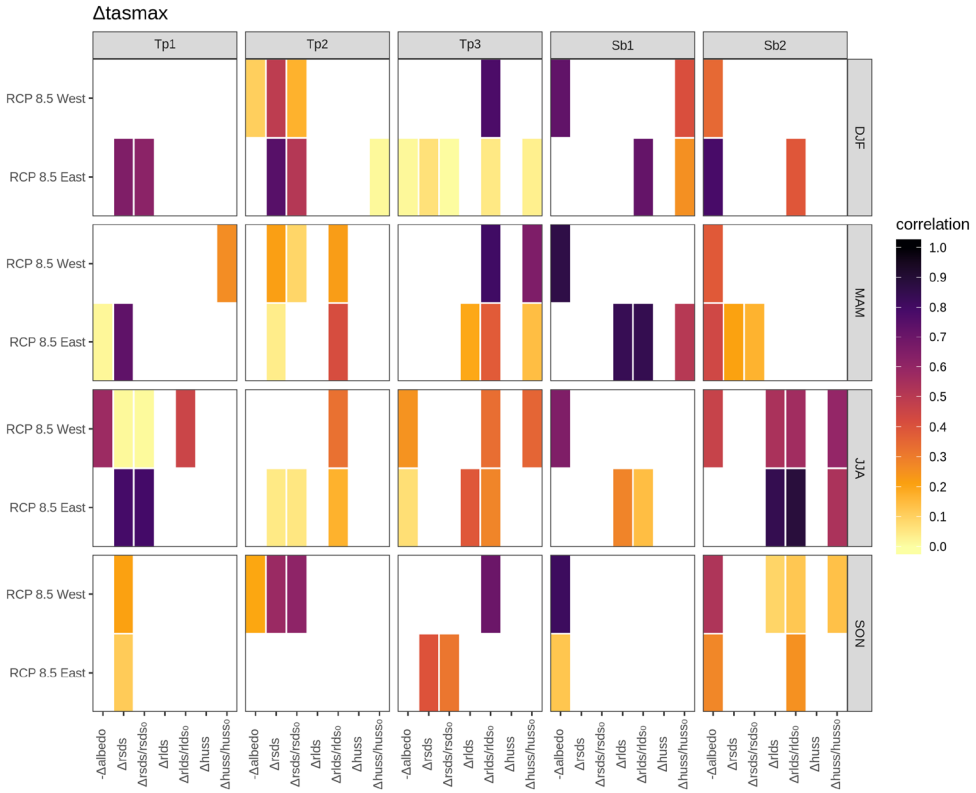

Fig. 9 Correlation coefficient between each of the seven possible EDW drivers and the maximum temperature change, for the RCP8.5 scenario, in the five areas areas (columns) and four seasons (rows) on each side of the Andean Cordillera. The drivers are displayed along the x-axis. White boxes identify the cases in which the correlation is negative and/or the elevational dependence of a given driver has not the same sign as EDW (see text for details)

and $\Delta rlds/rlds_0$ are the main drivers in the East (except that in SON). In Sb2, $\Delta albedo$ is the main driver in both the western side and the eastern side of the chain with the only exception of JJA where $\Delta rlds$ and $\Delta rlds/rlds_0$ show a significant correlation with the EDW signal. With the exception of $\Delta huss/huss_0$ in SON for the western side, all the EDW drivers associated with $\Delta tasmax$ are also associated with $\Delta tasmin$. This suggests that in the Subtropics the minimum and maximum temperature changes may be driven by the same drivers on each side of the Cordillera. The individual model pairs (Figs. S12 and S13 of the Supplementary Information) do agree with the identification of the changes in the downward shortwave radiation as the main drivers in Tp1 and Tp2 especially in the eastern side of the Cordillera. As for Tp3, while the main EDW driver for most individual models in the west side is $\Delta rlds/rlds_0$, coherently with the picture provided by the multi-model mean, in the eastern part the absolute and relative changes in *rsds* turn also out to be important. In the Subtropics, almost all individual models identify $\Delta albedo$ as one main EDW driver in the West, together with the changes in *rlds* and $\Delta huss/huss_0$ but only in Sb2 in JJA and SON. This partly applies to the eastern side of the Cordillera too, though the signal is more scattered and $\Delta rsds$ and $\Delta rsds/rsds_0$ also play a role in Sb1 (SON) and Sb2 (MAM).

To summarise, it might be useful to highlight the drivers presenting the highest correlations with the temperature changes for each area and side of the Cordillera:

- in Tp1, the changes in the minimum temperature (in both eastern and western sides of the Cordillera) are driven by the changes in *rlds* while the changes in the maximum temperature (especially in the East) are driven by the changes in *rsds*. This might explain the opposite EDW signals found in this region during nighttime and daytime (see e.g. Fig. 6). Also observed in all the individual GCM-RCM pairs, this result is very robust;
- the albedo change exists as an ubiquitous EDW driver in the Subtropics (in both west and east sides in Sb2, mainly in the west side in Sb1) where it always shows a high correlation with both the minimum temperature change and the maximum temperature change. In general, the model ensemble reproduces coherently this driver. In the Tropics, while for the minimum temperature the absence of $\Delta albedo$ as an EDW driver is quite clear, its role in driving the maximum temperature changes is less certain;
- the (absolute and relative) change in shortwave radiation is an evident EDW driver only for the maximum temperature in the Tropics;
- when the Tropics and Subtropics exhibit the same EDW signal, i.e. for the maximum temperature, in general no common drivers are identified in the two regions. On the other hand, when the Tropics and Subtropics show an opposite EDW signal, i.e. for the minimum temperature, the change in longwave radiation is a common driver

4 Discussion and conclusions

The Andean Cordillera extends over different latitudes in South America being exposed to different climate regimes, which offers a unique possibility to explore possible differences in EDW along the chain and how the possible various EDW drivers may act.

In this paper, the Cordillera was divided into five domains, three pertaining the Tropics and two the Subtropics. The study employed a small ensemble of eight regional climate model simulations belonging to the CORDEX-South American domain experiment together with their multi-model mean. For future projections, the RCP 8.5 IPCC emission scenario was considered. The analysis was also performed on the RCP 4.5 scenario, not shown in the paper, and no substantial differences were found.

The CORDEX models were first compared to MODIS and ERA5 data to assess their ability in reproducing snow cover and the temperature, respectively, over a historical period. As for the minimum temperature, the climatological annual cycle is well reproduced by the CORDEX models overall, though its amplitude is overestimated in east facing Tp1 and Tp2. A cold bias is observed in the model simulations compared to ERA5. As for the maximum temperature, the model bias is reduced particularly in the subtropical regions. Also, the shape of the annual cycle is overall well captured except in east facing Tp1 and Tp2 and in west facing Tp1. We found that CORDEX (the multi-model mean) overestimates the snow cover on the high Cordillera areas in the subtropics along the Chile–Argentina border, and underestimate snow cover around the latitude of 20 °S. Though the temperature comparison between CORDEX and ERA5 overall led to satisfactorily results, the snow cover biases could have implications for the interpretation of projected temperature changes through the albedo mechanism.

The EDW signal was assessed by means of linear, LOESS and piecewise regressions. The comparison among the three methods highlighted a clear bi-modal behaviour for most of the seasons in all the study areas and sides of the Cordillera. Remarkably, when using the piecewise regression, the regression lines before and after the breakpoint showed, for most GCM-RCM model pairs, very similar slopes. This suggested that describing the EDW with a bi-modal linear behaviour might be related to physical reasons, which were not analysed in this study but deserve future investigations. Here, we opted for a more standard EDW analysis, based on the use of a single slope to assess the EDW sign and

strength, in order to make the analysis of the results for the Andes more easily comparable to those published in the current EDW literature for this and other regions.

In all the three tropical regions an opposite EDW signal during daytime and nighttime (i.e. in the maximum and in the minimum temperature) was identified. The minimum temperatures, in fact, showed a negative EDW (warming rates are lower at higher elevations) while the maximum temperatures exhibited a positive EDW (amplification of warming rates with elevation). The minimum temperature elevational gradient in the Tropics also seemed to be similar in the eastern and the western sides of the mountain range, while for the maximum temperature the elevational gradient was larger in the western side. Contextually, our analysis on the possible EDW drivers showed that, in the Tropics, no common driver was identified for EDW in the maximum temperature (mostly driven by changes in downward shortwave radiation) and EDW in the minimum temperature (driven by changes in downward longwave radiation and in specific humidity), which may support the observation of the contrasting EDW signal found in the two variables. This is particularly true for Tp1 and Tp2, while in the west side of Tp3, *Δtasmin* and *Δtasmax* exhibit weak common drivers in DJF and SON.

In the subtropical Andes EDW is positive in every season and for both the minimum and the maximum temperature (in DJF, MAM and SON in the eastern side, EDW in *Δtasmin* is neutral). One clear and important EDW driver in the Subtropics, common to both nighttime and daytime temperatures, is the change in albedo. Longwave radiation and humidity are also significantly correlated to EDW in the Subtropics, but with different relevance for the minimum and maximum temperature throughout the seasons and the sides of the Andes. These findings reflect the results on EDW drivers reported in previous studies focused on mountain areas in the northern hemisphere mid-latitudes.

The analysis on the possible EDW drivers highlighted some differences between the tropical and subtropical sectors of the Andean chain, suggesting that the Tropic somehow marks a boundary, with Tp3 representing a transition area between different EDW behaviours.

It is important to stress that other possible drivers not included in this study, such as mechanisms related to aerosol particles or clouds, might influence EDW. Further, the potential cross-correlations between the drivers, that in principle may dampen or amplify the effect of the drivers taken individually, are here neglected.

A better understanding of climate changes in mountain regions and of their possible elevational gradients is of utmost importance, given the influence of high-altitude regions on downstream livelihood, economies and societies. This work showed the peculiarity of the elevational gradients of warming rates in the Andean chain, highlighting that different EDW patterns and driving mechanisms are at play in the tropical and subtropical Andes as well as in the eastern and western sides of the mountain range. Though being a crucial water reservoir for the Andean countries, this mountain range is still under-represented in the EDW literature. Further observational and model studies are thus required to deepen our knowledge on EDW and its mechanisms and to account for new or currently not well represented processes at play in this high-elevation region.

Supplementary Information The online version contains supplementary material available at https://doi.org/10.1007/s00382-021-06081-4.

Acknowledgements This study was financed in part by the Coordenação de Aperfeiçoamento de Pessoal de Nível Superior – Brasil (CAPES) – Finance Code 001. The authors acknowledge the World Climate Research Programme's Working Group on Regional Climate, and the Working Group on Coupled Modelling, former coordinating body of CORDEX and responsible panel for CMIP5, and they also thank the climate modelling groups which produced and made available their model outputs.

Declarations

Conflict of interest The authors declare that they have no conflicts of interest.

References

Aguilar-Lome J, Espinoza-Villar R, Espinoza JC, Rojas-Acuña J, Willems BL, Leyva-Molina WM (2019) Tropical Andes, land surface warming, remote sensing, high mountains, 77. Int J Appl Earth Observ Geoinf. https://doi.org/10.1016/j.jag.2018.12.013

Arora VK, Scinocca JF, Boer GJ, Christian JR, Denman KL, Flato GM, Kharin VV, Lee WG, Merryfield WJ (2011) Carbon emission limits required to satisfy future representative concentration pathways of greenhouse gases. Geophys Res Lett 38:L05805. https://doi.org/10.1029/2010GL046270

Bellouin N, Rae J, Jones A, Johnson C, Haywood J, Boucher O (2011) Aerosol forcing in the climate model intercomparison project (CMIP5) simulations by HadGEM2-ES and the role of ammonium nitrate. J Geophys Res 116:D20206. https://doi.org/10.1029/2011JD016074

Bendat JS, Piersol AG (2000) Random data: analysis and measurement procedures. Wiley, New York (**640 Pages**)

Bradley RS, Vuille M, Diaz HF, Vergara W (2006) Threats to water supplies in the tropical Andes. Science 312:1755–1756. https://doi.org/10.1126/science.1128087

Ceballos JL, Euscategui C, Ramirez J, Canon M, Huggel C, Haeberli W, Machguth H (2006) Fast shrinkage of tropical glaciers in Colombia. Ann Glaciol 43:194–201. https://doi.org/10.3189/172756406781812429

Chiu G, Lockhart R, Routledge R (2006) Bent-cable regression theory and applications. J Am Stat Assoc 101(474):542–553. https://doi.org/10.1198/016214505000001177

Chou SC, Lyra A, Mourão C, Dereczynski C, Pilotto I, Gomes J, Bustamante J, Tavares P, Silva A, Rodrigues D, Campos D, Chagas D, Sueiro G, Siqueira G, Marengo J (2014) Assessment of climate change over South America under RCP 4.5 and 8.5 downscaling scenarios. Am J Clim Chang 3(5):512–525

Delworth TL, Broccoli AJ, Rosati A, Stouffer RJ, Balaji V, Beesley JA, Cooke WF, Dixon K, Dunne J, Dunne KA, Durachta JW, Findell KL, Ginoux P, Gnanadesikan A, Gordon CT, Griffies SM, Gudgel R, Harrison MJ, Held IM, Hemler RS, Horowitz LW, Klein SA, Knutson TR, Kushner PJ, Langenhorst AR, Lee HC, Lin SJ, Lu J, Malyshev SL, Milly PCD, Ramaswamy V, Russell J, Schwarzkopf MD, Shevliakova E, Sirutis JJ, Spelman MJ, Stern WF, Winton M, Wittenberg AT, Wyman B, Zeng F, Zhang R (2006) GFDL's CM2 global coupled climate models part I: formulation and simulation characteristics. J Clim 19:643–674. https://doi.org/10.1175/JCLI3629.1

Dufresne JL, Foujols MA, Denvil S et al (2013) Climate change projections using the IPSL-CM5 Earth System Model: from CMIP3 to CMIP5. Clim Dyn 40:2123–2165. https://doi.org/10.1007/s00382-012-1636-1

Farr TG, Rosen PA, Caro E, Crippen R, Duren R, Hensley S, Kobrick M, Paller M, Rodriguez E, Roth L (2007) The shuttle radar topography mission. Rev Geophys 45:1–33. https://doi.org/10.1029/2005RG000183

Fernandez JPR, Franchito SH, Rao VB (2006) Simulation of the summer circulation over South America by two regional climate models. Part I: mean climatology. Theor Appl Climatol 86:247–260. https://doi.org/10.1007/s00704-005-0212-6

Garreaud RD (2009) The Andes climate and weather. Adv Geosci 22:3–11. https://doi.org/10.5194/adgeo-22-3-2009

Giorgetta MA, Jungclaus J, Reick C, Legutke S, Bader J, Bttinger M, Brovkin V, Crueger T, Esch M, Fieg K, Glushak K, Gayler V, Haak H, Hollweg HD, Ilyina T, Kinne S, Kornblueh L, Matei D, Mauritsen T, Mikolajewicz U, Mueller W, Notz D, Pithan F, Raddatz T, Rast S, Redler R, Roeckner E, Schmidt H, Schnur R, Segschneider J, Six KD, Stockhause M, Timmreck C, Wegner J, Widmann H, Wieners KH, Claussen M, Marotzke J, Stevens B (2013) Climate and carbon cycle changes from 1850 to 2100 in MPI-ESM simulations for the coupled model intercomparison project phase 5. J Adv Model Earth Syst 5:572–597. https://doi.org/10.1002/jame.20038

Giorgi F, Jones C, Asrar GR (2009) Addressing climate information needs at the regional level: the CORDEX framework. World Meteorol Organiz Bull 58(3):175–183

Giorgi F, Coppola E, Raffaele F (2014) A consistent picture of the hydroclimatic response to global warming from multiple indices: models and observations. J Geophys Res Atmos 119:11695–11708. https://doi.org/10.1002/2014JD022238

Hazeleger W, Wang X, Severijns C, Stefănescu S, Bintanja R, Sterl A, Wyser K, Semmler T, Yangm S, van den Hurk B, van Noije T, van der Linden E, van der Wiel K (2012) EC-Earth v2.2: description and validation of a new seamless earth system prediction model. Clim Dyn 39:2611–2629. https://doi.org/10.1007/s00382-011-1228-5

Hersbach H, Bell B, Berrisford P et al (2020) The ERA5 global reanalysis. Q J R Meteorol Soc 146:1999–2049. https://doi.org/10.1002/qj.3803

IPCC (2019) Summary for policymakers. In: Pörtner H- O, Roberts DC, Masson-Delmotte V, Zhai P, Tignor M, Poloczanska E, Mintenbeck K, Nicolai M, Okem A, Petzold J, Rama B, Weyer N (eds) IPCC special report on the ocean and cryosphere in a changing climate. (**In press**)

Karmalkar AV, Bradley RS, Diaz HF (2008) Climate change scenario for Costa Rican montane forests. Geophys Res Lett 35:L11702. https://doi.org/10.1029/2008GL033940

Kaser G (1999) A review of the modern fluctuations of tropical glaciers. Global Planet Change 22(1–4):93–103. https://doi.org/10.1016/S0921-8181(99)00028-4

Kohler T, Maselli D (2009) Mountains and Climate Change – From Understanding to Action. Published by Geographica Bernensia with the support of the Swiss Agency for Development and Cooperation (SDC), and an international team of contributors, Bern

Lenters JD, Cook KH (1997) On the origin of the Bolivian High and related circulation features of the South American climate. J Atmos Sci 54:656–678. https://doi.org/10.1175/1520-0469(1997)054<0656:OTOOTB>2.0.CO;2

Liu X, Cheng Z, Yin ZY (2009) Elevation dependency of recent and future minimum surface air temperature trends in the Tibetan Plateau and its surroundings. Glob Planet Change 68:164–174. https://doi.org/10.1016/j.gloplacha.2009.03.017

Mark BG, McKenzie JM (2007) Tracing increasing tropical Andean glacier melt with stable isotopes in water. Environ Sci Technol 41:6955–6960. https://doi.org/10.1021/es071099d

Minder JR, Letcher TW, Liu C (2018) The character and cause of elevation-dependent warming in high-resolution simulations of rocky mountain climate change. J Clim 31:2093–2113. https://doi.org/10.1175/JCLI-D-17-0321.1

Moss RH, Edmonds JA, Hibbard KA, Manning MR, Rose SK, van Vuuren DP, Carter TR, Emori S, Kainuma M, Kram T, Meehl GA, Mitchell JFB, Nakicenovic N, Riahi K, Smith S, Stouffer RJ, Thomson AM, Weyant JP, Wilbanks TJ (2010) The next generation of scenarios for climate change research and assessment. Nature 463:747–756. https://doi.org/10.1038/nature08823

Nogués-Bravo D, Araujo MB, Errea MP, Martinez-Rica JP (2007) Exposure of global mountain systems to climate warming during the 21st century. Global Environ Change 17:420–428. https://doi.org/10.1016/j.gloenvcha.2006.11.007

Palazzi E, Filippi L, Von Hardenberg J (2017) Insights into elevation-dependent warming in the Tibetan Plateau-Himalayas from CMIP5 model simulations. Clim Dyn 48(11–12):3991–4008

Palazzi E, Mortarini L, Terzago S, Hardenberg J (2019) Elevation dependent warming in global climate model simulations at high spatial resolution. Clim Dyn 52(5–6):2685–2702. https://doi.org/10.1007/s00382-018-4287-z

Pepin N, Bradley RS, Diaz HF, Baraër M, Caceres EB, Forsythe N, Miller JR (2015) Elevation-dependent warming in mountain regions of the world. Nat Clim Chang 5(5):424

Price M (2015) Mountains: a very short introduction. Oxford University Press, Oxford (**134 pp.**)

Rangwala I, Miller JR (2012) Climate change in mountains: a review of elevation-dependent warming and its possible causes. Clim Change 114:527–547. https://doi.org/10.1007/s10584-012-0419-3

Rangwala I, Sinsky E, Miller RJ (2013) Amplified warming projections for high altitude regions of the Northern hemisphere mid- latitudes from CMIP5 models. Environ Res Lett 8:024040. https://doi.org/10.1088/1748-9326/8/2/024040

Rangwala I, Sinsky E, Miller RJ (2016) Variability in projected elevation dependent warming in boreal midlatitude winter in CMIP5 climate models and its potential drivers. Clim Dyn 46(7):2115–2122. https://doi.org/10.1007/s00382-015-2692-0

Riahi K, Rao S, Krey V, Cho C, Chirkov V, Fischer G, Kindermann G, Nakicenovic N, Rafaj P (2011) RCP 8.5-a scenario of comparatively high greenhouse gas emissions. Clim Change 109:33–57. https://doi.org/10.1007/s10584-011-0149-y

Rotstayn LD, Jeffrey SJ, Collier MA, Dravitzki SM, Hirst AC, Syktus JI, Wong KK (2012) Aerosol- and greenhouse gas-induced changes in summer rainfall and circulation in the Australasian region: a study using single-forcing climate simulations. Atmos Chem Phys 12:6377–6404. https://doi.org/10.5194/acp-12-6377-2012

Saavedra FA, Kampf SK, Fassnacht SR, Sibold JS (2018) Changes in Andes snow cover from MODIS data, 2000–20016. Cryosphere 12:1027–1046. https://doi.org/10.5194/tc-12-1027-2018

Samuelsson P, Jones CG, Willén U, Ullerstig A, Gollvik S, Hansson U, Jansson C, Kjellström E, Nikulin G, Wyser K (2011) The Rossby Centre Regional Climate model RCA3: model description and performance. Tellus A 63:4–23. https://doi.org/10.1111/j.1600-0870.2010.00478.x

Seimon TA, Seimon A, Daszak P, Halloy SRP, Schloegel LM, Aguliar CA, Sowell P, Hyatt AD, Konecky B, Simmons JE (2007) Upward range extension of Andean anurans and chytridiomycosis to extreme elevations in response to tropical deglaciation. Global Change Biol 13:288–299. https://doi.org/10.1111/j.1365-2486.2006.01278.x

Solman SA (2013) Regional climate modeling over South America: a review. Adv Meteorol 18:1–13. https://doi.org/10.1155/2013/504357

Tennant CJ, Crosby BT, Godsey SE (2014) Elevation-dependent responses of streamflow to climate warming. Hydrol Process 29:991–1001. https://doi.org/10.1002/hyp.10203

Thompson LG, Mosley-Thompson E, Brecher H, Davis M, Leon B, Les D, Lin P-N, Mashiotta T, Mountain K (2006) Abrupt tropical climate change: past and present. Proc Natl Acad Sci USA 103(28):10536–10543. https://doi.org/10.1073/pnas.0603900103

Thomson AM, Calvin KV, Smith SJ, Kyle GP, Volke A, Patel P, Delgado-Arias S, Bond-Lamberty B, Wise MA, Clarke LE, Edmonds JA (2011) RCP 4.5: a pathway for stabilization of radiative forcing by 2100. Clim Change 109:77–94. https://doi.org/10.1007/s10584-011-0151-4

Toms JD, Lesperance ML (2003) Piecewise regression: a tool for identifying ecological thresholds. Ecology 84:2034–2041. https://doi.org/10.1890/02-0472

Urrutia R, Vuille M (2009) Climate change projections for the tropical Andes using a regional climate model: temperature and precipitation simulations for the end of the 21st century. J Geophys Res 114:D02108. https://doi.org/10.1029/2008JD011021

Viviroli D, Durr HH, Messerli B, Meybeck M, Weingartner R (2007) Mountains of the world - water towers for humanity: typology, mapping and global significance. Water Resour Res 43:1–13

Viviroli D, Archer DR, Buytaert W, Fowler HJ, Greenwood GB, Hamlet AF, Huang Y, Koboltschnig G, Litaor MI, López-Moreno JI, Lorentz S, Schädler B, Schreier H, Schwaiger K, Vuille M, Woods R (2011) Climate change and mountain water resources: overview and recommendations for research, management and policy. Hydrol Earth Syst Sci 15:471–504. https://doi.org/10.5194/hess-15-471-2011

Vuille M, Bradley RS (2000) Mean annual temperature trends and their vertical structure in the tropical Andes. Geophys Res Lett 27:3885–3888. https://doi.org/10.1029/2000GL011871

Vuille M, Bradley R, Werner M, Keimig F (2003) 20th century climate change in the tropical Andes: observations and model results. Clim Change 59(1–2):75–99. https://doi.org/10.1023/A:1024406427519

Vuille M, Francou B, Wagnon P, Juen I, Kaser G, Mark BG, Bradley RS (2008) Climate change and tropical Andean glaciers? Past, present and future. Earth Sci Rev 89:79–96. https://doi.org/10.1016/j.earscirev.2008.04.002

Watanabe M, Suzuki T, O'ishi R, Komuro Y, Watanabe S, Emori S, Takemura T, Chikira M, Ogura T, Sekiguchi M, Takata K, Yamazaki D, Yokohata T, Nozawa T, Hasumi H, Tatebe H, Kimoto M (2010) Improved climate simulation by MIROC5: mean states, variability, and climate sensitivity. J Clim 23:6312–6335. https://doi.org/10.1175/2010JCLI3679.1

You Q, Kang S, Pepin N, Flgel W-A, Yan Y, Behrawan H, Huang J (2010) Relationship between temperature trend magnitude, elevation and mean temperature in the Tibetan Plateau from homogenized surface stations and reanalysis data. Global Planet Chang 71(124):133. https://doi.org/10.1016/j.gloplacha.2010.01.020

Zazulie N, Rusticucci M, Raga GB (2017) Regional climate of the subtropical central Andes using high-resolution CMIP5 models?part I: past performance (1980–2005). Clim Dyn 49:3937. https://doi.org/10.1007/s00382-017-3560-x(2017)

Zazulie N, Rusticucci M, Raga GB (2018) Regional climate of the Subtropical Central Andes using high?resolution CMIP5 models. Part II: Future projections for the twenty-first century. Clim Dyn 51:2913. https://doi.org/10.1007/s00382-017-4056-4

Noname manuscript No.
(will be inserted by the editor)

Supplementary Information

Comparison of elevation-dependent warming and its drivers in the tropical and subtropical Andes

Osmar Toledo Bonfim · Elisa Palazzi* · Iván Mauricio Cely Toro · Luca Mortarini

Received: date / Accepted: date

In this document we first perform a comparison, limited to the snow cover and temperature variables, between the CORDEX models and some reference datasets. The reference dataset for snow cover is one among the MODIS satellite products (see the main text for details), while we used the most recent ERA5 reanalysis for the minimum and the maximum temperature

The evaluation of snow cover in the CORDEX models against an observational reference is motivated by the need of assessing the extent to which models with a relatively coarse spatial resolution are able to realistically reproduce snow cover, especially given the importance of snow processes and changes for EDW. Figures S1 and S2 show the climatological maps of snow cover for the multi-model mean of the GCM-RCM CORDEX ensemble and for MODIS. Figure S3 shows their anomaly (CORDEX–MODIS). To evaluate the anomaly, MODIS data were remapped on the CORDEX grid. Section 2.2 of the main text discusses the results of this comparison.

Figures S4 and S5 show, respectively, the time series of the minimum temperature and of the maximum temperature in the models (the black line indicates the multi-model mean, while the grey area represents the range of model

Osmar Toledo Bonfim
Universidade Federal de Santa Maria, Santa Maria (RS), Brazil

Elisa Palazzi
Institute of Atmospheric Sciences and Climate – National Research Council
corso Fiume 4, 10133, Torino, Italy
Tel.: +39-011-3839836
Fax: +39-011-6600364
E-mail: e.palazzi@isac.cnr.it

Iván Mauricio Cely Toro
Universidade Federal de Santa Maria, Santa Maria (RS), Brazil

Luca Mortarini
Institute of Atmospheric Sciences and Climate – National Research Council, Torino, Italy
Universidade Federal de Santa Maria, Santa Maria (RS), Brazil

variability) and in ERA5 (red line) for the five sub-domains and the East and West sides of Andean Cordillera.

These figures allow to evaluate, even though in a succinct way, the ability of the model in reproducing the historical temperature climatology and corroborate the comments made in the main text when presenting Figs. 2 and 3. Compared to ERA5, the models exhibit a cold bias in the minimum temperature. The bias, as well as the inter-model spread, is larger in the three tropical domains (Tp1, Tp2, and Tp3) than in the subtropical areas. The agreement between the models and ERA5 is higher for the maximum temperature: in this case a warm model bias is observed but limited to Tp1 and Tp2, for some subdomains only. We report in Table S1 the seasonal and annual bias (CORDEX–ERA5, following Figs. 2 and 3 of the main text) for the minimum and maximum temperature, each season, domain and side of the Cordillera. We also compare in Table S2 the annual bias with the future temperature change (i.e., the change of the minimum and of the maximum temperature between the average in the period 2071–2100 and the average in the period 1976–2005) in the RCP 8.5 scenario. As highlighted in the main text, the existence of a bias between the models and ERA5 does not compromise our results and does not call for the application of bias-correction methods. In fact, our EDW analysis is based on the calculation of the change between two temperature climatologies, thus any bias is removed. For completeness, Table S3 shows the trend values of the the minimum and maximum temperature time series in ERA5 (red figures) and in the CORDEX mean (black figures) while Table S4 shows the interannual variability of the temperature series, calculated as the standard deviation of the detrended time series shown in Figs. S4 and S5, in ERA5 and in the GCM-RCM ensemble.

Figures S6 and S7 show, respectively, the minimum and the maximum temperature change maps in all the seasons and for the five areas considered in this study. We recall that, in order to assess EDW, the relationship between these temperature changes and the elevation is calculated. When a linear regression is assumed, the EDW is quantified through the slope of the linear regression.

Figures S8 and S9 show the piecewise regression for the minimum and maximum temperatures for each individual GCM-RCM model pair in the RCP 8.5 scenario, for each season, study area and side of the Andean Cordillera.

Finally, Figs. S10 and S11 integrate the correlation analysis for the minimum temperature depicted in Fig. 8 of the main text plotting the correlation coefficients of each individual RCM member besides the one of their mean for the RCP 8.5 scenario in the western and eastern sides of the mountain range. Similarly, Figs. S12 and S13 integrate the correlation analysis for the maximum temperature depicted in Fig. 9 of the main text plotting the correlation coefficients of each individual RCM member besides the one of their mean for the RCP 8.5 scenario in the western and eastern sides of the mountain range.

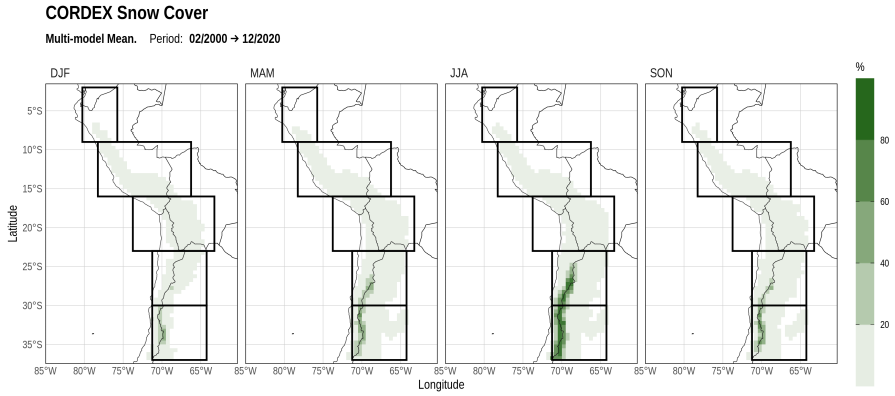

Fig. S1 Climatological seasonal maps of the Snow cover fraction for the multi-model mean of the GCM-RCM CORDEX ensemble for the years 2000–2020. Black rectangles delimit the five study areas.

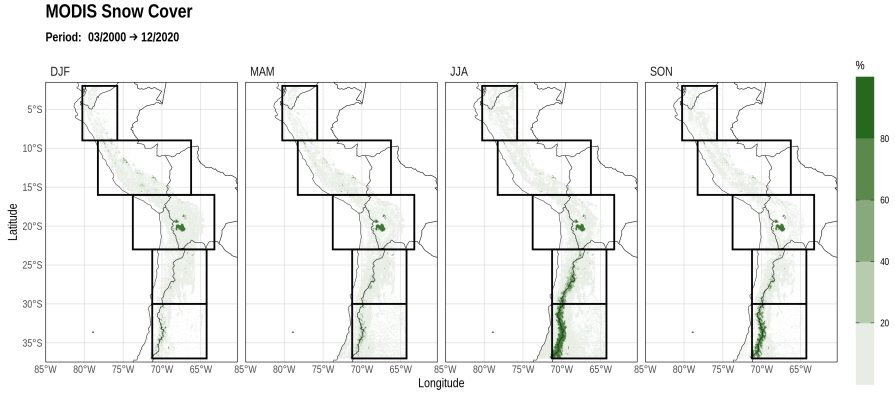

Fig. S2 Climatological seasonal maps of the snow cover fraction for the MODIS satellite data for the years 2000–2020. Black rectangles delimit the five study areas.

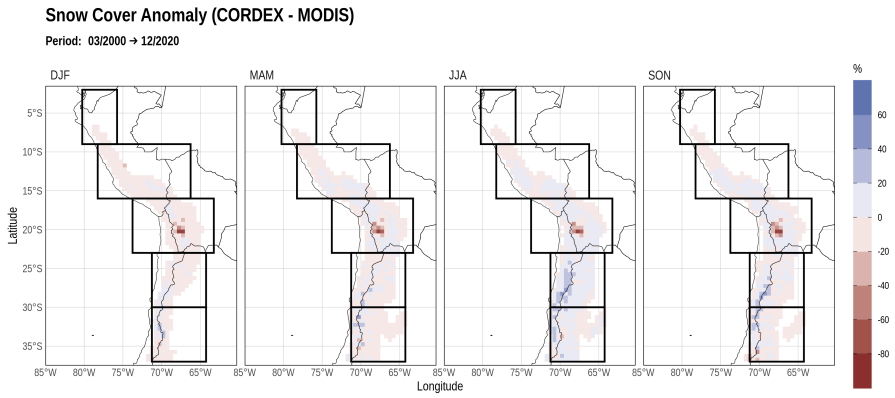

Fig. S3 Climatological seasonal map of the anomaly of the snow cover fraction between the MODIS satellite data and the the multi-model mean of the GCM-RCM CORDEX ensemble for the years 2000-2020. Black rectangles delimit the five study areas.

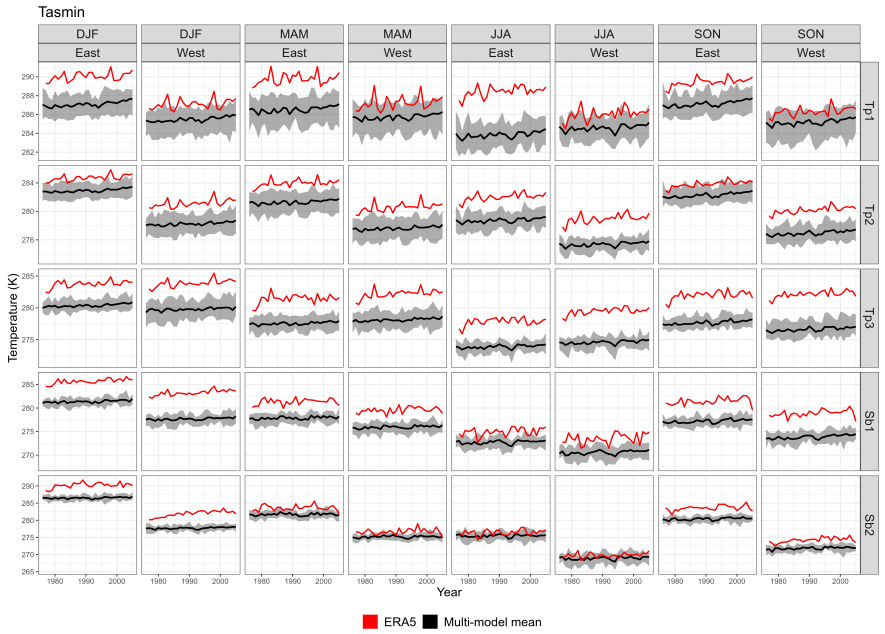

Fig. S4 Minimum temperature time series in the models (black line: multi-model mean; shaded grey area: range of model variability) and in ERA5 (red) for the five areas and the two sides of the Andean Cordillera. Corresponding trend values are shown in Table S3.

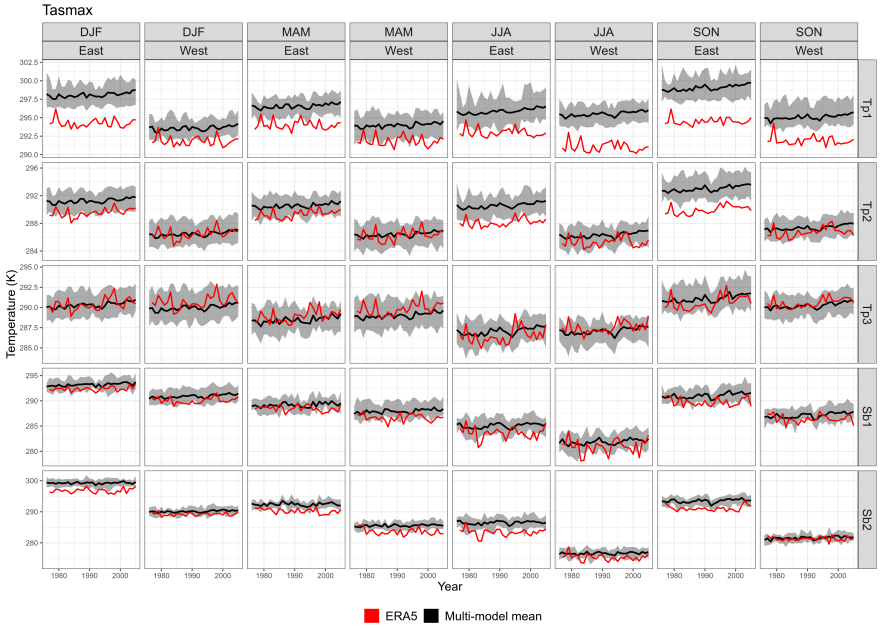

Fig. S5 The same as Fig. S4 but for the maximum temperature

.

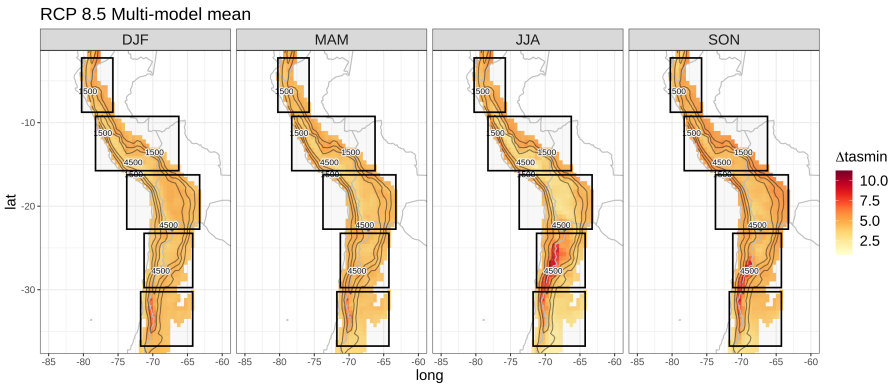

Fig. S6 Seasonal maps of the minimum temperature change.

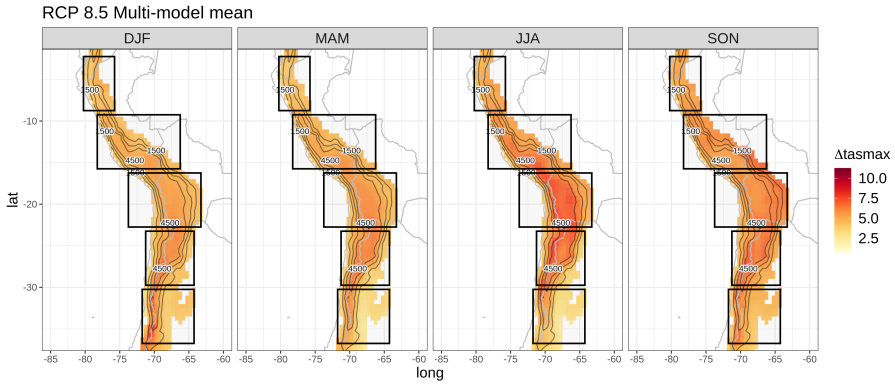

Fig. S7 Seasonal maps of the maximum temperature change.

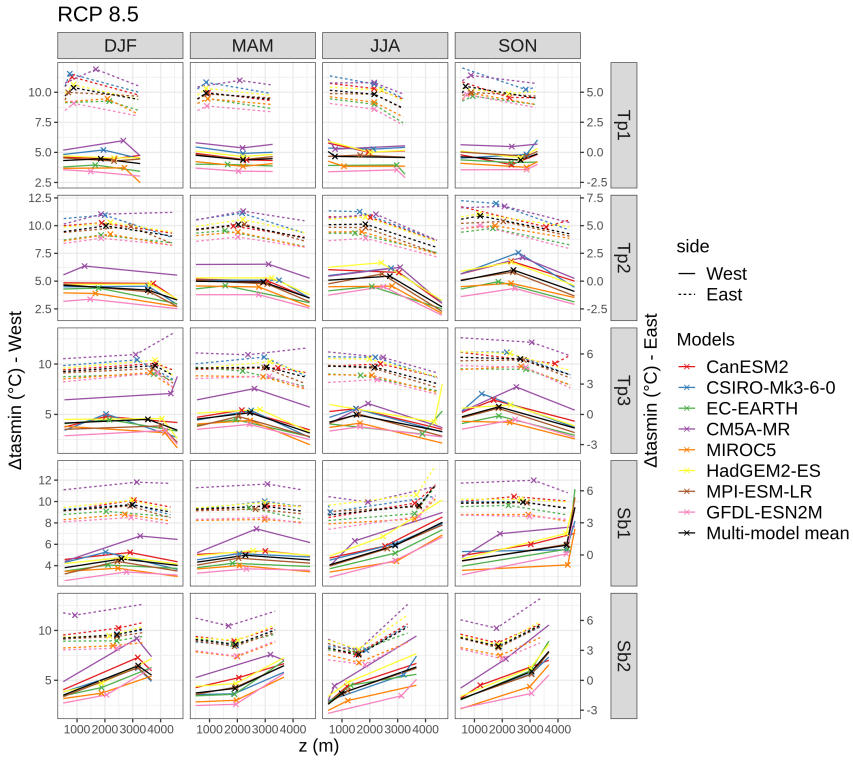

Fig. S8 Piecewise regression lines for the seasonal minimum temperature changes in the topical and subtropical study areas for each GCM-RCM model pair (colored lines) and for the multi-model mean (black) in the RCP 8.5 scenario. Results referring to the Western (continuous lines) and eastern (dashed lines) sides were shifted to improve readability; the left (right) y-axes refer to West (East). The cross symbols represent the breakpoints z_α.

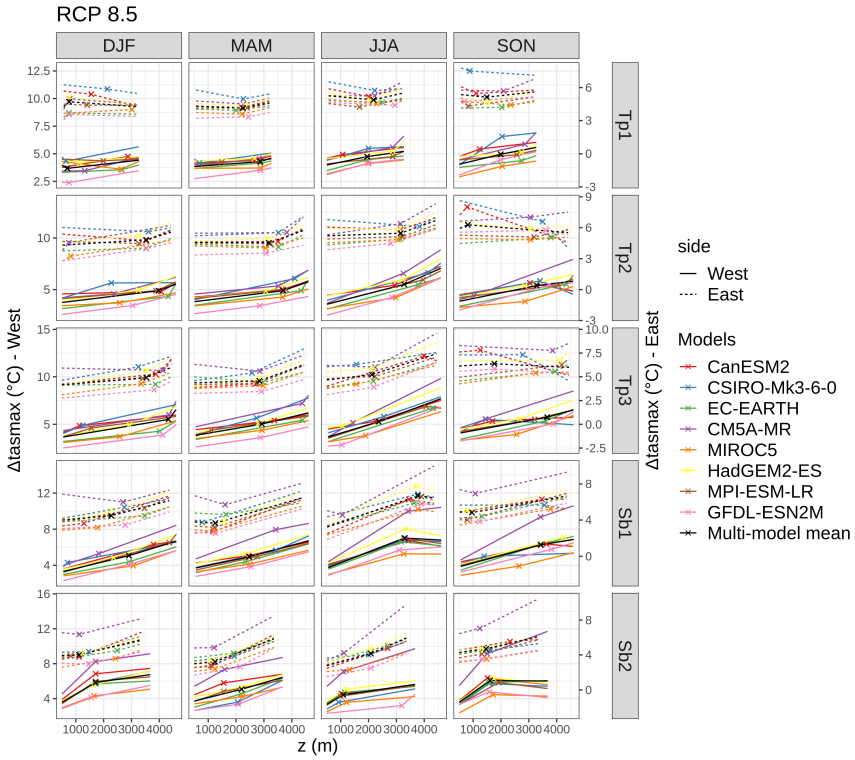

Fig. S9 The same as Fig. S8, but for the maximum temperature change.

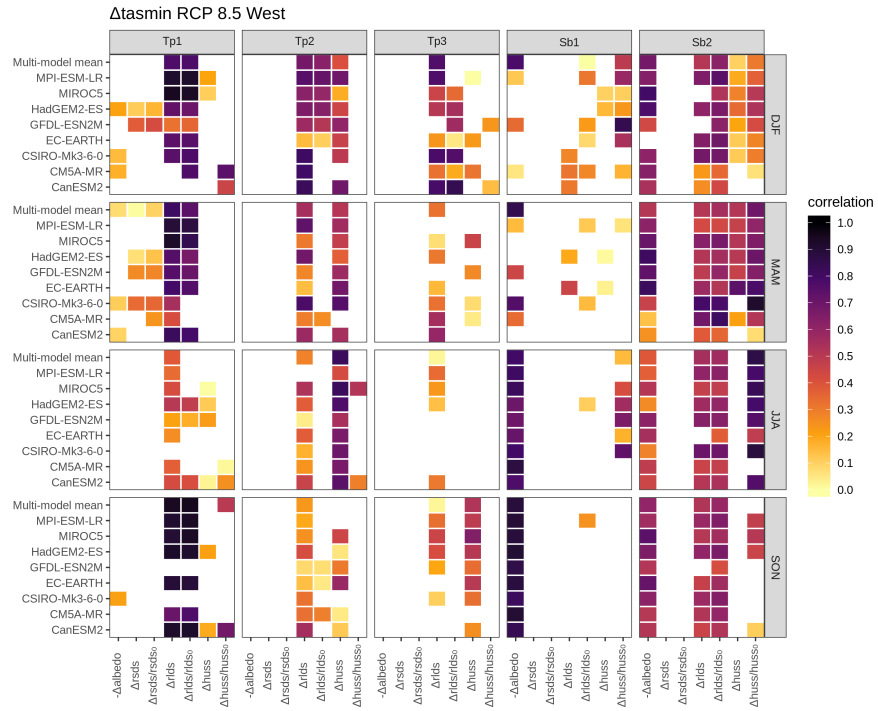

Fig. S10 Correlation coefficient between each of the seven possible EDW drivers and the minimum temperature change, for the RCP85 scenario, in the five areas areas (columns) and four seasons (rows) on the west the Andean Cordillera. The drivers are displayed along the x-axis. White boxes identify the cases in which the correlation is negative and/or the elevational dependence of a given driver has not the same sign as EDW (see text for details).

Fig. S11 Correlation coefficient between each of the seven possible EDW drivers and the minimum temperature change, for the RCP85 scenario, in the five areas areas (columns) and four seasons (rows) on the east the Andean Cordillera. The drivers are displayed along the x-axis. White boxes identify the cases in which the correlation is negative and/or the elevational dependence of a given driver has not the same sign as EDW (see text for details).

Fig. S12 Correlation coefficient between each of the seven possible EDW drivers and the maximum temperature change, for the RCP85 scenario, in the five areas areas (columns) and four seasons (rows) on the west the Andean Cordillera. The drivers are displayed along the x-axis. White boxes identify the cases in which the correlation is negative and/or the elevational dependence of a given driver has not the same sign as EDW (see text for details).

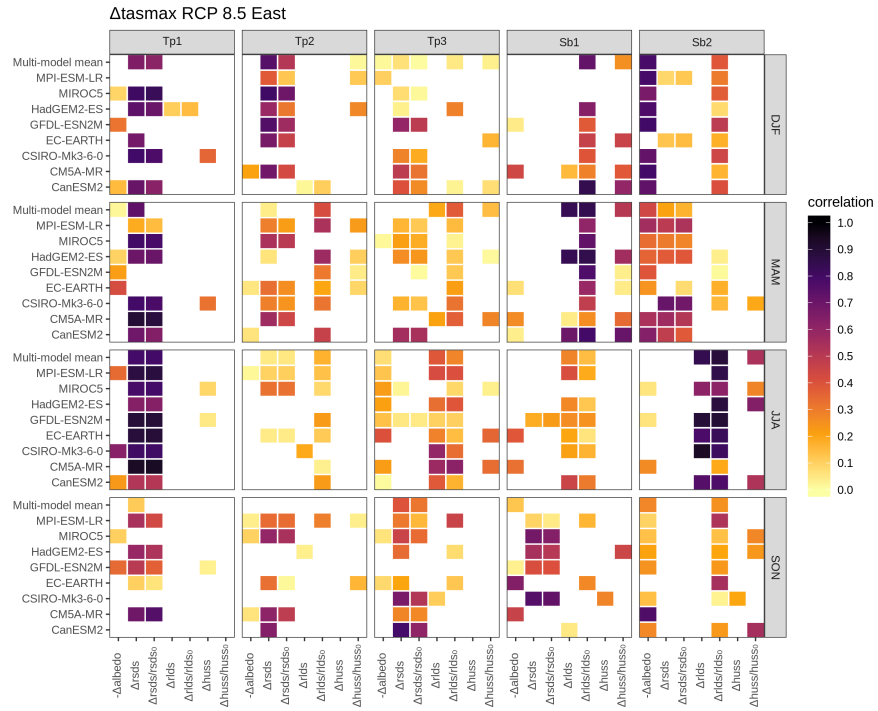

Fig. S13 Correlation coefficient between each of the seven possible EDW drivers and the maximum temperature change, for the RCP85 scenario, in the five areas areas (columns) and four seasons (rows) on the east the Andean Cordillera. The drivers are displayed along the x-axis. White boxes identify the cases in which the correlation is negative and/or the elevational dependence of a given driver has not the same sign as EDW (see text for details).

Table S1 Seasonal and annual bias (CORDEX–ERA5), following Figs. 2 and 3 of the main text. For CORDEX, only the multi-model mean values are reported.

	season	**Tp1**		**Tp2**		**Tp3**		**Sb1**		**Sb2**	
Tasmin		**West**	**East**	**West**	**East**	**West**	**East**	**West**	**East**	**West**	**East**
	DJF	-1.66	-2.97	-2.92	-1.82	-4.25	-3.44	-5.62	-4.35	-4.31	-3.82
	MAM	-1.54	-3.20	-3.02	-2.74	-4.16	-3.97	-3.64	-3.51	-1.50	-1.93
	JJA	-1.53	-4.66	-3.66	-3.34	-4.96	-4.04	-3.01	-2.27	-0.91	-1.01
	SON	-1.15	-2.34	-3.26	-1.57	-5.57	-4.42	-5.01	-4.24	-2.40	-3.19
	Annual	-1.47	-3.32	-3.21	-2.37	-4.71	-3.97	-4.32	-3.59	-2.28	-2.49
Tasmax		**West**	**East**	**West**	**East**	**West**	**East**	**West**	**East**	**West**	**East**
	DJF	0.69	2.70	-1.07	0.67	-1.67	-1.25	-0.58	-0.58	-0.53	0.78
	MAM	1.09	1.37	-1.05	0.09	-1.95	-1.92	-0.05	-0.82	0.65	0.53
	JJA	3.31	1.75	-0.45	1.11	-1.89	-1.28	-0.52	-0.28	0.01	1.41
	SON	2.23	3.46	-0.57	1.97	-1.45	-0.94	-0.52	-0.15	-0.75	0.90
	Annual	1.83	2.32	-0.78	0.96	-1.74	-1.35	-0.42	-0.46	-0.15	0.90

Table S2 Annual values of the CORDEX–ERA5 bias (as also shown in Table S1) and of the future temperature change (i.e., the change of the minimum and of the maximum temperature between the average in the period 2071–2100 and the average in the period 1976–2005) in the RCP 8.5 scenario.

		Tp1		**Tp2**		**Tp3**		**Sb1**		**Sb2**	
Tasmin		**West**	**East**	**West**	**East**	**West**	**East**	**West**	**East**	**West**	**East**
	Present bias	-1.47	-3.32	-3.21	-2.37	-4.71	-3.97	-4.32	-3.59	-2.28	-2.49
	Future change	2.17	2.29	2.55	1.96	2.41	2.61	2.19	2.51	2.19	2.31
Tasmax		**West**	**East**	**West**	**East**	**West**	**East**	**West**	**East**	**West**	**East**
	Present bias	1.83	2.32	-0.78	0.96	-1.74	-1.35	-0.42	-0.46	-0.15	0.90
	Future change	2.95	2.68	2.75	2.01	2.47	2.69	2.85	2.90	2.94	3.01

Table S3 Trend values (°C/decade) of the minimum and maximum temperature time series (shown in Figs. S4 and S5) in ERA5 (red) and in the CORDEX models mean (black) for the five areas, the two sides of the Andean Cordillera and each season.

Tasmin	**DJF**		**MAM**		**JJA**		**SON**	
	West	**East**	**West**	**East**	**West**	**East**	**West**	**East**
Tp1	0.15/0.24	0.13/0.28	0.18/0.25	0.07/0.29	0.19/0.19	0.19/0.23	0.18/0.24	0.20/0.30
Tp2	0.32/0.22	0.25/0.25	0.27/0.22	0.14/0.25	0.24/0.21	0.22/0.21	0.31/0.27	0.28/0.31
Tp3	0.31/0.18	0.16/0.22	0.28/0.22	0.02/0.20	0.20/0.20	0.02/0.18	0.22/0.23	0.14/0.26
Sb1	0.41/0.21	0.33/0.20	0.15/0.15	0.05/0.13	0.37/0.26	0.29/0.21	0.30/0.35	0.31/0.23
Sb2	0.73/0.20	0.18/0.14	0.23/0	-0.1/0	0.24/0.21	0.24/0.13	0.51/0.17	0.36/0.19
Tasmax	**DJF**		**MAM**		**JJA**		**SON**	
	West	**East**	**West**	**East**	**West**	**East**	**West**	**East**
Tp1	0.15/0.24	0.13/ 0.28	0.18/0.25	0.07/0.29	0.19/0.19	0.19/0.23	0.18/0.24	0.20/0.30
Tp2	0.32/0.22	0.25/0.25	0.27/0.22	0.14/0.25	0.24/0.21	0.22/0.21	0.31/0.27	0.28/0.31
Tp3	0.31/0.18	0.16/0.22	0.28/0.22	0.02/0.20	0.20/0.20	0.02/0.17	0.22/0.23	0.14/0.26
Sb1	0.41/0.21	0.33/0.20	0.15/0.15	0.05/0.13	0.37/0.27	0.29/0.21	0.30/0.35	0.31/0.27
Sb2	0.73/0.20	0.18/0.14	0.23/0	-0.1/-0.01	0.24/0.21	0.24/0.13	0.51/0.17	0.36/0.19

Table S4 Interannual variability of the minimum and maximum temperature series (calculated as the standard deviation of the detrended time series shown in Figs. S4 and S5) in ERA5 (single figure) and in the GCM-RCM ensemble (range of variability given by the minimum and maximum values, in parenthesis).

Tasmin	**DJF**		**MAM**		**JJA**		**SON**	
	West	**East**	**West**	**East**	**West**	**East**	**West**	**East**
Tp1	0.51 (0.26–0.6)	0.4 (0.21–0.52)	0.67 (0.31–0.81)	0.56 (0.38–0.9)	0.54 (0.37–0.91)	0.44 (0.32–0.9)	0.4 (0.32–0.69)	0.3 (0.27–0.59)
Tp2	0.47 (0.2–0.73)	0.35 (0.18–0.44)	0.54 (0.29–0.84)	0.43 (0.29–0.78)	0.49 (0.4–0.67)	0.38 (0.27–0.68)	**0.33 (0.34–0.6)**	0.27 (0.24–0.61)
Tp3	0.46 (0.33–0.56)	0.4 (0.25–0.44)	0.51 (0.38–0.6)	0.56 (0.34–0.61)	**0.39 (0.41–0.63)**	0.44 (0.4–0.61)	**0.37 (0.4–0.73)**	0.46 (0.35–0.61)
Sb1	0.4 (0.37–0.57)	0.39 (0.32–0.58)	0.6 (0.44–0.71)	0.6 (0.52–0.74)	1.05 (0.72–1.14)	0.83 (0.67–1.03)	0.68 (0.51–0.91)	0.72 (0.52–0.81)
Sb2	0.47 (0.41-0.77)	**0.61 (0.43–0.58)**	0.81 (0.44–0.93)	0.8 (0.64–0.93)	**0.66 (0.88–1.36)**	0.83 (0.77–1.13)	0.61 (0.5–0.89)	0.7 (0.48–0.89)
Tasmax	**DJF**		**MAM**		**JJA**		**SON**	
	West	**East**	**West**	**East**	**West**	**East**	**West**	**East**
Tp1	0.54 (0.3–1.13)	0.52 (0.2–0.81)	0.67 (0.37–1.02)	0.6 (0.39–1.14)	0.66 (0.29–0.7)	0.57 (0.41–1.02)	0.51 (0.33–0.72)	0.4 (0.26–0.94)
Tp2	0.67 (0.32–0.89)	0.53 (0.27–1)	0.74 (0.43–1.05)	0.51 (0.42–1.13)	0.69 (0.41–0.88)	0.49 (0.43–0.91)	0.54 (0.34–0.69)	0.42 (0.36–0.76)
Tp3	0.79 (0.3–1.08)	0.65 (0.37–1.08)	0.68 (0.45–1.15)	0.66 (0.5–1.14)	**0.46 (0.5–0.82)**	**0.58 (0.64–1.01)**	0.39 (0.37–0.69)	0.6 (0.49–0.8)
Sb1	0.48 (0.4–1)	0.5 (0.4–0.77)	0.66 (0.5–0.99)	0.67 (0.64–1.05)	1.35 (0.91–1.36)	1 (0.81–1.19)	0.79 (0.58–1.14)	0.79 (0.73–1.18)
Sb2	**0.45 (0.55–0.82)**	0.74 (0.57–0.95)	1 (0.63–1.03)	0.84 (0.72–1.15)	0.98 (0.68–1.19)	1.12 (0.96–1.39)	0.76 (0.65–1.23)	0.78 (0.67–1.27)

4 CONCLUSÕES

As análises das simulações do conjunto de oito de modelos climáticos regionais pertencentes ao CORDEX-SAM junto com a média multi-modelo mostraram que, não houve diferenças substanciais no sinal de EDW para projeções futuras quando comparado os cenários de alta emissão de CO_2 (RCP 8.5) e de estabilização das concentrações de CO_2 (RCP 4.5).

Na comparação dos modelos CORDEX com os dados de reanálise ERA5, os ciclos climatológicos de Tasmin e Tasmax foram bem reproduzidos. No entanto, a amplitude de Tasmin foi superestimada nas faces leste de Tp1 e Tp2 e uma tendência fria foi observada nas simulações dos modelos. Quanto à Tasmax, a tendência fria encontrada em Tasmin foi atenuada,principalmente nas regiões subtropicais. Além disso, a forma do ciclo anual foi bem simulada, exceto para a face leste de Tp1 e Tp2 e oeste Tp1.

Quando comparado o CORDEX (média multi-modelos) com os dados de satélite MODIS, o CORDEX superestima a cobertura de neve nas áreas elevadas da Cordilheira nos subtrópicos ao longo da fronteira Chile-Argentina, e subestimam a cobertura de neve em torno da latitude de 20 $^{\circ}$S. Embora a comparação de temperatura entre CORDEX e ERA5 demonstrou resultados satisfatórios, as tendências da cobertura de neve pode ter implicações para a interpretação de mudanças de temperatura através do mecanismo do albedo da neve.

A comparação entre os métodos de regressão linear, regressão local (LOESS) e regressão por partes na avaliação do sinal EDW, destacou um claro comportamento bimodal para a maioria das estações em todas as áreas de estudo e faces da Cordilheira. Notavelmente, ao usar a regressão por partes, as linhas de regressão antes e depois do ponto de mudança mostraram, para a maioria dos GCM-RCM, inclinações muito semelhantes. Isso sugere que descrever o EDW com um comportamento linear bimodal pode estar relacionado a razões físicas, que não foram analisadas neste estudo, mas merecem investigações futuras.

Em todas as três regiões tropicais foram identificados contrastes no sinal do EDW durante o dia e a noite (ou seja, na temperatura máxima e mínima). A $\triangle$tasmin, de fato, mostrou um EDW negativo (a taxa de aquecimento é menor em altitudes mais altas), enquanto a tasmax exibiu um EDW positivo (amplificação da taxa de aquecimento com a elevação). O gradiente de elevação da temperatura mínima nos trópicos também pareceu ser semelhante nas faces leste e oeste dos Andes, enquanto para a temperatura máxima o gradiente de altitude foi maior no lado oeste.

Contextualmente, na análise dos possíveis mecanismos condutores de EDW mostrou que, nos trópicos, nenhum mecanismo condutor comum de EDW foi identificado para $\triangle$tasmax (na maior parte impulsionado por mudanças na ROC) e $\triangle$tasmin (impulsionado

por mudanças na ROL e na umidade específica), o que pode contribuir para o sinal de EDW contrastante observados entre as duas variáveis. Isso é particularmente verdadeiro para Tp1 e Tp2, enquanto no lado oeste de Tp3, $\triangle$tasmin e $\triangle$tasmax exibiram mecanismos fracos semelhantes para DJF e SON.

Nos Andes Subtropicais, o EDW se mostrou positivo em todas as estações tanto para a $\triangle$tasmin quanto para $\triangle$tasmax (em DJF, MAM e SON no lado leste, o sinal de EDW é neutro para $\triangle$tasmin). Um mecanismo condutor de EDW claro e importante nos subtrópicos, comum às temperaturas noturnas e diurnas, é a mudança no albedo. A radiação de ondas longas e a umidade também estão significativamente correlacionadas com a EDW nos subtrópicos, mas com relevância diferente para a temperatura mínima e máxima ao longo das estações e faces da Cordilheira.

É importante ressaltar que outros possíveis fatores não incluídos neste estudo, como mecanismos relacionados a partículas de aerossol ou nuvens, podem influenciar o EDW. Além disso, as potenciais correlações cruzadas entre os mecanismos condutores, que em princípio podem amortecer ou amplificar o efeito dos mecanismos tomados individualmente, foram negligenciadas.

REFERÊNCIAS BIBLIOGRÁFICAS

AGHELPOUR, Pouya et al. Using the MODIS sensor for snow cover modeling and the assessment of drought effects on snow cover in a mountainous area. **Remote Sensing**, v. 12, n. 20, p. 3437, 2020. DOI: https://doi.org/10.3390/rs12203437

AGUILAR-LOME, Jaime et al. Elevation-dependent warming of land surface temperatures in the Andes assessed using MODIS LST time series (20002017). **International Journal of Applied Earth Observation and Geoinformation**, v. 77, p. 119-128, 2019. DOI: https://doi.org/10.1016/j.jag.2018.12.013

BELL, Bill et al. The ERA5 global reanalysis: Preliminary extension to 1950. **Quarterly Journal of the Royal Meteorological Society**, v. 147, n. 741, p. 4186-4227, 2021. DOI: https://doi.org/10.1002/qj.4174

BENISTON, Martin. Climatic change in mountain regions: a review of possible impacts. **Climatic Change**, v.59, p. 531, 2003.

BOLAÑO-ORTIZ, Tomas Rafael et al. Assessment of absorbing aerosols on austral spring snow albedo reduction by several basins in the Central Andes of Chile from daily satellite observations (20002016) and a case study with the WRF-Chem model. **SN Applied Sciences**, v.1, p.1-13, 2019. DOI: https://doi.org/10.1007/s42452-019-1256-z.

BRADLEY, Raymond et al. Threats to water supplies in the tropical Andes. **Science**, v. 312, p. 17551756, 2006. DOI: 10.1126/science.1128087.

BUYTAERT, Wouter et al. Uncertainties in climate change projections and regional downscaling in the tropical Andes: implications for water resources management. **Hydrol. Earth System Sci**. v.14, p.12471258, 2010. DOI: https://doi.org/10.5194/hess-14-1247-2010

C3S - COPERNICUS CLIMATE CHANGE SERVICE. ERA5: **Fifth generation of ECMWF atmospheric reanalyses of the global climate**. Copernicus Climate Change Service Climate Data Store (CDS), 2021.

CAMPOVERDE, Andrés Santiago Bustamante. Analysis of the urban heat island in the Andean environment of Cuenca-Ecuador. **Investigaciones Geograficas**, v.70, p.167-179, 2018. DOI: 10.14198/INGEO2018.70.08

CHIMBORAZO, Oscar; MINDER, Justin; VUILLE, Mathias. Observations and Simulated Mechanisms of Elevation-Dependent Warming over the Tropical Andes. **Journal of Climate**, v. 35, p. 1021-1044, 2022. DOI: 10.1175/JCLI-D-21-0379.1.

DELBART, Nicolas et al. Remote sensing of Andean Mountain snow cover to forecast water discharge of Cuyo rivers. **Journal of Alpine Research| Revue de géographie alpine**. v.103, 2015. DOI: https://doi.org/10.4000/rga.2903.

DUAN Anmin; WU Guoxiong. Change of cloud amount and the climate warming on the Tibetan Plateau. **Geophys Research Letters**, v.33, 2006. DOI: https://doi.org/10.1029/2006GL027946

FALCO, Magdalena et al. The potential added value of Regional Climate Models in South America using a multiresolution approach. **Climate Dynamics**, v. 54, p. 1553-1569, 2020. DOI: 10.1007/s00382-019-05073-9.

FAUSTO, Robert et al. Greenland ice sheet melt area from MODIS (20002014). **Geological Survey of Denmark and Greenland Bulletin**. v. 33, p.57-60, 2015. DOI: https://doi.org/10.34194/geusb.v33.4498

FLATO, Gregory; MAROTZKE, Jochem. (2013). Evaluation of climate models. Chapter 9. In Climate Change 2013: The Physical Science Basis. Contribution of Working Group I to the Fifth Assessment Report of the Intergovernmental Panel on Climate Change, Stocker TF, Qin D, Plattner G-K, Tignor M, Allen SK, Boschung J, Nauels A, Xia Y, Bex V, Midgley PM (eds). **Cambridge University Press: Cambridge**, UK and New York, NY, 126. doi:10.1017/CBO9781107415324.020

FRANCOU, Bernard et al. New evidence for an ENSO impact on low-latitude glaciers: Antizana, Andes of Ecuador, 0° 28'S. bf J. Geophysic Research, v.109, 2004. DOI:10.1029/2003JD004359.

FRANCOU, Bernard; VINCENT, Christian. **Les glaciers à lépreuve du climat**, IRD, Belin, Paris, 2007, 274 pp.

GARREAUD, René Dario et al. Present-day South America climate. **Palaeogeography, Palaeoclimatology, Palaeoecology**. v.281, p.180195, 2009. DOI: https://doi.org/10.1016/j.palaeo.2007.10.032.

GARREAUD, René Dario; VUILLE, Mathias; CLEMENT, Amy C. The climate of the Altiplano: observed current conditions and mechanisms of past changes. **Palaeogeography, Palaeoclimatology, Palaeoecology**. v.194, p.5-22, 2003. DOI: https://doi.org/10.1016/S0031-0182(03)00269-4

GARREAUD, René Dario. Multiscale analysis of the summertime precipitation over the Central Andes. **Monthly Weather Review**. v.127, p. 901-921, 1999. DOI:https://doi.org/10.1175/1520-0493(1999)127<0901:MAOTSP>2.0.CO;2

GARREAUD, René Dario. The Andes climate and weather. **Advances in Geosciences**. v. 22, p. 311, 2009. DOI: https://doi.org/10.5194/adgeo-22-3-2009.

GAUTAM, Ritesh et al. Satellite observations of desert dust-induced Himalayan snow darkening. **Geophysical Research Letters**. v. 40, p. 988993, 2013. DOI: https://doi.org/10.1002/grl.50226

GIORGI, Filippo et al. Editorial for the CORDEX-CORE experiment I special issue. **Climate Dynamics**. v. 57, p.1265-1268, 2021. DOI: https://doi.org/10.1007/s00382-021-05902-w

GIORGI, Filippo et al. Elevation dependency of the surface climate change signal: a model study. **Journal of Climate**. 10, 288296, 1997. DOI:https://doi.org/10.1175/1520-442(1997)010<0288:EDOTSC>2.0.CO;2

GIORGI, Filippo; JONES, Colin; ASRAR, Ghassem. Addressing climate information needs at the regional level: the CORDEX framework. **World Meteorological Organization Bulletin**, v.58, p.175183, 2009.

GUO, Donglin et al. Local changes in snow depth dominate the evolving pattern of elevation-dependent warming on the Tibetan Plateau. **Science Bulletin**, v.66, p.1146-1150, 2021. DOI: https://doi.org/10.1016/j.scib.2021.02.013

GUO, Donglin et al. Revisiting Recent Elevation Dependent Warming on the Tibetan Plateau Using Satellite Based Data Sets. **Journal of Geophysical Research**, v.124, p. 8511-8521, 2019. DOI: https://doi.org/10.1029/2019JD030666

IMMERZEEL, Walter et al. Importance and vulnerability of the worlds water towers. **Nature**, v. 577, p.364369, 2020. DOI: https://doi.org/10.1038/s41586-019-1822-y

IPCC - INTERGOVERNMENTAL PANEL ON CLIMATE CHANGE. CLIMATE CHANGE Climate Change 2007: Summary for policymakers. Contribution of working group I to the fourth assessment report of the Intergovernmental Panel on Climate Change. **Cambridge Univ. Press**, 2007.

IPCC - INTERGOVERNMENTAL PANEL ON CLIMATE CHANGE. CLIMATE CHANGE. Climate Change 2013: The Physical Science Basis. Contribution of Working Group I to the Fifth Assessment Report of the Intergovernmental Panel on Climate Change. **Cambridge Univ. Press**, 2013, 1535 pp.

IPCC - INTERGOVERNMENTAL PANEL ON CLIMATE CHANGE. CLIMATE CHANGE. The Physical Science Basis. Contribution of Working Group I to the Sixth Assessment Report of the Intergovernmental Panel on Climate. **Cambridge University Press**. 2021.

JUEN, Irmgard; KASER, Georg, GEORGES, Christian. Modeling observed and future runoff from a glacierized tropical catchment (Cordillera Blanca, Perú). **Global and Planetary Change**. v.59, p.3748, 2007. DOI: https://doi.org/10.1016/j.gloplacha.2006.11.038

KASER, Georg (1999) A review of the modern fluctuations of tropical glaciers. **Global and Planetary Change**. v.22, p.93103, 1999. DOI: 10.1016/S0921-8181(99)00028-4.

KUWAGATA, Tsuneo; NUMAGUTI, Atusi; ENDO, Nobuhiko. Diurnal variation of water vapor over the central Tibetan Plateau during summer. **J. Meteorol. Soc. Japan**. v.79, p. 401418, 2001. DOI: https://doi.org/10.2151/jmsj.79.401

LAU, William et al. Enhanced surface warming and accelerated snow melt in the Himalayas and Tibetan Plateau induced by absorbing aerosols. **Environmental Research Letters**. v.5, 2010. DOI: 10.1088/1748-9326/5/2/025204

LAWRIMORE, Jay H. et al. An overview of the Global Historical Climatology Network monthly mean temperature data set, version 3. **Journal of Geophysical Research**. v.116, 2011. DOI: https://doi.org/10.1029/2011JD016187

LENTERS, J.D.; COOK, K.H. On the Origin of the Bolivian High and Related Circulation Features of the South American Climate. **J. Atmosheric Sciences**. v.54, p. 656678, 1997. DOI: https://doi.org/10.1175/1520-0469(1997)054<0656:OTOOTB>2.0.CO;2

LIU Xiaodong et al. Temporal trends and variability of daily maximum and minimum, extreme temperature events, and growing season length over the eastern and central Tibetan Plateau during 19612003. **Journal Geophysical Research**. v. 111, 2006. DOI: https://doi.org/10.1029/2005JD006915

LIU, Hailong et al. Atlantic Warm Pool Variability in CMIP5 Simulations. **Journal of Climate**. v. 26, 2013. DOI: https://doi.org/10.1175/JCLI-D-12-00556.1

LIU, Xiaodong et al. Elevation dependency of recent and future minimum surface air temperature trends in the Tibetan Plateau and its surroundings. **Global and Planetary Change**, v. 68, p.164174, 2009. DOI: 10.1016/j.gloplacha.2009.03.017.

LUTZ, David A.; POWELL, Rebecca. L.; SILMAN, Milles. R. Four decades of Andean timberline migration and implications for biodiversity loss with climate change. **PLOS ONE**. v.8, 2013. DOI: https://doi.org/10.1371/journal.pone.0074496

MARK, Bryan G.; SELTZER, geoffrey O. Evaluation of recent glacier recession in the Cordillera Blanca, Peru (AD 19621999): spatial distribution of mass loss and climatic forcing. **Quaternay Science Reviews**. v. 24, p.22652280, 2005. DOI: https://doi.org/10.1016/j.quascirev.2005.01.003

MESSERLI, Bruno. The International Year of Mountains (IYM), The Mountains Research Initiative (MRI) and pages. **Editorial Pages New**, v.9, n.3., 2001. DOI: https://doi.org/10.22498/pages.9.3.2

MILLER, James R. et al. Elevation-dependent warming in the Eastern Siberian Arctic. **Environmental Research Letters**, v. 16, n. 2, p. 024044, 2021. DOI: https://doi.org/10.1088/1748-9326/abdb5e

MINDER, J. R.; LETCHER, T. W.; LIU, C. The character and causes of elevation-dependent warming in high-resolution simulations of Rocky Mountain climate change. **Journal of Climate**. v.31, p. 2093-2113, 2018. DOI: https://doi.org/10.1175/JCLI-D-17-0321.1

MRE- MINISTÉRIO DAS RELAÇÕES EXTERIORES. **Topografia do Brasil**, 2022. Disponível em: https://sistemas.mre.gov.br/kitweb/datafiles/Ancara/pt-br/territorio.xml

MUKHERJEE, Santanu; KUMAR, Manish. Cycling of black carbon and black nitrogen in the hydrogeosphere: Insights on the paradigm, pathway, and processes. **Science of the Total Environment**. v. 770, 2021. DOI: https://doi.org/10.1016/j.scitotenv.2020.144711

NIU, Xiaorui et al. Elevation Dependent Warming Over the Tibetan Plateau from an Ensemble of CORDEX EA Regional Climate Simulations. **Journal of Geophysical Research**. v. 126, 2021. DOI: https://doi.org/10.1029/2020JD033997

NOLIN, Anne W. Recent advances in remote sensing of seasonal snow. **J. Glaciology**. v. 56: p. 11411150, 2010. DOI: https://doi.org/10.3189/002214311796406077

OHMURA, Atsumu. (2012). Enhanced temperature variability in high-altitude climate change. **Theoretical and Applied Climatology**, v.110, p. 499-508, DOI:10.1007/s00704-012-0687-x.

ORSOLINI, Yvan et al. Evaluation of snow depth and snow cover over the Tibetan Plateau in global reanalyses using in situ and satellite remote sensing observations. **The Cryosphere**, v. 13, p. 2221-2239, 2019. DOI: https://doi.org/10.5194/tc-13-2221-2019

OYERINDE, Ganiyu. Titilope. A Review of the CMIP5 21 st Century Climate Change Projection in the Niger Basin. **Current Journal of Applied Science and Technology**. v.28, p.1-10, 2018. DOI: 10.9734/CJAST/2018/43060

PABÓN-CAICEDO, Jose Daniel et al.Observed and projected hydroclimate changes in the Andes. **Frontiers in Earth Science**. v.8, 2020. DOI: https://doi.org/10.3389/feart.2020.00061

PAINTER Thomas H. et al. Impact of disturbed desert soils on duration of mountain snow cover. **Geophysical Research Letters**, v. 34, 2007. DOI: https://doi.org/10.1029/2007GL03028

PALAZZI, Elisa et al. Elevation-dependent warming in global climate model simulations at high spatial resolution. **Climate Dynamics**, v. 52, p. 2685-2702, 2019. DOI: https://doi.org/10.1007/s00382-018-4287-z

PALAZZI, Elisa.; FILIPPI, Luca; VON HARDENBERG, Jost. Insights into elevation-dependent warming in the Tibetan Plateau-Himalayas from CMIP5 model simulations. **Climate Dynamics**, v. 48, p.39914008, 2017. DOI: 10.1007/s00382-016-3316-z

PEPIN N; LUNDQUIST J. Temperature trends at high elevations: patterns across the globe. **Geophysical Research Letters**, v. 35, 2008. DOI: https://doi.org/10.1029/2008GL034026

PEPIN, Nicholas et al. Elevation-dependent warming in mountain regions of the world. **Nature Climate Change**.v. 5, 2015. DOI: https://doi.org/10.1029/2010JD014769

PEPIN, Nicholas; DALY, Christopher; LUNDQUIST, Jessica. (2011). The influence of surface versus free-air decoupling on temperature trend patterns in the western United States. **Journal of Geophysical Reseasrch**. v.116, 2011. DOI: https://doi.org/10.1029/2010JD014769

PHILIPONA, Rolf et al. Anthropogenic greenhouse forcing and strong water vapor feedback increase temperature in Europe. **Geophysical Research Letters**. v.32, 2005. DOI: 10.1029/2005GL023624.

PISTONE, Kristina; EISENMAN, Ian; RAMANATHAN, Veerabhadran. Observational determination of albedo decrease cause by vanishing Arctic Sea ice. **Proceedings Nat. Academy Sciences**, v. 111, p. 3322-3326. 2014. DOI: 10.1073/pnas.1318201111

PRICE, Martin. Mountains: a very short introduction. **Oxford University Press**, Oxford. 2015, 134 pp. DOI: DOI:10.1093/actrade/9780199695881.001.0001

QIN, Jun et al. The altitudinal dependence of recent rapid warming over the Tibetan Plateau, **Climatic Change**. v.97, p.321327, 2009. DOI:10.1007/s10584-009-9733-9

RAMANATHAN , Veerabhadran; CARMICHAEL, Gregory. Global and regional climate changes due to black carbon. **Nature Geoscience**. v.1, p.221227, 2008. DOI: https://doi.org/10.1038/ngeo156

RAMANATHAN, Veerabhadran et al. Warming trends in Asia amplified by brown cloud solar absorption. **Nature**. v.448, p.575578, 2007. DOI: https://doi.org/10.1038/nature06019

RANGWALA Imtiaz et al. Using a global climate model to evaluate the influences of water vapor, snow cover and atmospheric aerosol on warming in the Tibetan Plateau during the twenty-first century. **Climate Dynamics**. v. 34, p.859872, 2010. DOI: 10.1007/s00382-009-0564-1

RANGWALA, Imtiaz; MILLER James. Climate change in mountains: a review of elevation-dependent warming and its possible causes. **Climatic Change**. v.114, p.527-547, 2012. DOI: https://doi.org/10.1007/s10584-012-0419-3

RANGWALA, Imtiaz; MILLER, James; XU, Ming. Warming in the Tibetan Plateau: possible influences of the changes in surface water vapor. **Geophysical Research Letters**. v.36, 2009. DOI: https://doi.org/10.1029/2009GL037245

RANGWALA, Imtiaz; SINSKY, Eric; MILLER, James. Variability in projected elevation dependent warming in boreal midlatitude winter in CMIP5 climate models and its potential drivers. **Climate Dynamics**. v.46, p.21152122, 2016. DOI:https://doi.org/10.1007/s00382-015-2692-0

RANGWALA, Imtiaz. Amplified water vapour feedback at high altitudes during winter. **Int. Journal of Climatology**. v.33, p.897903, 2013. DOI: https://doi.org/10.1002/joc.3477

RASMUSSEN Roy et al. How well are we measuring snow? The NOAA/FAA/NCAR winter precipitation test bed. **Bull. Am. Meteorological Society**. v.93, p.811829, 2012. DOI: https://doi.org/10.1175/BAMS-D-11-00052.1

REMEDIO, Armelle Reca. et al. Evaluation of new CORDEX simulations using an updated KöppenTrewartha climate classification. **Atmosphere**. v.10, 2019. DOI: https://doi.org/10.3390/atmos10110726

RUCKSTUHL, Christian et al. Observed relationship between surface specific humidity, integrated water vapor, and longwave downward radiation at different altitudes. **J Geophysical Research**. v.112, 2007. DOI: https://doi.org/10.1029/2006JD007850

SAAVEDRA, Freddy et al. Changes in Andessnow cover from MODIS data, 2000 2016. **The Cryosphere**. v. 12, p. 1027-1046, 2018. DOI: https://doi.org/10.5194/tc-12-1027-2018

SHEN, Liucheng et al. Changes in snow depth under elevation-dependent warming over the Tibetan Plateau. **Atmospheric Science Letters**. v. 22, 2021.DOI: https://doi.org/10.1002/asl.1041

SICART, Jean Emmanuel et al. Radiative properties of clouds over a tropical Bolivian glacier: seasonal variations and relationship with regional atmospheric circulation. **Int. Journal Climatology**. v.36, p. 3116-3128, 2016. DOI: https://doi.org/10.1002/joc.4540

STEHR, Alejandra et al. Combining the Soil and Water Assessment Tool (SWAT) and MODIS imagery to estimate monthly flows in a data-scarce Chilean Andean basin. **Hydrological Sciences Journal**. v.54, 2009. DOI: https://doi.org/10.1623/hysj.54.6.1053

TERZAGO, Silvia et al. Snow water equivalent in the Alps as seen by gridded data sets, CMIP5 and CORDEX climate models. **The Cryosphere**. v.11, p.16251645, 2017. DOI: https://doi.org/10.5194/tc-11-1625-2017

THÉPAUT, Jean-Noel et al. The Copernicus programme and its climate change service. In:

IEEE INTERNATIONAL GEOSCIENCE AND REMOTE SENSING SYMPOSIUM, Valencia, Spain. **IGARSS 2018**, pp. 15911593, 2018.

TUDOROIU, Marin et al. Negative elevation-dependent warming trend in the Eastern Alps. **Environmental Research Letters**. v.11, 2016. DOI: 10.1088/1748-9326/11/4/044021

URRUTIA, Rocío; VUILLE, Mathias. Climate change projections for the tropical Andes using a regional climate model: Temperature and precipitation simulations for the end of the 21st century. **Journal of Geophysical Research**. v.114, 2009. DOI: https://doi.org/10.1029/2008JD011021

VIVIROLI, Daniel; WEINGARTNER, Rolf. The hydrological significance of mountains: from regional to global scale. **Hydrology and Earth System**, v.8, p.1016-1029, 2004. DOI: https://doi.org/10.5194/hess-8-1017-2004

VUILLE, Mathias et al. 20th century climate change in the tropical Andes: observations and model results. **Climatic Change**, v.59, p.7599, 2003. DOI: 10.1007/978-94-015-1252-75

VUILLE, Mathias et al. Climate change and tropical Andean glaciers: Past, present and future. **Earth Science Reviews**. v.89, p.7996, 2008a. DOI: https://doi.org/10.1016/j.earscirev.2008.04.002

VUILLE, Mathias; BRADLEY, Raymond; KEIMIG, Frank. Interannual climate variability in the Central Andes and its relation to tropical Pacific and Atlantic forcing. **Journal of Geophysical Research**. v.105, p.1244712460, 2000. DOI: https://doi.org/10.1029/2000JD900134

VUILLE, Mathias; BRADLEY, Raymond. Mean annual temperature trends and their vertical structure in the tropical Andes. **Geophysical Research Letters**. v.27, p.38853888, 2000. DOI: https://doi.org/10.1029/2000GL011871

VUILLE, Mathias; KASER, Georg; JUEN, Irmgard. Glacier mass balance variability in the Cordillera Blanca, Peru and its relationship with climate and the large-scale circulation. **Global and Planetary Change**. v. 62, p. 1428, 2008b. DOI: https://doi.org/10.1016/j.gloplacha.2007.11.003

WANG, Qixiang; FAN, Xiaohui; WANG, Mengben. Evidence of high-elevation amplification versus Arctic amplification. **Scientific reports**. v.6, p.1-8, 2016. DOI: https://doi.org/10.1038/srep19219

WANG, Wenli et al. Characterizing surface albedo of shallow fresh snow and its importance for snow ablation on the interior of the Tibetan Plateau. **Journal of Hydrometeorology**. v.21, p.815-827, 2020. DOI: https://doi.org/10.1175/JHM-D-19-0193.1

WU, Peiming et al. Diurnal variation of GPS-derived precipitable water over the Tibetan Plateau during summer. In: PROC. INTERNATIONAL WORKSHOPS ON GPS METEOROLOGY GPS METEOROLOGY: GROUND-BASED AND SPACE-BORNE APPLICATIONS. Tsukuba, Japan, **Anais [...]**, p.3-28, 2003.

XU, Baiqing et al. Black soot and the survival of Tibetan glaciers. Proceedings Nat. **Academy Sciences**. v.106, p.221142211, 2009. DOI: https://doi.org/10.1073/pnas.0910444106

YOU, Qinglong et al. Relationship between temperature trend magnitude, elevation and mean temperature in the Tibetan Plateau from homogenized surface stations and reanalysis data. **Global and Planetary Change**, v.71, p.124-133, 2010. DOI: https://doi.org/10.1016/j.gloplacha.2010.01.020

YOU, Qinglong et al. Robust elevation dependency warming over the Tibetan Plateau under global warming of 1.5°C and 2°C. **Climate Dynamics**. v. 53, p.2047-2060, 2019. DOI: https://doi.org/10.1007/s00382-019-04775-4

ZAZULIE, Natalia; RUSTICUCCI, Matilde; RAGA, Graciela B. Regional climate of the Subtropical Central Andes using high-resolution CMIP5 models. Part II: Future projec-

tions for the twenty-first century. **Climate Dynamics**, v.51, p.2913-2925, 2018. DOI: 10.1007/s00382-017-4056-4

ZHAO, Lei et al. Global multi-model projections of local urban climates. **Nature Climate Change**. v. 11, p.152-157, 2021. DOI: https://doi.org/10.1038/s41558-020-00958-8